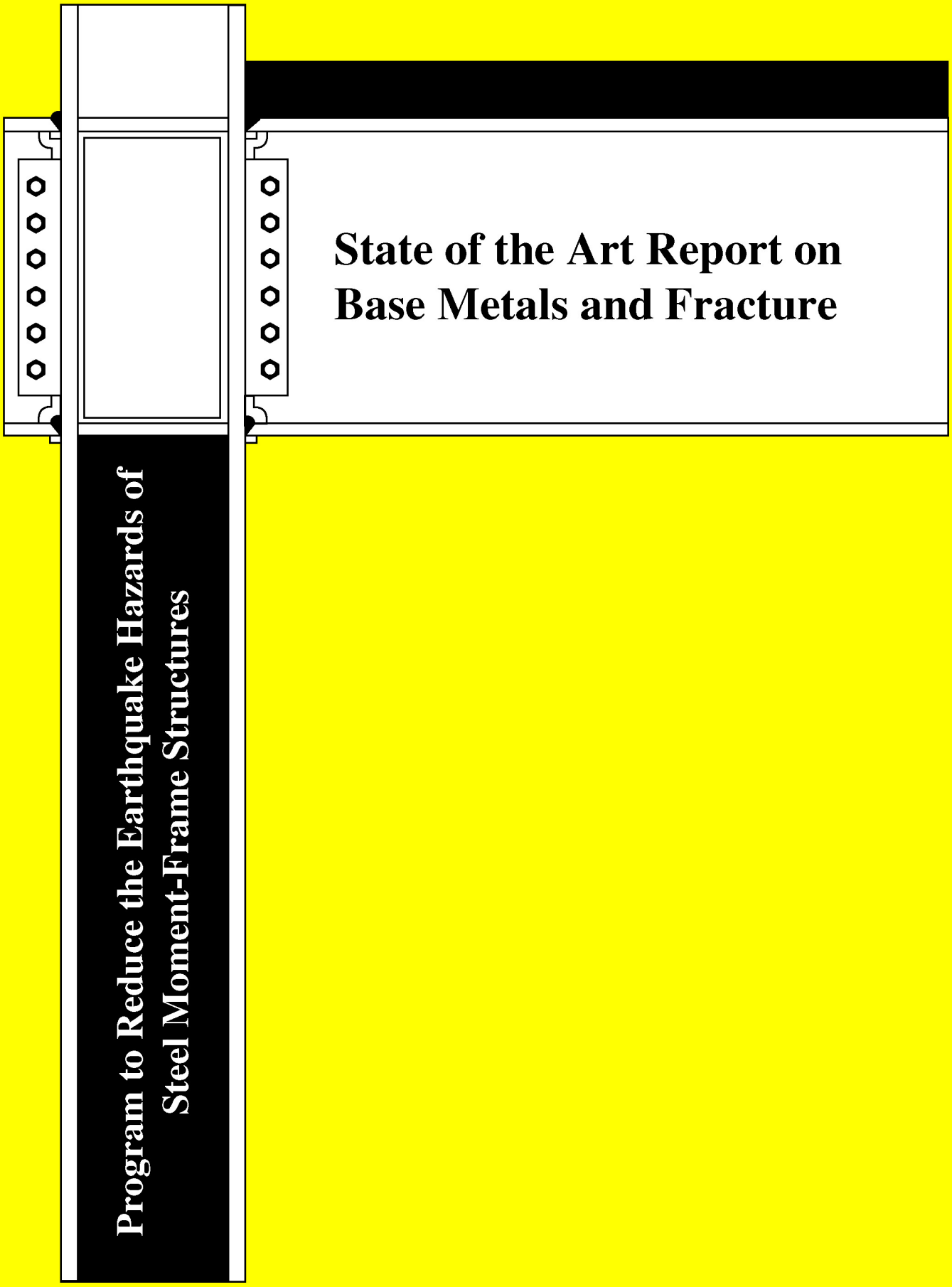

State of the Art Report on Base Metals and Fracture

Program to Reduce the Earthquake Hazards of Steel Moment-Frame Structures

DISCLAIMER

This document provides practicing engineers and building officials with a resource document for understanding the behavior of steel moment-frame buildings in earthquakes. It is one of the set of six State of the Art Reports containing detailed derivations and explanations of the basis for the design and evaluation recommendations prepared by the SAC Joint Venture. The recommendations and state of the art reports, developed by practicing engineers and researchers, are based on professional judgment and experience and supported by a large program of laboratory, field, and analytical research. **No warranty is offered with regard to the recommendations contained herein, by the Federal Emergency Management Agency, the SAC Joint Venture, the individual joint venture partners, or the partner's directors, members or employees. These organizations and their employees do not assume any legal liability or responsibility for the accuracy, completeness, or usefulness of any of the information, products or processes included in this publication. The reader is cautioned to review carefully the material presented herein and exercise independent judgment as to its suitability for application to specific engineering projects.** This publication has been prepared by the SAC Joint Venture with funding provided by the Federal Emergency Management Agency, under contract number EMW-95-C-4770.

Cover Art. The beam-column connection assembly shown on the cover depicts the standard detailing used in welded, steel moment-frame construction, prior to the 1994 Northridge earthquake. This connection detail was routinely specified by designers in the period 1970-1994 and was prescribed by the *Uniform Building Code* for seismic applications during the period 1985-1994. It is no longer considered to be an acceptable design for seismic applications. Following the Northridge earthquake, it was discovered that many of these beam-column connections had experienced brittle fractures at the joints between the beam flanges and column flanges.

State of the Art Report on Base Metals and Fracture

SAC Joint Venture

A partnership of
Structural Engineers Association of California (SEAOC)
Applied Technology Council (ATC)
California Universities for Research in Earthquake Engineering (CUREe)

Prepared for the SAC Joint Venture Partnership by
Karl H. Frank
University of Texas at Austin
John M. Barsom
Barsom Consulting, Ltd.
Ronald O. Hamburger
EQE International

Project Oversight Committee
William J. Hall, Chair

Shirin Ader
John M. Barsom
Roger Ferch
Theodore V. Galambos
John Gross
James R. Harris
Richard Holguin
Nestor Iwankiw
Roy G. Johnston
Len Joseph
Duane K. Miller
John Theiss
John H. Wiggins

SAC Project Management Committee

SEAOC: William T. Holmes
ATC: Christoper Rojahn
CUREe: Robin Shepherd
Program Manager: Stephen A. Mahin
Project Director for Topical Investigations: James O. Malley
Project Director for Product Development: Ronald O. Hamburger

Topical Investigation Team

Robert Dexter
Karl H. Frank

Technical Advisory Panel

John M. Barsom
Serge Bouchard
Michael F. Engstrom
Nestor Iwankiw
Dean C. Krouse
Frederick V. Lawrence
Robert F. Preece
Raymond H. R. Tide

SAC Joint Venture
SEAOC: www.seaoc.org
ATC: www.atcouncil.org
CUREe: www.curee.org

September 2000

THE SAC JOINT VENTURE

SAC is a joint venture of the Structural Engineers Association of California (SEAOC), the Applied Technology Council (ATC), and California Universities for Research in Earthquake Engineering (CUREe), formed specifically to address both immediate and long-term needs related to solving performance problems with welded, steel moment-frame connections discovered following the 1994 Northridge earthquake. SEAOC is a professional organization composed of more than 3,000 practicing structural engineers in California. The volunteer efforts of SEAOC's members on various technical committees have been instrumental in the development of the earthquake design provisions contained in the *Uniform Building Code* and the 1997 *National Earthquake Hazards Reduction Program (NEHRP) Recommended Provisions for Seismic Regulations for New Buildings and other Structures*. ATC is a nonprofit corporation founded to develop structural engineering resources and applications to mitigate the effects of natural and other hazards on the built environment. Since its inception in the early 1970s, ATC has developed the technical basis for the current model national seismic design codes for buildings; the *de facto* national standard for postearthquake safety evaluation of buildings; nationally applicable guidelines and procedures for the identification, evaluation, and rehabilitation of seismically hazardous buildings; and other widely used procedures and data to improve structural engineering practice. CUREe is a nonprofit organization formed to promote and conduct research and educational activities related to earthquake hazard mitigation. CUREe's eight institutional members are the California Institute of Technology, Stanford University, the University of California at Berkeley, the University of California at Davis, the University of California at Irvine, the University of California at Los Angeles, the University of California at San Diego, and the University of Southern California. These laboratory, library, computer and faculty resources are among the most extensive in the United States. The SAC Joint Venture allows these three organizations to combine their extensive and unique resources, augmented by subcontractor universities and organizations from across the nation, into an integrated team of practitioners and researchers, uniquely qualified to solve problems related to the seismic performance of steel moment-frame buildings.

ACKNOWLEDGEMENTS

Funding for Phases I and II of the SAC Steel Program to Reduce the Earthquake Hazards of Steel Moment-Frame Structures was principally provided by the Federal Emergency Management Agency, with ten percent of the Phase I program funded by the State of California, Office of Emergency Services. Substantial additional support, in the form of donated materials, services, and data has been provided by a number of individual consulting engineers, inspectors, researchers, fabricators, materials suppliers and industry groups. Special efforts have been made to maintain a liaison with the engineering profession, researchers, the steel industry, fabricators, code-writing organizations and model code groups, building officials, insurance and risk-management groups, and federal and state agencies active in earthquake hazard mitigation efforts. SAC wishes to acknowledge the support and participation of each of the above groups, organizations and individuals. In particular, we wish to acknowledge the contributions provided by the American Institute of Steel Construction, the Lincoln Electric Company, the National Institute of Standards and Technology, the National Science Foundation, and the Structural Shape Producers Council. SAC also takes this opportunity to acknowledge the efforts of the project participants – the managers, investigators, writers, and editorial and production staff – whose work has contributed to the development of these documents. Finally, SAC extends special acknowledgement to Mr. Michael Mahoney, FEMA Project Officer, and Dr. Robert Hanson, FEMA Technical Advisor, for their continued support and contribution to the success of this effort.

In Memory of Egor Popov, Professor Emeritus, University of California at Berkeley

TABLE OF CONTENTS

LIST OF FIGURES vii

LIST OF TABLES xi

1. INTRODUCTION 1-1
   - 1.1 Purpose 1-1
   - 1.2 Background 1-2
   - 1.3 Scope 1-9
   - 1.4 Special Acknowledgement 1-9

2. OVERVIEW OF STEEL MAKING AND PROCESSING 2-1
   - 2.1 Steel Making 2-1
     - 2.1.1 Blast Furnace 2-1
     - 2.1.2 Open Hearth Furnace (OHF) Steel Making 2-2
     - 2.1.3 Basic Oxygen Furnace (BOF) Steel Making 2-2
     - 2.1.4 Electric Furnace Steel Making 2-2
     - 2.1.5 Ladle Metallurgy 2-4
   - 2.2 Steel Casting and Characteristics 2-5
     - 2.2.1 Ingot Casting 2-6
     - 2.2.2 Continuous Casting 2-6
   - 2.3 Characteristics 2-7
     - 2.3.1 Microstructure 2-7
     - 2.3.2 Steel Composition 2-8
       - 2.3.2.1 Killed and Semi-Killed Steels 2-8
       - 2.3.2.2 Segregation 2-10
         - 2.3.2.2.1 Segregation and Other Defects in Ingot-Based Products 2-10
     - 2.3.3 Influence of Thermal History 2-11
       - 2.3.3.1 Phase Transformations 2-11
       - 2.3.3.2 Grain Growth 2-13
     - 2.3.4 Hot Rolling 2-13
   - 2.4 Surface and Embedded Imperfections 2-15

3. MECHANICAL PROPERTIES OF STEELS 3-1
   - 3.1 Strength 3-1
     - 3.1.1 Stress-Strain Curves 3-1
     - 3.1.2 Yield Strength and Tensile Strength 3-2
     - 3.1.3 Effects of Stress (Strain) State and Constraint on Strength 3-4
     - 3.1.4 Effects of Temperature on Strength 3-6
     - 3.1.5 Effects of Loading Rates on Strength 3-7
   - 3.2 Ductility 3-9
     - 3.2.1 Effects of Stress (Strain) State and Constraint on Ductility 3-9
     - 3.2.2 Effects of Temperature on Ductility 3-11
     - 3.2.3 Effects of Loading Rate on Ductility 3-12
   - 3.3 Fracture Toughness 3-12

3.3.1 Charpy V-Notch Fracture Toughness 3-13
3.3.2 Fracture Mechanics Concepts 3-13
3.3.2.1 Effect of Stress (Strain) State and Constraint on Fracture Toughness 3-14
3.3.2.2 Effect of Temperature on Linear-Elastic Fracture Toughness 3-15
3.3.2.3 Effect of Loading Rate on Linear-Elastic Fracture Toughness 3-16
3.4 Effects of Plastic Deformation on Steel Properties 3-17

4. TENSILE PROPERTIES OF STRUCTURAL STEELS 4-1
4.1 General 4-1
4.2 Mill Practice 4-1
4.3 Tensile Properties of Currently Produced Rolled Shapes 4-1
4.3.1 Effect of Coupon Location upon Yield Strength 4-3
4.3.2 Effect of Strain Rate upon Yield Strength 4-5
4.3.3 Yield to Tensile Strength Ratio 4-5
4.3.4 Inelastic Stress-Strain Behavior of Steels 4-6
4.4 Strength of Historic Steels 4-7
4.5 Influence of Dual Graded Steels upon Expected Strength 4-9
4.5.1 Recommended Changes to ASTM Specification 4-12
4.6 Summary 4-12

5. THROUGH-THICKNESS STRENGTH OF ROLLED SECTION FLANGES 5-1
5.1 Introduction 5-1
5.2 Causes of Anisotropic Behavior of Steel 5-1
5.3 Typical Through-Thickness Properties 5-2
5.4 Evaluation of Welded T-Joint Connections 5-5
5.5 Conclusions 5-8

6. CHARPY V-NOTICH TOUGHNESS OF ROLLED SHAPES AND PLATE 6-1
6.1 Introduction 6-1
6.2 Toughness Surveys 6-1
6.2.1 Plate 6-1
6.2.2 Wide Flange Shape 6-3
6.3 Summary and Comparison of CVN Toughness Surveys 6-9

7. MATERIAL PROPERTIES AT k-AREA REGION OF WIDE FLANGE SHAPES 7-1
7.1 Introduction 7-1
7.2 k-Area Properties of Rolled Shapes 7-1
7.3 Conclusions 7-5

8. STRENGTH VARIATION IN A913 STEEL 8-1
8.1 Hardness Survey of Shapes 8-1
8.2 Notch Toughness 8-2
8.3 Strength Variations 8-2

8.4 Conclusions 8-3

REFERENCES, FEMA REPORTS, SAC REPORTS, AND ACRONYMS R-1

SAC PHASE II PROJECT PARTICIPANTS S-1

LIST OF FIGURES

Figure 1-1 Typical Welded Moment-Resisting Connection Prior to 1994 1-4
Figure 1-2 Common Zone of Fracture Initiation in Beam-Column Connection 1-4
Figure 1-3 Fractures of Beam-to-Column Joints 1-5
Figure 1-4 Column Fractures 1-5
Figure 1-5 Vertical Fracture through Beam Shear Plate Connection 1-6
Figure 2-1 Comparison of Relative Shapes and Sizes of Rolled Steel Governing Nomenclature of Products of Primary and Billet Mills 2-5
Figure 2-2 Section Schematic of a Continuous Caster 2-7
Figure 2-3 Schematic Representation of Segregation in Plate and Structural Shapes from Ingots 2-11
Figure 2-4 Toughness Anisotropy in As-Rolled Low-Carbon Steel Plate 2-14
Figure 3-1 Tensile Stress-Strain Curve 3-1
Figure 3-2 Schematic Representation of Tensile Stress-Strain Curves for Structural Steels of Various Strengths 3-2
Figure 3-3 Schematic Stress-Strain Curves for Structural Steels 3-3
Figure 3-4 Planes of Maximum Shear Stress 3-4
Figure 3-5 Mohr's Circle of Stress Analysis for Stresses in a Structure 3-5
Figure 3-6 Origins of Constraint Effects 3-6
Figure 3-7 Yield Stresses of Eight Steels 3-6
Figure 3-8 Ultimate Tensile Strengths of Eight Steels 3-7
Figure 3-9 Stress-Strain Curve for ASTM A852 Steel 3-8
Figure 3-10 Difference Between Static Yield Strength and Yield Strength Measured at the Minimum ASTM Loading Rate 3-8
Figure 3-11 Fracture Strain in Round Tension Specimen for Eight Steels 3-10
Figure 3-12 State of Strain for Axisymmetric and Plane-Strain Tension Tests 3-10
Figure 3-13 Plane-Strain Tensile Ductility at Fracture for Four Steels as a Function of Temperature 3-11
Figure 3-14 Fracture Strain of Eight Steels 3-12
Figure 3-15 Schematic Illustration of Relationship Among Stress, Flaw Size and Material Toughness 3-14
Figure 3-16 Effects of Thickness on K_c 3-15
Figure 3-17 Plane-Strain Fracture-Toughness Transition Behavior as a Function of Temperature 3-15
Figure 3-18 Effect of Temperature and Strain Rate on Plane-Strain Fracture-Toughness Behavior of ASTM A36 Type Steel 3-16
Figure 3-19 Effect of Yield Strength on Shift in Transition Temperature Between Impact and Static Plane-Strain Fracture-Toughness Curve 3-17

Figure 3-20 Effects of Strain Hardening 3-18
Figure 3-21 Effects of Strain Aging 3-19
Figure 4-1 Idealized Stress-Strain Curve 4-2
Figure 4-2 Location of Tensile Specimens 4-4
Figure 4-3 Distribution of Yield to Tensile Ratio F_y/F_u 4-6
Figure 4-4 Average Flange Stress-Strain Curve 4-7
Figure 4-5 Results of AISI SU/19 Survey, A36 Steel 4-9
Figure 4-6 Histogram of Yield Strength for Grade 50 Material 4-10
Figure 4-7 Yield Point Histogram of A36 Grade Material 4-11
Figure 5-1 Reference Axes for Steel 5-1
Figure 5-2 Reduction in Area as a Function of Sulfur Content 5-3
Figure 5-3 Comparison of Through-Thickness and Longitudinal Properties 5-4
Figure 5-4 Sulfur Content from Survey SU/17 5-4
Figure 5-5 Sulfur Content of Recent Sales 5-5
Figure 5-6 Typical Column Flange Through-Thickness Test Specimen 5-6
Figure 5-7 Typical Tee-Joint Test Setup in the 2670 kN Capacity Universal Testing Machine Showing Location of Strain Gages and LVDTs 5-7
Figure 5-8 View of Divot-Type Fracture of Column Flange in Specimen with No Continuity Plates 5-7
Figure 6-1 Typical CVN Curve 6-2
Figure 6-2 Longitudinal CVN A572 Plate 1972-73 6-3
Figure 6-3 Transverse CVN A572 Plate 1972-73 6-3
Figure 6-4 Distribution of CVN Toughness Values A36 Shape (AISC, 1995) 6-5
Figure 6-5 Distribution of CVN Toughness Values, A572, Grade 50 Shape (AISC, 1995) 6-5
Figure 6-6 Transition Curve for Flange Materials, A572, Grade 50 W24x162 Shape 6-6
Figure 6-7 Transition Curve for Core Material, A572, Grade 50 W24x162 Shape 6-7
Figure 6-8 Transition Curve for Web Materials, A572, Grade 50 W24x162 Shape 6-7
Figure 6-9 Distribution of Upper-Shelf CVN Values 6-8
Figure 6-10 Distribution of CVN Transition Temperature, A572, Grade 50 Shape 6-8
Figure 7-1 Locations of k-Area Samples 7-2
Figure 7-2 Locations of Hardness Tests 7-3
Figure 7-3 Hardness Profile of Web – W24x62 7-3
Figure 7-4 Hardness Profile of Flange – W24x62 7-4
Figure 7-5 Charpy V-Notch Toughness Results of W24x62 from Producer 1 7-4
Figure 7-6 Charpy V-Notch Toughness Results of W24x62 from Producer 2 7-5
Figure 8-1 Hardness Testing in Web of ASTM A913 Material 8-1
Figure 8-2 Hardness Testing in Flange of ASTM A913 Material 8-2

Figure 8-3 Transition Curve for k-Area Material, ASTM A913 Section 8-3
Figure 8-4 Variations in Flange Strength of QST Shapes 8-4

LIST OF TABLES

Table 2-1 Effects of Alloying Elements 2-9
Table 4-1 Comparison of Web and Flange Tensile Properties – Contemporary Production 4-4
Table 4-2 Ratio of Static to Dynamic Yield Strengths 4-5
Table 4-3 Flange Test Values 4-7
Table 4-4 1950 Shape Test Data (A7, A373) 4-8
Table 4-5 Distribution of Steel Strength, Dual and Single Grade Producers 4-11
Table 4-6 Summary of Mill Yield Point Statistics 4-13
Table 6-1 Statistics on Upper Shelf CVN Energy for A572, Grade 50 Structural Steel 6-7
Table 6-2 Statistics for Transition Temperature (°F) A572, Grade 50 Shape 6-8
Table 6-3 Summary of Toughness Data 1973 - Present 6-10

1. INTRODUCTION

1.1 Purpose

This report, *FEMA-355A – State of the Art Report on Base Metals and Fracture*, summarizes the present state of knowledge related to the mechanical properties of structural steel shapes produced in the United States and is important to understanding the probable behavior of moment-resisting steel frames when subjected to strong earthquake ground shaking. This State of the Art Report was prepared in support of the development of a series of Recommended Design Criteria documents, prepared by the SAC Joint Venture on behalf of the Federal Emergency Management Agency (FEMA) and addressing the issue of the seismic performance of moment-resisting steel frame structures. These publications include:

- *FEMA-350 – Recommended Seismic Design Criteria for New Steel Moment-Frame Buildings.* This publication provides recommended criteria, supplemental to *FEMA-302 – 1997 NEHRP Recommended Provisions for Seismic Regulations for New Buildings and Other Structures*, for the design and construction of steel moment-frame buildings and provides alternative performance-based design criteria.
- *FEMA-351 – Recommended Seismic Evaluation and Upgrade Criteria for Existing Welded Steel Moment-Frame Buildings.* This publication provides recommended methods to evaluate the probable performance of existing steel moment-frame buildings in future earthquakes and to retrofit these buildings for improved performance.
- *FEMA-352 – Recommended Postearthquake Evaluation and Repair Criteria for Welded Steel Moment-Frame Buildings.* This publication provides recommendations for performing postearthquake inspections to detect damage in steel moment-frame buildings following an earthquake, evaluating the damaged buildings to determine their safety in the postearthquake environment, and repairing damaged buildings.
- *FEMA-353 – Recommended Specifications and Quality Assurance Guidelines for Steel Moment-Frame Construction for Seismic Applications.* This publication provides recommended specifications for the fabrication and erection of steel moment frames for seismic applications. The recommended design criteria contained in the other companion documents are based on the material and workmanship standards contained in this document, which also includes discussion of the basis for the quality control and quality assurance criteria contained in the recommended specifications.

Detailed derivations and explanations of the basis for these design and evaluation recommendations may be found in a series of State of the Art Report documents prepared by the SAC Joint Venture in parallel with these design criteria. These reports include:

- *FEMA-355A – State of the Art Report on Base Metals and Fracture*. This report summarizes current knowledge of the properties of structural steels commonly employed in building construction, and the production and service factors that affect these properties.
- *FEMA-355B – State of the Art Report on Welding and Inspection*. This report summarizes current knowledge of the properties of structural welding commonly employed in building

construction, the effect of various welding parameters on these properties, and the effectiveness of various inspection methodologies in characterizing the quality of welded construction.

- *FEMA-355C – State of the Art Report on Systems Performance of Steel Moment Frames Subject to Earthquake Ground Shaking.* This report summarizes an extensive series of analytical investigations into the demands induced in steel moment-frame buildings designed to various criteria, when subjected to a range of different ground motions. The behavior of frames constructed with fully restrained, partially restrained and fracture-vulnerable connections is explored for a series of ground motions, including motion anticipated at near-fault and soft-soil sites.
- *FEMA-355D – State of the Art Report on Connection Performance.* This report summarizes the current state of knowledge of the performance of different types of moment-resisting connections under large inelastic deformation demands. It includes information on fully restrained, partially restrained, and partial strength connections, both welded and bolted, based on laboratory and analytical investigations.
- *FEMA-355E – State of the Art Report on Past Performance of Steel Moment-Frame Buildings in Earthquakes.* This report summarizes investigations of the performance of steel moment-frame buildings in past earthquakes, including the 1995 Kobe, 1994 Northridge, 1992 Landers, 1992 Big Bear, 1989 Loma Prieta and 1971 San Fernando events.
- *FEMA-355F – State of the Art Report on Performance Prediction and Evaluation of Steel Moment-Frame Buildings.* This report describes the results of investigations into the ability of various analytical techniques, commonly used in design, to predict the performance of steel moment-frame buildings subjected to earthquake ground motion. Also presented is the basis for performance-based evaluation procedures contained in the design criteria documents, *FEMA-350, FEMA-351,* and *FEMA-352*.

In addition to the recommended design criteria and the State of the Art Reports, a companion document has been prepared for building owners, local community officials and other non-technical audiences who need to understand this issue. *A Policy Guide to Steel Moment Frame Construction (FEMA-354)* addresses the social, economic, and political issues related to the earthquake performance of steel moment-frame buildings. *FEMA-354* also includes discussion of the relative costs and benefits of implementing the recommended criteria.

1.2 Background

For many years, the basic intent of the building code seismic provisions has been to provide buildings with an ability to withstand intense ground shaking without collapse, but potentially with some significant structural damage. In order to accomplish this, one of the basic principles inherent in modern code provisions is to encourage the use of building configurations, structural systems, materials, and details that are capable of ductile behavior. A structure is said to behave in a ductile manner if it is capable of withstanding large inelastic deformations without significant degradation in strength, and without the development of instability and collapse. The design forces specified by building codes for particular structural systems are related to the amount of ductility the system is deemed to possess. Generally, structural systems with more

ductility are designed for lower forces than less ductile systems, as ductile systems are deemed capable of resisting demands that are significantly greater than their elastic strength limit. Starting in the 1960s, engineers began to regard welded steel moment-frame buildings as being among the most ductile systems contained in the building code. Many engineers believed that steel moment-frame buildings were essentially invulnerable to earthquake-induced structural damage and thought that should such damage occur, it would be limited to ductile yielding of members and connections. Earthquake-induced collapse was not believed possible. Partly as a result of this belief, many large industrial, commercial and institutional structures employing steel moment-frame systems were constructed, particularly in the western United States.

The Northridge earthquake of January 17, 1994 challenged this paradigm. Following that earthquake, a number of steel moment-frame buildings were found to have experienced brittle fractures of beam-to-column connections. The damaged buildings had heights ranging from one story to 26 stories, and a range of ages spanning from buildings as old as 30 years to structures being erected at the time of the earthquake. The damaged buildings were spread over a large geographical area, including sites that experienced only moderate levels of ground shaking. Although relatively few buildings were located on sites that experienced the strongest ground shaking, damage to buildings on these sites was extensive. Discovery of these unanticipated brittle fractures of framing connections, often with little associated architectural damage, was alarming to engineers and the building industry. The discovery also caused some concern that similar, but undiscovered, damage may have occurred in other buildings affected by past earthquakes. Later investigations confirmed such damage in a limited number of buildings affected by the 1992 Landers, 1992 Big Bear and 1989 Loma Prieta earthquakes.

In general, steel moment-frame buildings damaged by the Northridge earthquake met the basic intent of the building codes. That is, they experienced limited structural damage, but did not collapse. However, the structures did not behave as anticipated and significant economic losses occurred as a result of the connection damage, in some cases, in buildings that had experienced ground shaking less severe than the design level. These losses included direct costs associated with the investigation and repair of this damage as well as indirect losses relating to the temporary, and in a few cases, long-term, loss of use of space within damaged buildings.

Steel moment-frame buildings are designed to resist earthquake ground shaking based on the assumption that they are capable of extensive yielding and plastic deformation, without loss of strength. The intended plastic deformation consists of plastic rotations developing within the beams, at their connections to the columns, and is theoretically capable of resulting in benign dissipation of the earthquake energy delivered to the building. Damage is expected to consist of moderate yielding and localized buckling of the steel elements, not brittle fractures. Based on this presumed behavior, building codes permit steel moment-frame buildings to be designed with a fraction of the strength that would be required to respond to design level earthquake ground shaking in an elastic manner.

Steel moment-frame buildings are anticipated to develop their ductility through the development of yielding in beam-column assemblies at the beam-column connections. This yielding may take the form of plastic hinging in the beams (or, less desirably, in the columns), plastic shear deformation in the column panel zones, or through a combination of these

mechanisms. It was believed that the typical connection employed in steel moment-frame construction, shown in Figure 1-1, was capable of developing large plastic rotations, on the order of 0.02 radians or larger, without significant strength degradation.

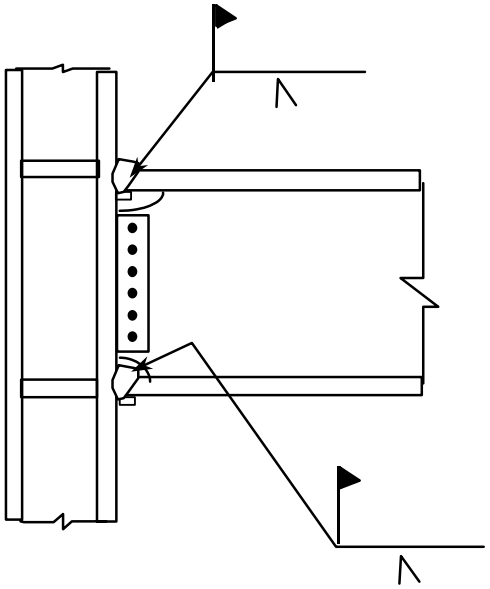

Figure 1-1 Typical Welded Moment-Resisting Connection Prior to 1994

Observation of damage sustained by buildings in the 1994 Northridge earthquake indicated that, contrary to the intended behavior, in many cases, brittle fractures initiated within the connections at very low levels of plastic demand, and in some cases, while the structures remained essentially elastic. Typically, but not always, fractures initiated at the complete joint penetration (CJP) weld between the beam bottom flange and column flange (Figure 1-2). Once initiated, these fractures progressed along a number of different paths, depending on the individual joint conditions.

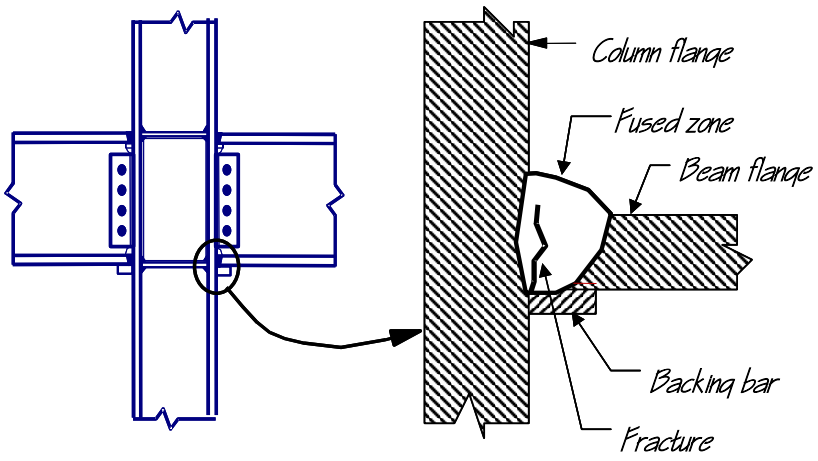

Figure 1-2 Common Zone of Fracture Initiation in Beam-Column Connection

In some cases, the fractures progressed completely through the thickness of the weld, and when fire protective finishes were removed, the fractures were evident as a crack through exposed faces of the weld, or the metal just behind the weld (Figure 1-3a). Other fracture patterns also developed. In some cases, the fracture developed into a crack of the column flange material behind the CJP weld (Figure 1-3b). In these cases, a portion of the column flange remained bonded to the beam flange, but pulled free from the remainder of the column. This fracture pattern has sometimes been termed a “divot” or “nugget” failure.

A number of fractures progressed completely through the column flange, along a near-horizontal plane that aligns approximately with the beam lower flange (Figure 1-4a). In some cases, these fractures extended into the column web and progressed across the panel zone (Figure 1-4b). Investigators have reported some instances where columns fractured entirely across the section.

a. Fracture at Fused Zone

b. Column Flange "Divot" Fracture

Figure 1-3 Fractures of Beam-to-Column Joints

a. Fractures through Column Flange

b. Fracture Progresses into Column Web

Figure 1-4 Column Fractures

Once such fractures have occurred, the beam-column connection has experienced a significant loss of flexural rigidity and strength to resist those loads that tend to open the crack. Residual flexural strength and rigidity must be developed through a couple consisting of forces transmitted through the remaining top flange connection and the web bolts. However, in

providing this residual strength and stiffness, the bolted web connections can themselves be subject to failures. These include fracturing of the welds of the shear plate to the column, fracturing of supplemental welds to the beam web or fracturing through the weak section of shear plate aligning with the bolt holes (Figure 1-5).

Despite the obvious local strength impairment resulting from these fractures, many damaged buildings did not display overt signs of structural damage, such as permanent drifts or damage to architectural elements, making reliable postearthquake damage evaluations difficult. In order to determine if a building has sustained connection damage it is necessary to remove architectural finishes and fireproofing, and perform detailed inspections of the connections. Even if no damage is found, this is a costly process. Repair of damaged connections is even more costly. At least one steel moment-frame building sustained so much damage that it was deemed more practical to demolish the building than to repair it.

Figure 1-5 Vertical Fracture through Beam Shear Plate Connection

Initially, the steel construction industry took the lead in investigating the causes of this unanticipated damage and in developing design recommendations. The American Institute of Steel Construction (AISC) convened a special task committee in March, 1994 to collect and disseminate available information on the extent of the problem (AISC, 1994a). In addition, together with a private party engaged in the construction of a major steel building at the time of the earthquake, AISC participated in sponsoring a limited series of tests of alternative connection details at the University of Texas at Austin (AISC, 1994b). The American Welding Society (AWS) also convened a special task group to investigate the extent to which the damage was related to welding practice, and to determine if changes to the welding code were appropriate (AWS, 1995).

In September 1994, the SAC Joint Venture, AISC, the American Iron and Steel Institute and National Institute of Standards and Technology jointly convened an international workshop (SAC, 1994) in Los Angeles to coordinate the efforts of the various participants and to lay the foundation for systematic investigation and resolution of the problem. Following this workshop, FEMA entered into a cooperative agreement with the SAC Joint Venture to perform problem-focused studies of the seismic performance of steel moment-frame buildings and to develop recommendations for professional practice (Phase I of SAC Steel Project). Specifically, these

recommendations were intended to address the following: the inspection of earthquake-affected buildings to determine if they had sustained significant damage; the repair of damaged buildings; the upgrade of existing buildings to improve their probable future performance; and the design of new structures to provide reliable seismic performance.

During the first half of 1995, an intensive program of research was conducted to explore more definitively the pertinent issues. This research included literature surveys, data collection on affected structures, statistical evaluation of the collected data, analytical studies of damaged and undamaged buildings, and laboratory testing of a series of full-scale beam-column assemblies representing typical pre-Northridge design and construction practice as well as various repair, upgrade and alternative design details. The findings of these tasks formed the basis for the development of *FEMA-267 – Interim Guidelines: Evaluation, Repair, Modification, and Design of Welded Steel Moment Frame Structures*, which was published in August, 1995. *FEMA-267* provided the first definitive, albeit interim, recommendations for practice, following the discovery of connection damage in the 1994 Northridge earthquake.

In September 1995, the SAC Joint Venture entered into a contractual agreement with FEMA to conduct Phase II of the SAC Steel Project. Under Phase II, SAC continued its extensive problem-focused study of the performance of moment-resisting steel frames and connections of various configurations, with the ultimate goal of developing reliable seismic design criteria for steel construction. This work has included: extensive analyses of buildings; detailed finite element and fracture mechanics investigations of various connections to identify the effects of connection configuration, material strength, and toughness and weld joint quality on connection behavior; as well as more than 120 full-scale tests of connection assemblies. As a result of these studies, and independent research conducted by others, it is now known that the typical moment-resisting connection detail employed in steel moment-frame construction prior to the 1994 Northridge earthquake, and depicted in Figure 1-1, had a number of features that rendered it inherently susceptible to brittle fracture. These included the following:

- The most severe stresses in the connection assembly occur where the beam joins to the column. Unfortunately, this is also the weakest location in the assembly. At this location, bending moments and shear forces in the beam must be transferred to the column through the combined action of the welded joints between the beam flanges and column flanges and the shear tab. The combined section properties of these elements, for example the cross sectional area and section modulus, are typically less than those of the connected beam. As a result, stresses are locally intensified at this location.
- The joint between the bottom beam flange and the column flange is typically made as a downhand field weld, often by a welder sitting on top of the beam top flange, in a so-called "wildcat" position. To make the weld from this position each pass must be interrupted at the beam web, with either a start or stop of the weld at this location. This welding technique often results in poor quality welding at this critical location, with slag inclusions, lack of fusion and other defects. These defects can serve as crack initiators, when the connection is subjected to severe stress and strain demands.
- The basic configuration of the connection makes it difficult to detect hidden defects at the root of the welded beam-flange-to-column-flange joints. The backing bar, which was

typically left in place following weld completion, restricts visual observation of the weld root. Therefore, the primary method of detecting defects in these joints is through the use of ultrasonic testing (UT). However, the geometry of the connection also makes it very difficult for UT to detect flaws reliably at the bottom beam flange weld root, particularly at the center of the joint, at the beam web. As a result, many of these welded joints have undetected significant defects that can serve as crack initiators.

- Although typical design models for this connection assume that nearly all beam flexural stresses are transmitted by the flanges and all beam shear forces by the web, in reality, due to boundary conditions imposed by column deformations, the beam flanges at the connection carry a significant amount of the beam shear. This results in significant flexural stresses on the beam flange at the face of the column, and also induces large secondary stresses in the welded joint. Some of the earliest investigations of these stress concentration effects in the welded joint were conducted by Richard, et al. (1995). The stress concentrations resulting from this effect resulted in severe strength demands at the root of the complete joint penetration welds between the beam flanges and column flanges, a region that often includes significant discontinuities and slag inclusions, which are ready crack initiators.
- In order that the welding of the beam flanges to the column flanges be continuous across the thickness of the beam web, this detail incorporates weld access holes in the beam web, at the beam flanges. Depending on their geometry, severe strain concentrations can occur in the beam flange at the toe of these weld access holes. These strain concentrations can result in low-cycle fatigue and the initiation of ductile tearing of the beam flanges after only a few cycles of moderate plastic deformation. Under large plastic flexural demands, these ductile tears can quickly become unstable and propagate across the beam flange.
- Steel material at the center of the beam-flange-to-column-flange joint is restrained from movement, particularly in connections of heavy sections with thick column flanges. This condition of restraint inhibits the development of yielding at this location, resulting in locally high stresses on the welded joint, which exacerbates the tendency to initiate fractures at defects in the welded joints.
- Design practice in the period 1985-1994 encouraged design of these connections with relatively weak panel zones. In connections with excessively weak panel zones, inelastic behavior of the assembly is dominated by shear deformation of the panel zone. This panel zone shear deformation results in a local kinking of the column flanges adjacent to the beam-flange-to-column-flange joint, and further increases the stress and strain demands in this sensitive region.

In addition to the above, additional conditions contributed significantly to the vulnerability of connections constructed prior to 1994.

- In the mid-1960s, the construction industry moved to the use of the semi-automatic, self-shielded, flux-cored arc welding process (FCAW-S) for making the joints of these connections. The welding consumables that building erectors most commonly used inherently produced welds with very low toughness. The toughness of this material could be further compromised by excessive deposition rates, which unfortunately were commonly employed by welders. As a result, brittle fractures could initiate in welds with large defects,

at stresses approximating the yield strength of the beam steel, precluding the development of ductile behavior.

- Early steel moment frames tended to be highly redundant and nearly every beam-column joint was constructed to behave as part of the lateral-force-resisting system. As a result, member sizes in these early frames were small and much of the early acceptance testing of this typical detail was conducted with specimens constructed of small framing members. As the cost of construction labor increased, the industry found that it was more economical to construct steel moment-frame buildings by moment-connecting a relatively small percentage of the beams and columns and by using larger members for these few moment-connected elements. The amount of strain demand placed on the connection elements of a steel moment frame is related to the span-to-depth ratio of the member. Therefore, as member sizes increased, strain demands on the welded connections also increased, making the connections more susceptible to brittle behavior.
- In the 1960s and 1970s, when much of the initial research on steel moment-frame construction was performed, beams were commonly fabricated using A36 material. In the 1980s, many steel mills adopted more modern production processes, including the use of scrap-based production. Steels produced by these more modern processes tended to include micro-alloying elements that increased the strength of the materials so that despite the common specification of A36 material for beams, many beams actually had yield strengths that approximated or exceeded that required for grade 50 material. As a result of this increase in base metal yield strength, the weld metal in the beam-flange-to-column-flange joints became under-matched, potentially contributing to its vulnerability.

At this time, it is clear that, in order to obtain reliable ductile behavior of WSMF construction a number of changes to past practices in design, materials, fabrication, erection, and quality assurance are necessary. The recommendations contained in this document, and the companion publications, are based on an extensive program of research into materials, welding and inspection technology, frame system behavior, and laboratory and analytical investigations of different connection details.

1.3 Scope

The information contained in this State of the Art Report is presented at a summary level and encapsulates the pertinent results of a series of investigations performed under the aegis of the SAC Joint Venture, as well as additional information contained in the literature. The intent of this State of the Art Report is to provide the interested reader with summary information on the important technical factors considered in the development of the recommended design criteria publications, referenced above.

1.4 Special Acknowledgement

The information presented in this report was largely made possible through the efforts of the Steel Shape Producers Council (SSPC), an industry association of steel producers. SSPC donated material, data, and technical consultation that were invaluable to the production of this report and its related publications.

2. OVERVIEW OF STEEL MAKING AND PROCESSING

In addition to the overall design and structural system, including the detailing of the connections and the fabrication process, the behavior of steel structures in earthquakes is dependent on key mechanical properties of the structural steel material that forms the structure, including its strength, ductility, and toughness. These properties, in turn, are dependent on the processes used to produce the material. This chapter presents a brief overview discussion of the steel making process, methods of steel production and processing, and the effects of these production processes on the mechanical properties of structural steel important to structural engineering application. Later chapters of this report present more detailed information on the range of properties that may be anticipated for steel of the various grades commonly used in structural applications.

2.1 Steel Making

Structural steels are a mixture of iron and carbon with varying amounts of other elements – primarily manganese, phosphorus, sulfur, and silicon. These and other elements are either unavoidably present or intentionally added in various combinations to achieve specific characteristics and properties of the finished steel product. The following sections present a brief description of the steel making process. More complete information can be found in various references (Lankford, 1985; Fruehan, 1998).

Various steel making furnaces have been developed over the years. The modern age production of bulk steel was initiated with the Thomas/Bessemer and open hearth processes. The Thomas/Bessemer process can now be considered extinct. Also, the open hearth process has lost most of its significance and is no longer used in the USA. The following is a brief description of the predominant steel conversion processes currently in use world wide.

2.1.1 Blast Furnace

The basic ingredients of the blast furnace mixture are iron ore and other iron bearing materials, coke, and limestone. Coke is a carbon rich material obtained by baking coal in an oxygen-free environment. It is the primary source of carbon in iron.

The basic ingredients are charged into the top of large steel shells lined with heat-resistant bricks called a blast furnace. The iron ore and other iron-bearing materials, coke, and limestone proceed slowly down through the body of the furnace as they are exposed to a blast of hot air that blows upwards from the bottom. The blast of air burns the coke, releasing heat and gas, which reduce the iron ore to metallic iron. The limestone acts as a cleaning agent by reacting with impurities in the ore.

The molten iron collects at the bottom of the furnace. This iron contains several chemical elements including carbon, manganese, sulfur, phosphorus, and silicon in amounts higher than permitted for steel. Thus, it is drawn off periodically, to be refined further in a steel making furnace.

Although steel shape is often produced by the Electronic-Arc Furnace (EAF) processes (see Section 2.1.4), which do not use the blast furnace directly, blast furnace ironmaking is an important part of shape production through its importance in overall steel manufacture, and through its contribution to the alternative iron sources which are used in EAF processes.

2.1.2 Open Hearth Furnace (OHF) Steel Making

An open hearth furnace is a shallow steel making area called a "hearth" in which molten iron, limestone, and scrap steel are charged. The open hearth process has been phased out of use in the USA and the countries of the European Union.

2.1.3 Basic Oxygen Furnace (BOF) Steel Making

In this process, hot metal from the blast furnace, along with steel scrap and fluxes, are charged into the BOF where oxygen is introduced into the molten metal to react with impurities and remove or reduce their level. Fluxes are added to reduce the sulfur and phosphorus contents to desired levels. The size of a typical BOF heat is about 270 to 300 tons.

Most world steel production, and much production of steel shape outside the USA, is by BOF steelmaking methods.

2.1.4 Electric Furnace Steel Making

Presently, all structural shapes produced domestically, and a significant portion of structural shape produced by foreign steel producers for consumption in the United States, are produced through melting in electric-arc furnaces (EAF). There are many variations of EAF. Power may be supplied by DC or three-phase AC current. Configuration may be the eccentric-bottom-tapping (EBT) variety, or a runner-tap type. The EAF may be of conventional shell design, twin shell arrangement, or "shaft-furnace" type. All configurations of electric-arc furnaces operate on the same principle; it is the purpose of an EAF to melt its burden (or charge).

The EAF burden is comprised of four major components:

- Steel scrap
- "Alternate" or supplementary iron units
- Additives
- Slag formers

Steel scrap is categorized or "typed" by source (previous application), physical shape and size, and by chemical make-up. Steel makers blend the various scrap types to optimize cost, packing density, melting efficiency, and "melt-in" chemistry. Typically steel scrap will comprise more than 90% of the metallic charge burden. The balance of the burden may be completed with "alternate" or supplemental iron units such as pig iron, direct reduced iron (DRI), or hot briquetted iron (HBI). These alternate iron units often contain 92 – 96% iron and 2 - 4% carbon and are very low in residual elements. Lime is also blended in the charge burden as a slag former. Coke or coal is a common burden additive as a source of additional carbon.

Burdens are built and charged into the EAF in lots, (or buckets). Depending upon shop preference, two to three charges are made to produce one heat lot.

The primary melting energy in the EAF melting process is the electric arc. Once an EAF has been charged, an arc is struck between the graphite electrode(s) and the scrap. Operating voltages of 800 – 1100 VAC and 40,000 – 80,000 Amps are not uncommon in AC – EAF operation. The 6000°F arc-plasma melts the scrap at the point of contact. A computer-feedback system constantly monitors the instantaneous electrical condition of the furnace and adjusts the spacing between the electrodes and the scrap. As the scrap melts away from the electrode tips, the feedback system lowers the electrodes deeper into the charge. Essentially, the arcs bore holes into the scrap. The charge pile placed in the furnace is consumed (melted) as solid pieces at the edges of the holes cave into the holes and are melted by the plasma. Any lime contacted by either the arc-plasma, or liquid steel generated by the arc-plasma, will also melt. Both liquids ultimately drain to the bath level (bottom) of the EAF. In multiple charge operations, the initial charge is usually the largest in volume. Melting is performed until sufficient furnace volume is available to accept a second or third charge. Only after all charges have been introduced to the furnace does melting to completion (no remaining solid scrap) occur.

Simultaneous to the electric melting, chemical energy is used to assist the melting. EAF's often have multiple gas-fired burners located around the circumference of the furnace shell. Burner flames are used to locally preheat the metallic charge. Commercially pure oxygen is blown into the furnace either through consumable pipes (lances), or through water-cooled lances (or both). In the early stages of a melt, the lancing of oxygen acts as a cutting torch, reducing large pieces of scrap to smaller, more readily melted sizes. As the melt progresses and a liquid pool can be contacted, the lanced oxygen "burns" dissolved oxidizable elements, such as carbon, manganese, silicon, and aluminum contained in the liquid; the energy from this reaction elevates the temperature of the liquid metal pool. In the final stages of melting, the oxygen is used to decarburize the melt. Sacrificial carbon is also commonly blown into the covering slag layer to react with excess oxygen. This reaction liberates additional energy. A second product of this reaction is carbon monoxide gas, which forms in the slag, and causes the slag to foam. The slag foaming improves the efficiency of arc-energy transfer to the bath.

In a typical operation, the furnace is not entirely drained of its liquid between heats. A hot liquid "heel" of 10 to 20 tons is maintained. The liquid heel aids in melting the next furnace charge by preheating the solid charge, dissolving solids, and allowing the carbon additives and alternative iron units to contact the liquid heel as soon as possible. As the heel's carbon content increases, its melting point becomes depressed; this aids in rapid dissolution of the remaining solid scrap.

Once the final charge has been entirely melted, the highly oxidized slag that has formed over the top of the pool is flushed from the furnace to minimize contamination of the next heat. Working (heating and decarburization) of the steel continues until the desired tap temperature and carbon level have been obtained. When this has occurred, the heat will be tapped into a refractory-lined ladle. Typical EAF heats range from 80 to 360 tons.

2.1.5 Ladle Metallurgy

Steel producers have varying degrees of control over the numerous elements that constitute steel. During EAF or BOF melting, the steel producer, through oxygen blowing, has a high degree of control over the final carbon level of the steel. With slag practices, the phosphorous and sulfur levels in the steel can be controlled to a limited extent. During melting, highly oxidizable elements, such as silicon, aluminum, and manganese are all but eliminated from the heat. Other elements, such as copper, nickel, molybdenum, tin, and to a lesser extent, chromium are only minimally oxidized during melting. Control of these latter elements can be accomplished by the careful control of scrap mix and composition. In BOF steels, the content of these elements is generally very low because of the use of blast furnace iron, which is made from iron ore of low residual element content.

Common structural steels are of the carbon-manganese family of steels. The primary elements comprising these steels are iron, carbon, and manganese. During melting, the steel producer can control the carbon level, but manganese is decreased due to oxidation. Ladle metallurgy is used to change the heat chemistry from the as-melted/as-tapped condition to a desired composition. Some steel producers add alloys to the ladle in a controlled manner during the tapping operation, while other producers use a ladle metallurgy furnace (LMF). The LMF practice is more flexible and controllable than the at-tap method.

During tapping, slag-formers are added to the molten tap stream to "build" a new ladle slag. Some quantity of EAF or BOF slag "carry-over" to the ladle is unavoidable. Melting slags are oxygen saturated. Additionally, the liquid steel itself contains a quantity of dissolved oxygen. Steels that are to be continuously cast must be "killed," that is, the dissolved oxygen content must be reduced to the point that oxygen will not form carbon monoxide bubbles during solidification. Killing is accomplished by the addition of highly oxidizable elements such as silicon and/or aluminum. Killing of a heat also reduces the losses of less oxidizable elements such as manganese when additions are made to alloy the steel. There exists a chemical equilibrium between slag and metal, thus for effective killing, the ladle slag must also be deoxidized (treated). Treating the slag also renders it suitable as a collector for sulfur.

After creating and treating the slag, the dissolved oxygen content of the steel is reduced by the addition of killing elements (typically silicon or aluminum). Alloying elements (manganese, vanadium, columbium/niobium, etc.) are then added to obtain the desired steel chemistry. Samples of the liquid steel are analyzed and "trim" additions made when necessary to meet specification-required limits. During the alloying process, inert gas is either bubbled or injected into the ladle to stir the steel, or it may be stirred by electromagnetic stirring (EMS). The stirring allows for more rapid dissolution of alloying elements, promotes desulfurization by improving metal-to-slag contact, and promotes uniformity of both steel temperature and composition in the ladle.

Alloying "at-tap" restricts the time available for post-tap slag treatments and trim alloy additions, which must be made carefully so that steel temperatures do not drop too low for casting. Higher steel temperature (superheat) is needed when LMF facilities are not available. Careful control of super-heat is very important in this case. In LMF operations, superheat is less

critical, as the LMF is capable of supplemental heating. This allows the time for the alloying process to be extended, facilitating a greater control.

Desulfurization is a time-dependent and temperature-dependent reaction. The ability to desulfurize a heat decreases as temperature decreases. The rate of desulfurization also diminishes with sulfur content and process time. Therefore, longer times are required to drive sulfur levels lower. Sulfur removal from liquid steel is accomplished by conditioning the slag so that sulfur retention by the slag is favored. In the absence of stirring, the sulfur must then diffuse to the slag/metal interface before the slag can absorb it. In "at-tap" systems, post-tap stirring (rinsing) is continued to encourage good metal-to-slag contact and improve the desulfurization reaction. Inert gas stirring is also used during LMF processing. In addition, arc heating in the LMF causes agitation and mixing of the slag/metal interface and increases the interface surface area, further improving the desulfurization reaction.

2.2 Steel Casting and Characteristics

Once the liquid steel has been processed to achieve the desired chemistry and temperature, it must be put into a solid form suitable for use by the rolling mill. The process of producing this solid product is known as casting. Either ingot or continuous casting methods may be used. Figure 2-1 indicates the cast forms of slabs, blooms, and billets.

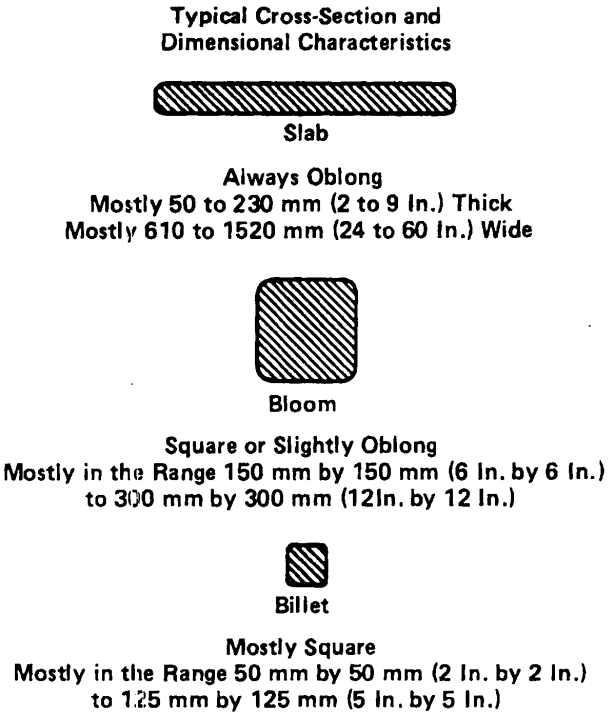

Figure 2-1 Comparison of Relative Shapes and Sizes of Rolled Steel Governing Nomenclature of Products of Primary and Billet Mills

2.2.1 Ingot Casting

In traditional (historic) steel making, the liquid steel was poured (teemed) from the ladle into a series of cast iron molds. The liquid steel cooled in the cast iron mold and solidified into an ingot. The rate of solidification was dependent upon the liquid steel temperature, the ingot size (geometry and cross-section), and steel chemistry. The final size, product form, and rolling mill capacity determine the size of the ingot cast.

Ingot casting could be used with killed, semi-killed, and non-killed (rimmed or capped) types of steel. The slow solidification rates (a 20-ton ingot could take three to four hours to solidify) can lead to segregation of carbon, sulfur, and phosphorus.

2.2.2 Continuous Casting

The use of continuous casting offers a more cost and quality effective casting method as compared to ingot casting. All structural shapes of domestic origin and the majority of foreign-produced shapes are continuously cast. Continuously cast shapes include billets, blooms, slabs, beam blanks, and near net shapes. Several foreign manufacturers still produce high quality ingot castings for jumbo shapes.

In continuous casting, schematically shown in Figure 2-2, liquid steel of the desired chemistry and temperature is teemed from the ladle into the tundish. The tundish is a refractory lined vessel that serves as a distribution box and molten metal reservoir. The tundish holds sufficient molten steel so that when a ladle has been drained of its contents, casting can continue uninterrupted while a full ladle is swapped for the empty one. Nozzles located in the bottom of the tundish deliver simultaneous streams of steel to one or more casting molds located directly below.

The continuous casting molds are made of copper, formed in the cross-sectional shape and size of the desired casting, and water-cooled. During steady-state casting, the steel streams from the tundish into the open top of the mold and fills the mold cross-section. Shrouding of the stream by various mechanical or gas devices may be employed to prevent or reduce the re-oxidation of the steel, which otherwise may lead to a deterioration in steel cleanliness. Liquid steel that comes in direct contact with the water-cooled mold surface quenches to form a solid shell and joins to the existing shell already formed along the perimeter of the mold. As the shell forms, it is continually withdrawn from the bottom of the mold. Shell growth is entirely due to heat extraction. The casting mold is oscillated up and down, and lubricated with either oil or powder to prevent the cast shell from sticking to the mold. During the short residence time within the mold, the thermal transfer is sufficient such that the shell grows to a thickness that is capable of maintaining its cross-sectional shape while containing a core of liquid steel. Outside of the mold, water and/or air sprays are employed to continue shell thickening. Mechanical restraint may also be used to help maintain the cast shape.

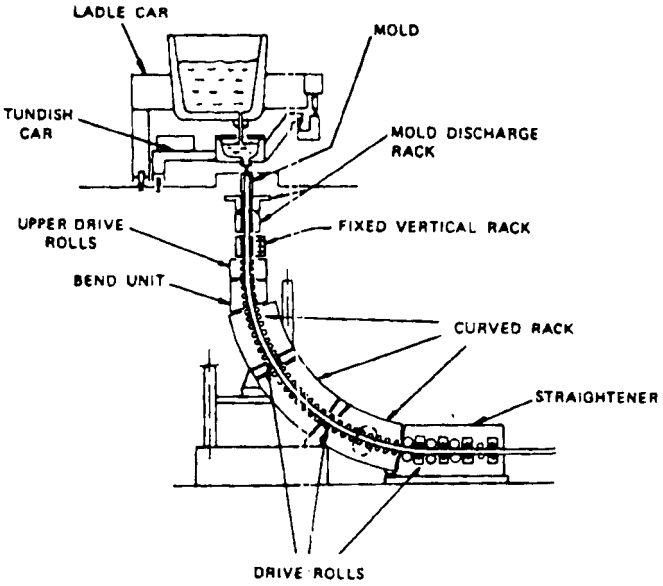

Figure 2-2 Section Schematic of a Continuous Caster

The continued integrity of the cast shell is critical to the success of continuous casting. As the distance below the top of the mold increases, so too does the internal pressure of the casting increase as a result of the height and weight of the central liquid column. Imperfections in the thin shell can weaken its ability to contain the liquid steel. The shell is particularly vulnerable upon exit of the mold. Should the shell be broached, the liquid core will drain away, destroying the cast strand and causing costly damage to the casting machine. Non-killed and semi-killed steels are known, from ingot casting, to promote flawed shells, hence *only killed steels are capable of being continuously cast*. Reduced sulfur content, particularly in larger cross-section castings, is helpful in promoting shell integrity. Poor surface quality can lead to "stickers," or "tears," within the mold, which "breakout" as the shell is withdrawn from the mold.

A pinch roller drive unit continuously withdraws the cast strand from the mold. A straightener, usually used in combination with the drive rolls, bends the strand from a radiused orientation to flat and horizontal. Once the strand has reached the straightener, sufficient heat has been extracted, and the cross-section is solid. The cast strand is then cut to the desired length.

2.3 Characteristics

2.3.1 Microstructure

On the microstructural level, all metals are composed of grains. Grains are a three-dimensional matrix of atoms arranged in a regular and repeating crystal structure. The characteristics and properties of steels are a function of the microstructure and grain distribution. Microstructure, in turn, is determined by the chemistry, deformation, and thermal history of the steel.

The microstructure of most common structural steels consists of a primary matrix of ferrite grains with a small dispersion of pearlite. The characteristics of the ferritic grain structure of steel dictate the properties and behavior at normal service temperatures. A fine grain size promotes increased strength, toughness, and weldability.

2.3.2 Steel Composition

Most structural steels are of the carbon-manganese family of steels; their primary constituents are iron, carbon, and manganese. Carbon is the principal hardening element in steel. Increases in carbon content result in greater hardness and tensile strength, but also result in a decrease in ductility, toughness, and weldability. Carbon has a moderate tendency to segregate. Similar to carbon, but to a lesser degree, manganese increases the hardness and tensile strength. Manganese also combines with sulfur to form manganese sulfides and thus control the undesirable effects of sulfur (decreased ductility, toughness, and weldability).

Other alloying elements may be present as a result of additions, or by inclusion in the raw materials. In addition to carbon and manganese, Table 2-1 presents the more common alloying elements. Of this list, silicon and aluminum are notable for their use as de-oxidizers (killing agents), and vanadium, columbium (niobium), and aluminum for their contribution to grain size control during hot working. Careful examination of Table 2-1 reveals that some elements have both positive and negative influence on the steel. The steelmaker carefully selects alloying elements to balance these influences and yield a product that meets both chemical composition specifications and performance requirements.

2.3.2.1 Killed and Semi-Killed Steels

In the liquid state, steel has a considerable capacity to dissolve gases such as oxygen. The solubility of gases decreases with decreasing temperature. As the steel temperature decreases during casting, oxygen will come out of solution and will be free to react with its surroundings. If the steel's carbon content is sufficient, the oxygen will react with carbon to form carbon monoxide bubbles. Typically, some of these bubbles are trapped in the body of the casting as voids, or escape through the thin casting wall leaving behind a "pinhole" as an artifact of its evolution.

To prevent these oxygen reactions, elements which have a stronger affinity to react with oxygen than does carbon, such as silicon or aluminum, are added to reduce (or "kill") the dissolved oxygen content of the steel. The products of these reactions are non-metallic inclusions. Normally, the killing operation will be carried out during the ladle metallurgy phase of steelmaking, allowing sufficient time for flotation and removal of most of the non-metallic reaction products, leading to cleaner steel.

Table 2-1 Effects of Alloying Elements

ELEMENT	EFFECT(s)
Carbon (C)	Principal hardening element in steel Increases strength and hardness Decreases ductility, toughness, and weldability Moderate tendency to segregate
Manganese (Mn)	Increases strength and toughness Controls negative effects of sulfur
Phosphorus (P)	Increases strength and hardness Decreases ductility and toughness Considered as an impurity, but sometimes added for atmospheric corrosion resistance Strong tendency to segregate
Sulfur (S)	Considered undesirable except for machinability Decreases ductility, toughness, and weldability Adversely affects surface quality Strong tendency to segregate
Silicon (Si)	Used to deoxidize or “kill” molten steel Increases strength
Aluminum (Al)	Used to deoxidize or “kill” molten steel Refines grain size, thus increasing strength and toughness
Vanadium (V) and Columbium/Niobium (Cb/Nb)	Small additions increase strength Refines grain size, thus increasing strength and toughness
Titanium (Ti)	Small amounts refine the grain size, thus increasing toughness
Nickel (Ni)	Increases strength and toughness
Chromium (Cr)	Increases strength Increases atmospheric corrosion resistance
Copper (Cu)	Primary contributor to atmospheric corrosion resistance Increases strength
Nitrogen (N)	Increases strength and hardness May decrease ductility and toughness
Boron (B)	Small amounts (0.0005%) increase hardenability, used only in aluminum killed steels Most cost effective at low carbon levels

Steels in which the dissolved oxygen content has not been reduced sufficiently to prevent carbon monoxide evolution during casting are known as semi-killed or non-killed steels (rimming steels). Rimming steels contain a high void percentage and are not suitable for structural steel applications. Semi-killed steels were commonly produced when ingot casting was the dominant industry casting process. The incomplete killing of the steel results in carbon monoxide evolution, however the rate of the evolution was much less than that in rimming steels. Semi-killed steel is more dense than rimming steel, is less costly than killed steel, but requires careful control of the deoxidation practice. Neither rimmed nor semi-killed steels can be routinely continuously cast; therefore killed steels are the norm today. Killed steels are also the norm for jumbo shapes that are still produced from ingots.

2.3.2.2 Segregation

Segregation of chemical elements in casting is frequently expressed as a local departure from the "average" chemical composition. Segregation of elements in steel is due to the fact that steel is an alloy. In solidification of a pure element, freezing of the metal occurs at a unique melting/freezing temperature. In alloys, freezing occurs over a temperature range. Within this range, the alloy becomes "mushy" (part solid, part liquid). During solidification, the higher melting point phases and metallic compounds will freeze first. The lower melting point elements and metallic compounds will be rejected into the liquid portion of the mushy zone, enriching it in these elements and compounds. In steel, relatively pure iron tends to be the first to solidify within the mushy zone. Sulfur has the highest tendency to segregate. The following elements (in descending order) also tend to segregate, but to a lesser degree: phosphorous, carbon, silicon, and manganese.

The rate of segregation is inversely dependent on the rate of solidification. When steels solidify rapidly, segregation does not have the time to occur. In such circumstances, the solid steel formed is of the same chemical composition as the liquid. Additionally, due to chemical reactions occurring during solidification, segregation of some elements may be more pronounced in semi-killed or non-killed steels. In general, continuously cast steel is less segregated and contains negligible porosity and pipe as compared to ingot steel. The higher solidification rate of killed steels processed by continuous casting methods results in greater uniformity of composition and properties as compared to ingot cast steels.

2.3.2.2.1 Segregation and Other Defects In Ingot-Based Products

Chemical segregation, porosity, and piping (shrinkage cavities) are inherent characteristics of the ingot solidification process. The magnitude of these characteristics in the final product is a function of several parameters including liquid metal composition and temperature, deoxidation practice, ingot size, and amount of metal cropped and discarded from the top and bottom of the ingot.

Killed steels, however, experience shrinkage at the top of the ingot during solidification. This condition can lead to large internal defects that do not heal during subsequent hot rolling. Generally, ingots made from killed steel are made with sinkheads (a reservoir of liquid steel at the ingot top) to feed this shrinkage cavity as the ingot solidifies. The sinkhead is subsequently removed and discarded.

The amount of ingot segregation remaining in semi-finished and finished products depends on many factors. However the relative location, shape, and distribution of the segregation in the product follows three simple principles (Barsom, 1991):

1. The center of the ingot cross-section remains the center of the cross-section of the final product.
2. The contours that describe the cross-section of the ingot remain contours that describe the cross-section geometry of the finished product.

3. The ratios of the areas within the contours remain constant as the ingot is rolled into the finished product.

The application of these principles indicate that segregation, if present, would occur along the mid-thickness plane of plate products and in the shape of a dog bone for a wide-flange structural shape, as shown in Figure 2-3 (Barsom, 1991). The redistribution of segregation, porosity, and pipe as a result of the elongation and shaping of ingots into the finished products may result in variations in properties within the final products.

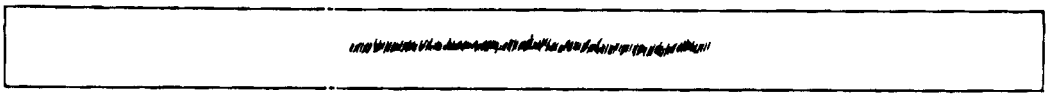

Plate

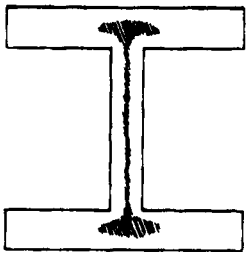

Structural Shape

Figure 2-3 Schematic Representation of Segregation in Plate and Structural Shapes from Ingots

2.3.3 Influence of Thermal History

The past thermal history of steel has significant influence upon properties of steel products. The principal thermal history effects are due to phase transformations and grain growth events.

2.3.3.1 Phase Transformations

Steel is an unusual material in that, as its temperature decreases from the liquid state to ambient, it not only undergoes a liquid to solid state change (freezing), but also two separate and distinct solid state phase transformations.

Very simplistically, solid steel grains are composed of a three-dimensional crystal matrix of regularly arranged iron atoms. The atomic diameter of carbon is roughly half the size of iron. Thus, carbon atoms easily fit into the interstices (spaces) between the iron atoms. The packing arrangement, and hence the interstitial hole size and distribution, is different in the different solid state phases.

Structural steel grades, upon solidification, form a solid phase known as delta-iron (δ-iron). This phase exists only at highly elevated temperatures. Phase transformations, to and from δ-

iron, other than melting, have no commercial application, and have no influence on the properties of steel at normal service temperatures.

Upon further cooling, the atomic arrangement of iron atoms in δ-iron transforms to a different packing configuration known as austenite or gamma-iron (γ-iron). Atomic packing density of iron in the austenitic state is such that up to 2% of carbon can be dissolved into the iron matrix. Further cooling of austenite will induce the iron matrix to transform to a higher packing density known as ferrite or alpha-iron (α-iron). The volume of interstices in the new matrix is reduced, resulting in a maximum carbon solubility of 0.02%.

The transformation from austenite to ferrite occurs over a temperature range that is dependent on chemical composition. Under equilibrium conditions, as the temperature is decreased through the transformation range, the excess carbon that is rejected by the formation of ferrite, diffuses through the solid steel, concentrates, and forms iron carbide. Iron carbide forms in islands of alternating ferrite and iron carbide, known as pearlite. The total percentage of pearlite developed within steel depends on the carbon content. The pearlite lath spacing is a function of temperature and time of formation. The size of the pearlite islands and the spacing between laths strongly influence the hardness, ductility and strength of the steel. Examples of structural steels having ferrite-pearlite microstructure are ASTM A36, A572, A588, and A992.

The solid state diffusion (transport) of carbon atoms through the solid steel matrix is dependent on both time and temperature. If the temperature of the steel is rapidly lowered (quenched) through the transformation range such that sufficient time for carbon diffusion is not provided (quenched), metastable low temperature transformation products bainite or martensite will form. These phases are characterized as being harder, stronger, less ductile and often less tough than ferrite – pearlite steels. Controlling the quenching rate can control the fraction of these phases. Once below the austenite to ferrite transformation completion temperature, insufficient thermal energy is available for any carbon diffusion to occur and the matrix is essentially “locked” into its transformed or partially transformed state.

If the steel’s temperature is then raised, the system will have restored to it sufficient thermal energy for solid state carbon diffusion to reinitiate. Given sufficient time and temperature, phase transformation products will decompose. Ductility and toughness of the steel will be improved, but at the expense of the strength and hardness that bainite and martensite offer. By carefully controlling the temperature and time of the reheating, the amount of decomposition can be controlled and thus a balance between increased strength and hardness can be obtained, with acceptable toughness and ductility. This process is known as tempering.

Quenched and tempered plate steels, such as A852, A514, and A517 are produced by this type of thermal processing. These plate steels are rarely used in buildings. ASTM A913 is an example of a structural shape building grade that is processed through controlling thermo-mechanical history. Immediately after the final hot rolling reduction, the A913 shape is subjected to a controlled water spray to quench its outer surface. The internal residual heat of rolling then re-heats the quenched shell and tempers the bainite that has formed. This form of thermo-mechanical processing (TMCP) is known as quenching and self-tempering (QST).

2.3.3.2 Grain Growth

As previously described, solid metals are comprised of grains which impinge upon one another. The region where the grains impinge is known as the grain boundary. In the austenite temperature range, sufficient thermal energy is available to allow grain boundary atoms to migrate across the boundary and occupy a stable lattice site in a neighboring grain. Grains with the highest total potential energy will generally see loss of grain boundary atoms to those neighboring grains of lower total energy. In this manner, the total energy of the system is decreased as the number of atoms occupying lower energy bulk lattice sites increases and total grain boundary surface contained within the system decreases. The observable effect is for large grains to grow larger at the expense of smaller grains. This process is known as grain growth. The rate of grain growth is highly dependent upon both time and temperature. Chemical composition also has a significant effect on the process. The presence of high temperature precipitate phases, such as aluminum nitride, vanadium nitride, columbium (niobium) carbide, etc., can act to "pin" grain boundary motion and help preserve a fine grain structure at elevated temperatures.

The practical result of grain growth is that shapes that are hot rolled at "hotter" temperatures will tend to exhibit a coarser grain size than those shapes rolled at "cooler" temperatures. In shapes where there are areas of large thermal mass concentrations, differential cooling rates will be experienced and the grain sizes will vary. This effect contributes to the lower toughness in the "core" region of heavy wide flange shapes. Equipment is available to apply "selective cooling" during hot rolling to regions of higher thermal mass to lessen the rate of grain growth and thus preserve toughness.

2.3.4 Hot Rolling

The purpose of hot rolling is to work a semi-finished piece of steel into a desired shape, while improving the mechanical properties of the finished shape by modifying the original cast structure.

The process of hot rolling consists of passing material between a set of rolls revolving in opposite directions, and spaced such that the distance between the rolls is less than the thickness of the material entering the rolls. The rolls grip the piece, reducing its cross-sectional area, and increasing its length. The amount of reduction and shape of the piece govern the amount of lateral spreading that occurs on each pass through the rolls.

Hot rolling causes distortion to the grains and grain boundaries, and is performed at elevated temperatures (within the austenitic range for steels) to minimize the energy required for plastic deformation. Hot working causes the deformed grains to recrystallize into more numerous, finer grains. The recrystallized grain structure is essentially strain-free. This process is a form of grain refinement.

Hot rolling causes grain refinement, and elongation of those grains, deformable inclusions and inhomogeneities in the rolling direction. The preferential alignment of structure along the rolling direction results in a shape with anisotropic properties. This is particularly true for ductility and fracture toughness. Specimens of plate taken parallel to the rolling direction

(longitudinal – LT and LS specimens) exhibit higher fracture toughness than specimens taken perpendicular to the rolling direction (transverse – TL specimens). Specimens that are notched parallel to the surface (LS) exhibit higher fracture toughness than those notched at right angles to the plate surface. Figure 2-4 shows the effect of specimen and notch orientation on the Charpy V-notch energy for an as-rolled carbon steel plate (ASM, 1985).

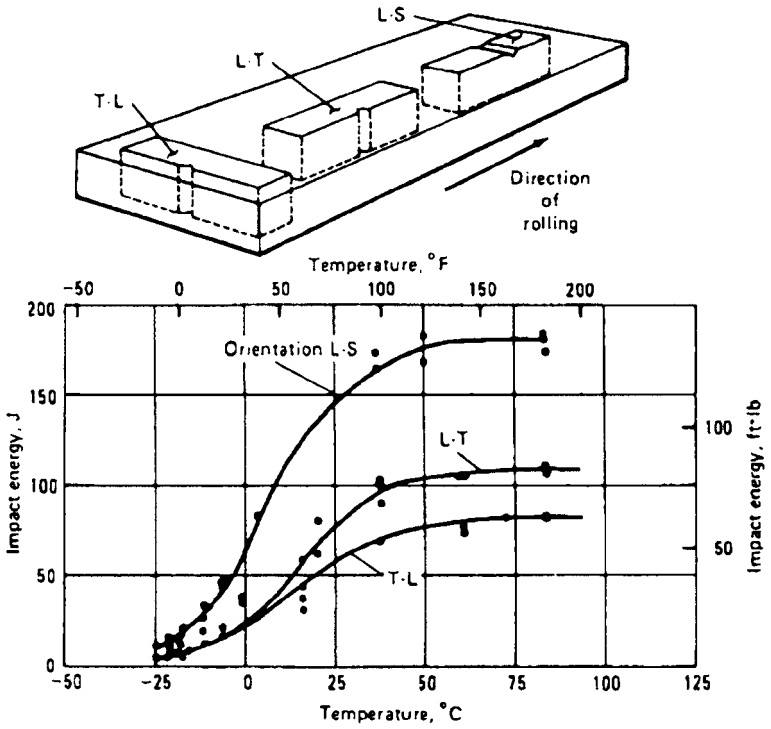

Figure 2-4 Toughness Anisotropy in As-Rolled Low-Carbon Steel Plate

Fracture paths for through–thickness specimens are parallel to the plate or structural shape surfaces and are the same planes in which elongated inhomogeneities reside. Consequently, this orientation can exhibit less fracture toughness than either the longitudinal or transverse orientations. The properties in the through-thickness direction are of little consequence in many applications, but may become important in design and fabrication when the steel is subjected to significant through-thickness stresses resulting from applied structural loads or from welding shrinkage (particularly in the case of thick members with highly restrained welded joints). In applications utilizing plate steels, plates can be specially processed to improve through-thickness properties. Some producers can manufacture shapes with improved through-thickness properties; however, this requires expensive steelmaking and rolling techniques. For structural shapes, tests on column shapes have demonstrated that the effective through-thickness strength of column flanges in constrained conditions, as typically exist in beam-to-column welded connections, exceed the maximum possible demands from the beam flanges (both grade 50 ksi and 65 ksi steels) (Dexter, 2000).

The yield and tensile strengths of steel plates and their elongation and reduction of area values are generally similar for the longitudinal and transverse directions. Plate steels that are

not specifically produced to have improved through-thickness properties tend to exhibit significantly less elongation, reduction of area, and fracture toughness, in the through-thickness direction. However, they generally have similar yield and tensile strengths in all three orientations (Barsom, 1991). Reduction of area is rarely determined for structural steels because of the predominant use of rectangular tension test specimens.

2.4 Surface and Embedded Imperfections

In general, imperfections occur to some degree on the surface of, and within the body of, all products (AISI, 1985). The mere existence of imperfections should not dictate a lack of suitability for a product for a given application. Instead, suitability for service should be based on the severity of the imperfections, measured in accordance with applicable specifications and analyses. Acceptability of structural quality plates and shapes that contain surface and edge imperfections may be conditioned in accordance with materials delivery standards.

The severity of an imperfection is governed by its size, shape, and orientation, and by the magnitude and direction of the design and fabrication stresses. In general, the severity of imperfections increases as the size increases, the shape becomes more planar, and the orientation becomes more perpendicular to the direction of the tensile stresses (Barsom, 1999). Thus, a crack-like imperfection lying in a plane parallel to the tensile stress could be innocuous. Furthermore, for a given size and shape, a surface imperfection in a plane perpendicular to the tensile stresses is more severe than a similarly oriented embedded imperfection.

Embedded imperfections can be observed by ultrasonic or by radiographic non-destructive testing procedures, or by various non-destructive methods when exposed on cut or sheared edges. Usually, the surfaces of plates and shapes in the as-rolled condition are inspected visually to ensure their freedom from injurious imperfections.

3. MECHANICAL PROPERTIES OF STEELS

The primary steel properties that affect structural performance are yield strength, tensile strength, ductility, and fracture (notch) toughness. Each of these properties depends on constraint (state of stress and strain), temperature and loading rate, as well as the chemistry and thermo-mechanical processing history of the steel. These mechanical properties of steel are discussed in this section.

3.1 Strength

Most mechanical properties important for the design and evaluation of steel structures are determined from a tension test. In this test, a machined specimen is loaded in a universal testing machine while load-elongation data are recorded. The specimen may have either a circular or a rectangular cross-section depending on the appropriate product specification. The recorded data define the tensile stress-strain behavior of the steel.

3.1.1 Stress-Strain Curves

Figure 3-1 (Barsom, 1991) is a schematic of an idealized tensile stress-strain curve for structural steels. This curve is an engineering tensile stress-strain curve, as opposed to a true tensile stress-strain curve, because the plotted stresses are calculated by dividing the instantaneous load on the specimen by its original, rather than the reduced, cross-sectional area. Also, the strains are calculated by dividing the specimen's instantaneous elongation of a gage length by its original gage length.

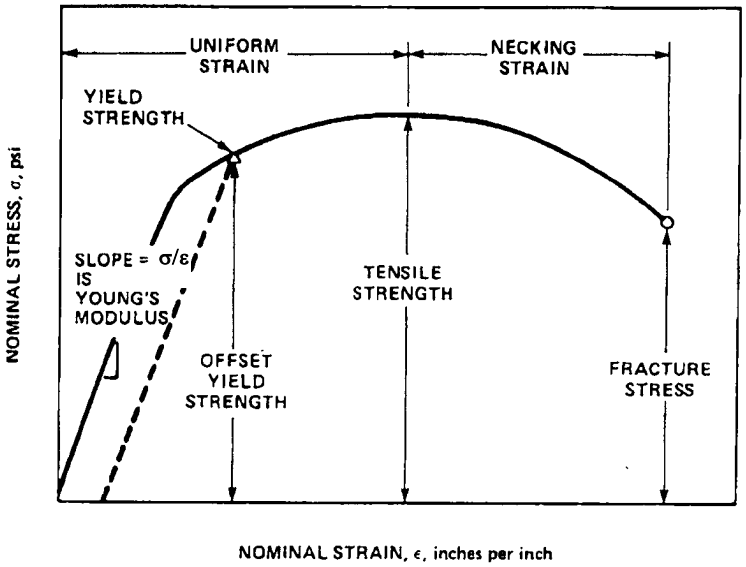

Figure 3-1 Tensile Stress-Strain Curve

The initial straight line segment of the stress-strain curve represents the specimen's elastic behavior where stress is linearly related to strain. In this region the strain is fully recoverable and the specimen returns to its original length when the load is removed. The slope of the line—the ratio of stress and strain in the elastic region—is termed the Modulus of Elasticity or Young's Modulus, and is approximately equal to 29 x 10^6 psi for structural steels at room temperature. As the load increases, stresses and strains become nonlinear, and the specimen experiences permanent plastic deformation. The stress corresponding to the initial deviation from linearity represents the yield strength of the material and the beginning of the plastic region. Usually, the stress required to produce additional plastic strain increases with increasing strain—thus, the steel strain-hardens. The rate at which stress increases with plastic strain is the strain-hardening modulus.

Figure 3-2 presents schematic representation of room-temperature tensile stress-strain curves for a few structural steels.

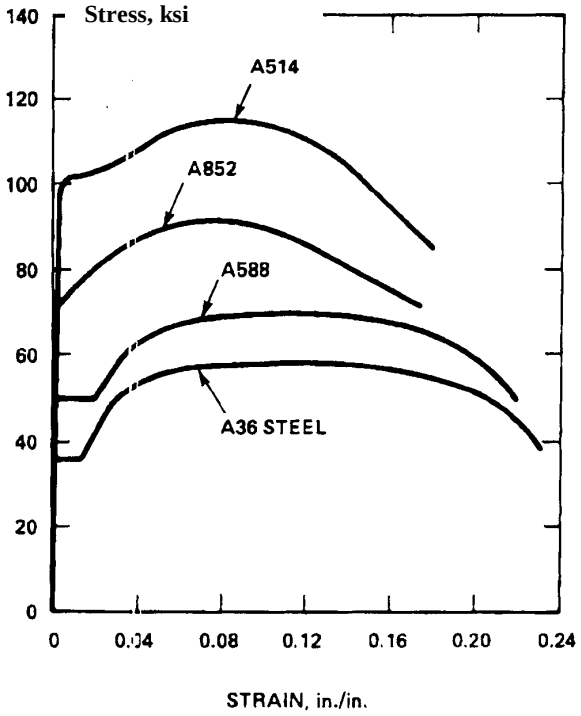

Figure 3-2 Schematic Representation of Tensile Stress-Strain Curves for Structural Steels of Various Strengths

3.1.2 Yield Strength and Tensile Strength

Tensile stress-strain curves for structural steels can be divided into two types that exhibit different behavior in the plastic region (Figure 3-3, Barsom, 1991). One such curve, Figure 3-3a, exhibits a smooth deviation from linearity with the stress continuously increasing to a maximum value, then decreasing until the specimen fractures. The second type of curve, represented by Figure 3-3b, reaches a peak immediately after the stress-strain curve deviates from linearity, dips slightly, and then remains at a constant value for a considerable amount of additional strain.

Thereafter, the steel strain hardens and the stress increases with strain to a maximum and then decreases until the specimen fractures. The stress corresponding to the peak value on this second type of curve is termed the Yield Point. Yield Strength, σ_{ys}, is the stress at which the material exhibits a specific limiting deviation from linearity of stress and strain. The deviation may be expressed as a 0.2% offset or a 0.005 inch/inch total extension under load (Figure 3-3). Maximum stress exhibited by the engineering stress-strain curve corresponds to the Tensile Strength, σ_u, of a given steel.

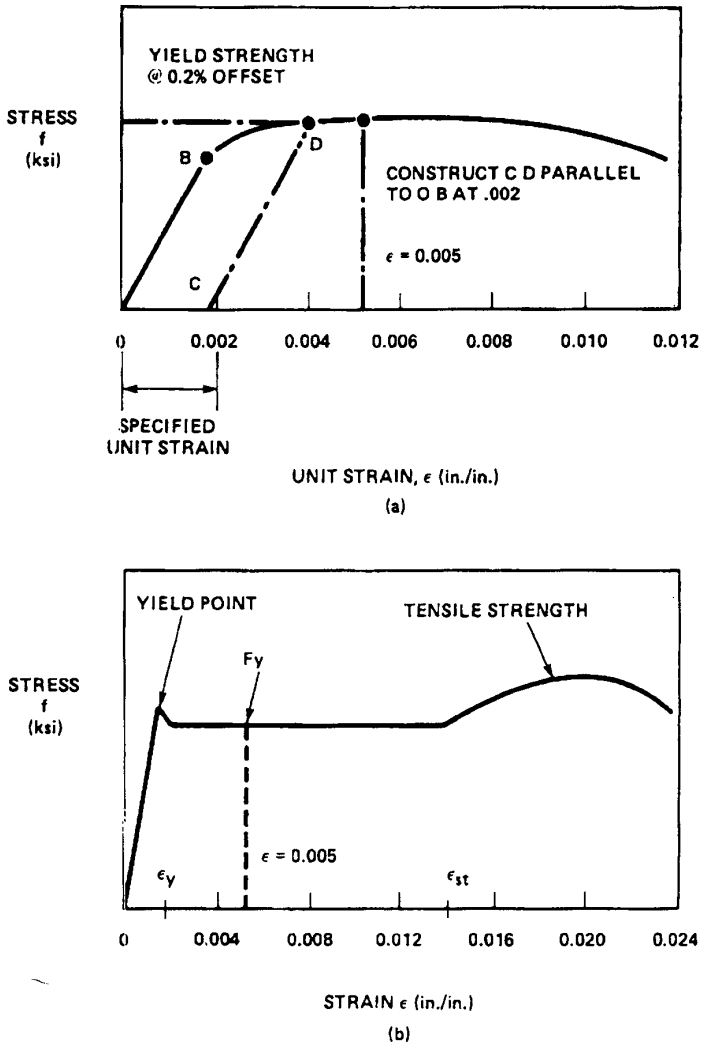

Figure 3-3 Schematic Stress-Strain Curves for Structural Steels

The room-temperature tensile stress-strain curves illustrated in Figure 3-2, represent the unimpeded plastic deformation that occurs in a uniaxially loaded coupon having a circular cross-section. Under this simple loading condition, once the stress exceeds the yield strength of the material, shear deformation occurs at many planes inclined 45 and 60 degrees to the axial stress. At large strains, this plastic deformation causes lateral contraction (i.e., localized necking) that leads to fracture of the specimen.

The inelastic properties and behavior of steels obtained from a simple uniaxial tension test are basic measures of material properties. However, like other properties, these fundamental properties differ for different states of stress and strain (i.e., constraint), temperature, and rate of loading.

3.1.3 Effects of Stress (Strain) State and Constraint on Strength

The stress field for a material element can be described by three principal stresses that are aligned normal to each other (Figure 3-4). Shear stresses acting along any plane inclined with regard to these surfaces can be calculated from the principal stress components. Assuming that σ_1 in Figure 3-4 is the largest and σ_3 is the smallest principal stress, the maximum shear stress component is given by the equation:

$$\tau_{max} = \frac{(\sigma_1 - \sigma_3)}{2} \tag{3-1}$$

For the uniaxial tension test specimen, $\sigma_1 = \sigma_{max}$ and $\sigma_2 = \sigma_3 = 0$. Therefore:

$$\tau_{max} = \frac{\sigma_1}{2} = \frac{\sigma_{max}}{2} \tag{3-2}$$

Since plastic deformation occurs when τ_{max} reaches a critical value, a change in the relationship between τ_{max} and σ_{max} represents a change in the plastic deformation behavior of the material. Note that yielding occurs when the shear stress, τ_{max}, reaches a critical value, not when σ_{max} reaches a critical value.

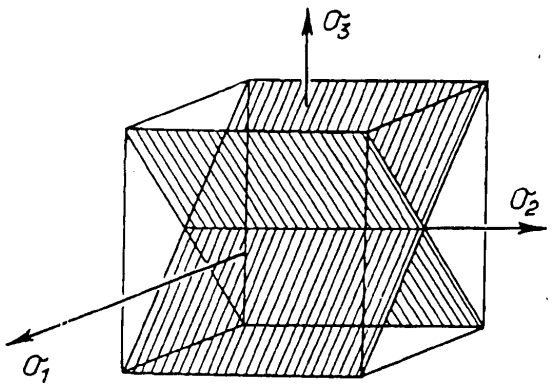

Figure 3-4 Planes of Maximum Shear Stress

The relationship between the shear stress and the normal stresses, σ_1, σ_2, and σ_3, can result in either yielding and relaxation of constraint or no yielding and increased constraint. This behavior is illustrated in Figure 3-5 using Mohr's circle of stress (Barsom, 1999). Figure 3-5a shows the principal stress directions, with the largest being σ_1. For uniaxial loading, such as the

case of a standard tension test, σ_1 = the applied stress and $\sigma_2 = \sigma_3 = 0$. At $\sigma_1 = \sigma_{max}$, $\tau_{max} = \sigma_{max}/2$, as shown in Figure 3-5b, and yielding occurs when $\tau_{max} = \sigma_{ys}/2$.

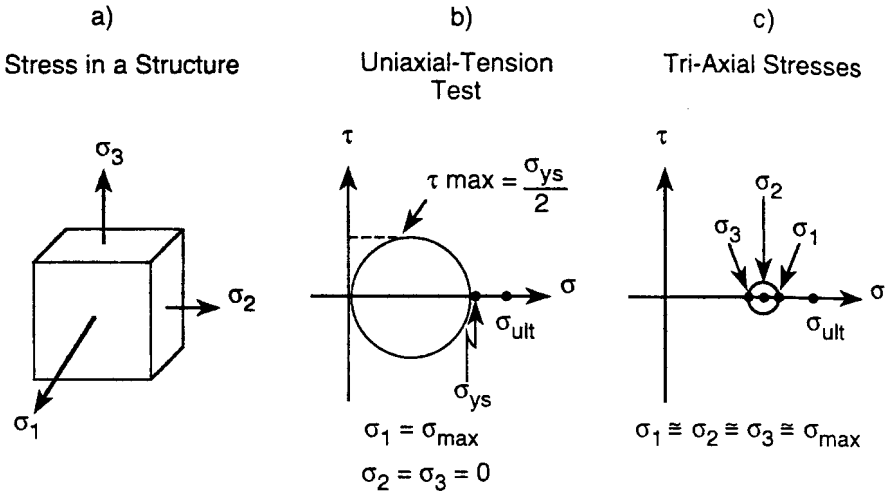

Figure 3-5 Mohr's Circle of Stress Analysis for Stresses in a Structure

In contrast to the simple tension test, Figure 3-5c represents a triaxial tensile state of stress such as would be expected in highly constrained connections such as the joint of beam flange to column flange in the beam-to-column connection of welded moment-resisting frame structures. As the magnitude of the triaxial stresses approach unity in tension, the diameter of Mohr's circle and the shear in the element approach zero. Yielding of the element is suppressed. Because of the triaxial stress loading, the stresses approach the ultimate stress and yielding may not occur.

The potential effect of structural detailing on yield strength and plastic deformation may be illustrated by considering the inelastic behavior of a material obtained from a smooth tension test and from a tension test with a circular notch (Figure 3-6 (Pellini, 1973)). The reduced section in the notched tension test bar deforms inelastically while the surrounding material is still elastic. Since the amount of elastic contraction (Poisson's ratio) is small compared with the inelastic contraction of the reduced section, a restriction to plastic flow develops. This restriction corresponds to a reaction-stress system such that the σ_2 and σ_3 stresses restrict or constrain the flow in the σ_1 (load) direction (Figure 3-6). Thus, the uniaxial stress state of the smooth bar is changed to a triaxial tensile stress system in the notched bar. Because plastic flow is restricted, the yield strength exhibited by the notched bar is higher than for the smooth bar. In other words, the notched bar behaves elastically at higher stress than the smooth bar. Thus, the strength and ductility in a smooth tension test referred to in design specifications does not characterize the behavior of highly constrained and notched details.

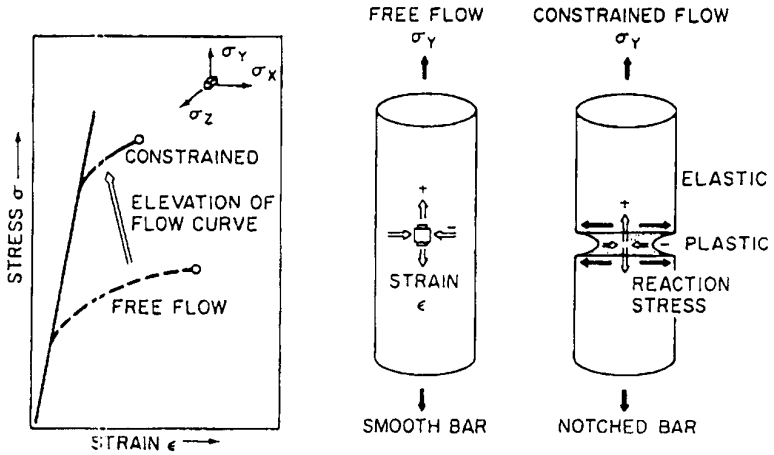

Figure 3-6 Origins of Constraint Effects

3.1.4 Effects of Temperature on Strength

In general, tensile properties of steels vary with temperature. Tensile data for various steels show that their yield strength and ultimate tensile strength increase by approximately 60 ksi when the temperature decreases from 70 to –320 ^{o}F (Figures 3-7 and 3-12 (Barsom, 1991)). Since absolute increases are about the same for all steels, the percentage increase is much larger for low-strength steels. More importantly, the data show that in the temperature range of interest for most structures (-60 ^{o}F<T<120 ^{o}F) structural steel yield strengths, and ultimate tensile strengths remain essentially constant.

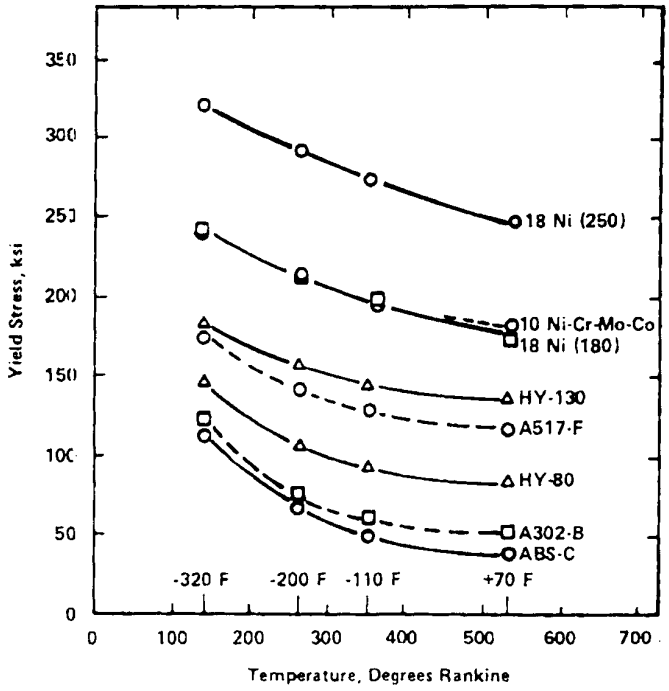

Figure 3-7 Yield Stresses of Eight Steels

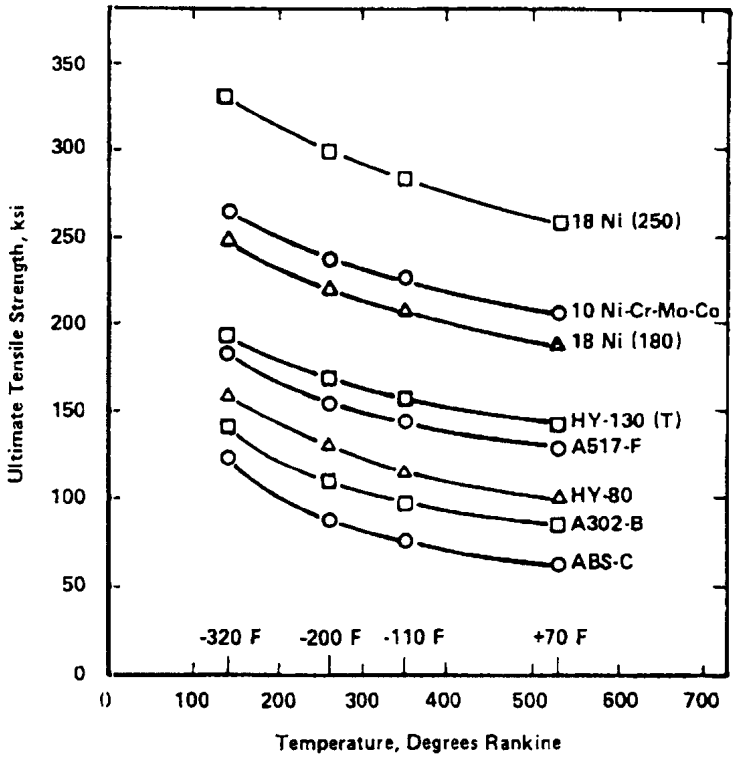

Figure 3-8 Ultimate Tensile Strengths of Eight Steels

3.1.5 Effect of Loading Rates on Strength

Tensile data for various steels subjected to monotonic dynamic loads show that the yield strength increases by about 4 to 5 ksi for each order of magnitude increase in rate of loading. The difference between "static" yield strength measured in accordance with the ASTM A370 specification and full impact loading (time to fracture $\leq$ 0.001 second) is about 25 ksi. The response time of most structures and their components is much longer than the rate of load application. Most structures respond in about 1 to 2 seconds to very rapidly applied loads such as severe wave loads on off-shore structures, highway traffic on bridges, ship slamming, and earthquake loading on bridges and buildings.

ASTM Standard A370 limits the speed for standard tension tests to a maximum 1.5 mm (1/16 inch) of crosshead motion per 25 mm (1 inch) of gage length per minute in determining the yield stress. "In any event, the minimum speed of testing shall not be less than 1/10 the specified maximum rates for determining yield point or yield strength and tensile strength." As an alternative, the speed of the machine "may be adjusted so that the rate of stressing does not exceed 100,000 psi (690 MPa)/min. However, the minimum rate of stressing shall not be less than 10,000 psi (70 MPa)/min." The minimum and maximum limits on loading rates differ by one order of magnitude. Therefore, materials tested at the maximum rate of loading may exhibit a yield strength about 4 ksi higher than when tested at the minimum rate of loading. Tests are usually conducted at an intermediate rate of loading such that fracture occurs in about one minute. Even at these low strain rates, the yield stress and tensile strength will be slightly higher than values obtained in a "static" test where the loading is stopped incrementally and the

specimen is allowed to relax. Studies have shown that the static (gravity) yield stress is typically about 28 MPa (4 ksi) less than the yield stress obtained from a standard test such as conducted by producing mills. Figures 3-9 and 3-10 (Barsom, 1996) demonstrate this behavior for two ASTM A852 steels. The data were obtained at the 10,000 psi/min. rate, the minimum rate allowed by the ASTM A370 specification. However, unlike ASTM requirements, the tests were conducted on an 8-inch flat bar with an 8-inch clip gage rather than by following "the elongation is measured in a 2-inch (50 mm) gage length that includes the fracture, and shows the greatest elongation." The static yield strength values were obtained by pausing the test for about 15 seconds. The data in Figure 3-10 show that static yield strength was about 2 ksi lower than the value obtained at the lowest rate permitted by ASTM A370. Therefore, the difference between data generated at the midrate and at the fastest rate allowed by ASTM, and the true static (gravity) yield strength should be about 4 and 6 ksi, respectively.

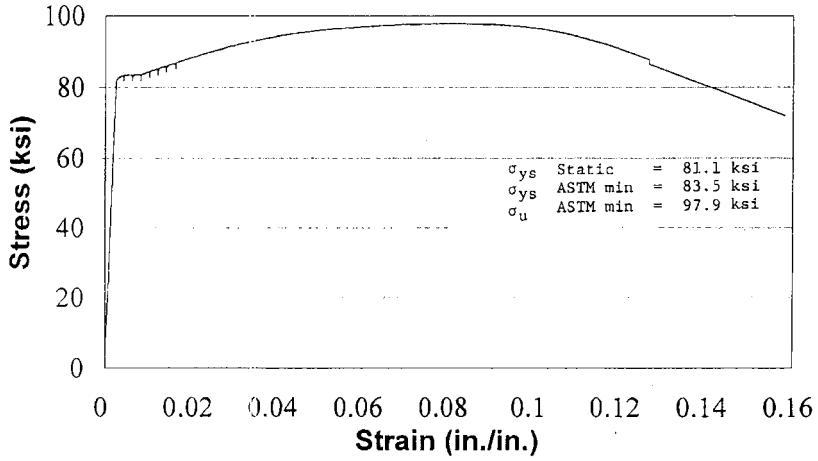

Figure 3-9 Stress-Strain Curve for ASTM A852 Steel

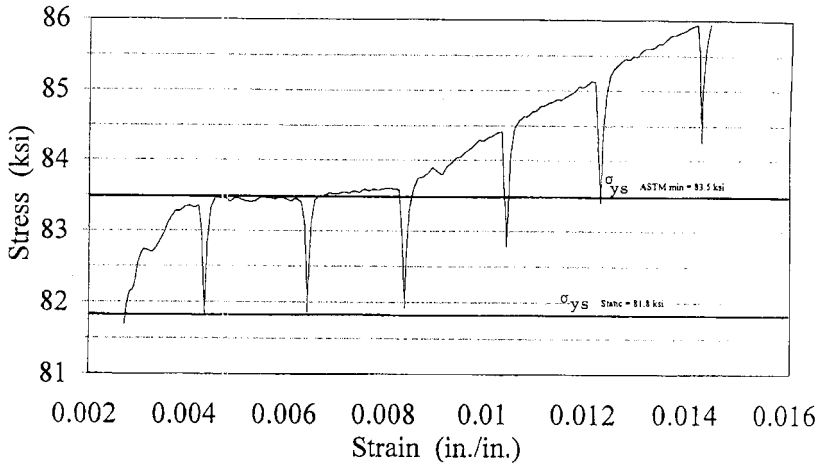

Figure 3-10 Difference Between Static Yield Strength and Yield Strength Measured at the Minimum ASTM Loading Rate

In summary, gravity-load yield strength is about 4 to 6 ksi lower than mill reported yield strength. The dynamic yield strength for loading rates of 1 to 2 seconds to maximum load, which represents fast loading on most structures, is about 4 to 6 ksi higher than mill reported data. The significance of these values and their relationship to structural performance must be established by the designer. However, test results obtained in accordance with ASTM requirements are good indicators of basic material properties.

3.2 Ductility

Ductility is an important index of the ability of a material to withstand inelastic deformation without fracture. It must be present at an adequate level to allow redistribution of local stresses, such as those associated with abrupt geometrical changes, and large inelastic deformations anticipated of structures subjected to strong ground motion.

The ductility of steels is usually expressed either as a total elongation or reduction of area obtained by testing a uniaxially loaded, smooth, cylindrical (axisymmetric) specimen. The total elongation is the difference between the initial, l_0, and the final, l_f, gage length after fracture, expressed as a percentage of the initial length. Similarly, the reduction of area is equal to the difference between the initial, A_0, and the final, A_f, cross-sectional area after fracture, expressed as a percentage of the original area. Both of these properties are strongly affected by specimen geometry. The percent elongation decreases as the gage length increases, and the reduction of area of round specimens is not directly comparable to that of rectangular specimens. ASTM specifications dictate the minimum allowable elongation for every steel and the standard procedures for measurements.

Ductility may be expressed in terms of true strain at fracture, $\varepsilon_{tr,f}$:

$$\varepsilon_{tr,f} = \ln\left(\frac{l_f}{l_0}\right) = \ln\left(\frac{A_0}{A_f}\right) \qquad (3\text{-}3)$$

where ln is the natural logarithm.

Room-temperature true fracture strain data from axisymmetric tension specimens indicate that the tensile ductility of eight structural steels ranging in yield strength from 39 to 248 ksi do not depend on yield strength (Figure 3-11 (Clausing, 1969)).

3.2.1 Effects of Stress (Strain) State and Constraint on Ductility

Specifications for structural steels require minimum elongation values for tension tests. These requirements ensure ductile fracture of the axisymmetric tension test specimens.

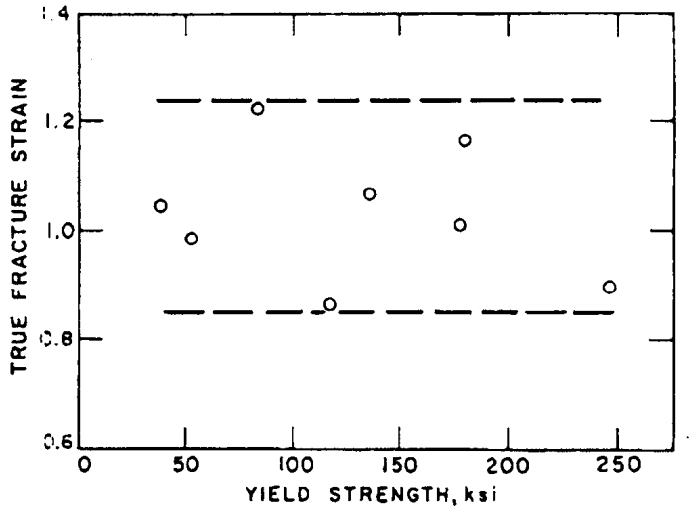

Figure 3-11 Fracture Strain in Round Tension Specimen for Eight Steels

The state of strain for most structural components containing geometric discontinuities or notches is plane strain at the zone of maximum stresses and strain. A state of plane strain is defined as having $\varepsilon_1 = -1$, $\varepsilon_2 = 0$, and $\varepsilon_3 = +1$. The plane-strain tension specimen (Figure 3-12 (Clausing, 1970; Barsom, 1971)), was developed to study the effect of state of strain on fracture ductility and to establish the plane-strain fracture behavior of steels. The specimen was proportioned so that the material on both sides of the reduced section remains elastic during loading to fracture and so that the approximate plane strain is achieved in the center region of the reduced section. Thus, contraction along the 1-inch width of the specimen is severely restricted.

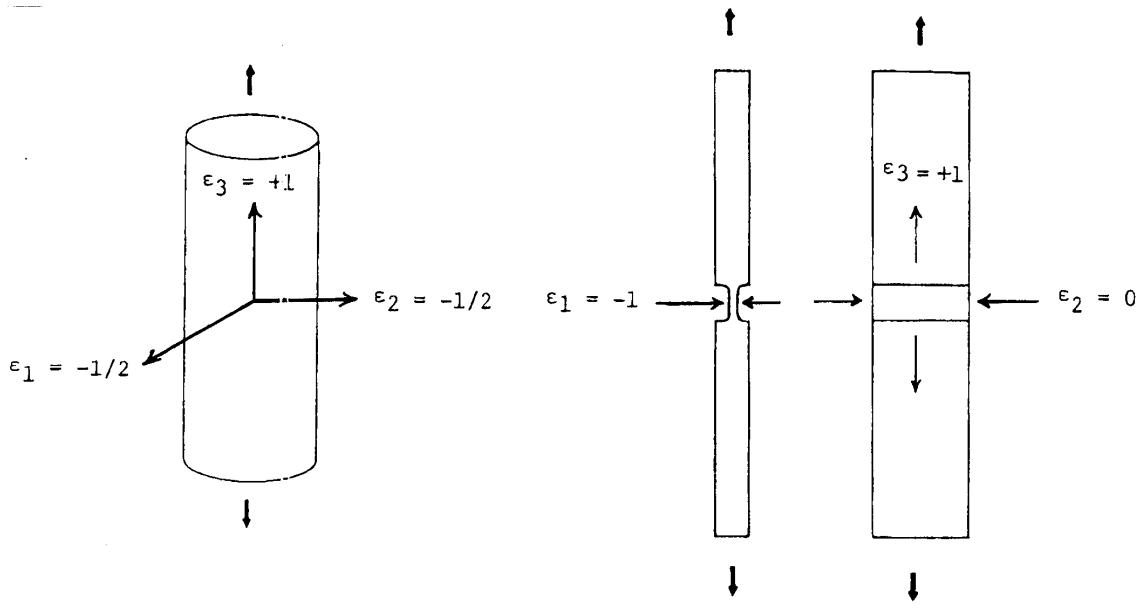

Figure 3-12 State of Strain for Axisymmetric and Plane-Strain Tension Tests

Test results on steels ranging in yield strength from 39 to 248 ksi showed that the tensile ductility of these steels was reduced substantially when the plastic-strain state was changed from axisymmetric to plane strain (Figure 3-13 (Barsom, 1971)).

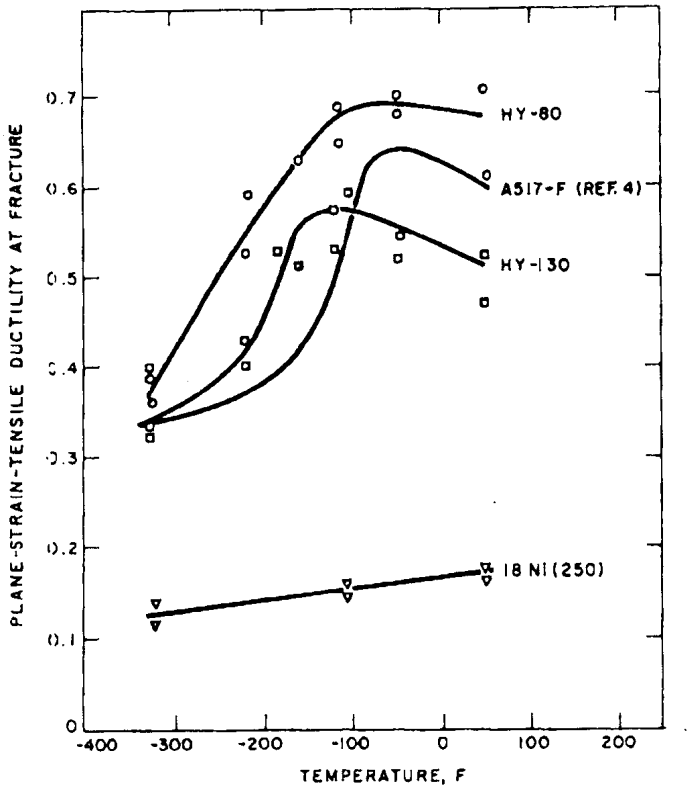

Figure 3-13 Plane-Strain Tensile Ductility at Fracture for Four Steels as a Function of Temperature

These data demonstrate the significant effect of the geometry of a structural detail on the performance of the connection. Plastic deformation decreases as the thickness of the connected members increases and as the geometry of the detail becomes more severe and more complex and as the state of stress and strain becomes more triaxial.

3.2.2 Effects of Temperature on Ductility

The axisymmetric strain ductility for steels is essentially independent of temperature in the range 70 to 200 ^{o}F (Figure 3-14 (Clausing, 1969)). Also, fracture strain has little dependence on yield strength. On the other hand, the plane-strain tensile ductility increases to a maximum value with increasing temperature (Figure 3-13 (Barsom, 1971)). Plane-strain ductility exhibits a transition behavior as a function of temperature. The transition temperature at which plane-strain ductility values increase rapidly is a unique characteristic of the tested material. At temperatures that approach room temperature, the change in plane-strain ductility for a given steel is very small.

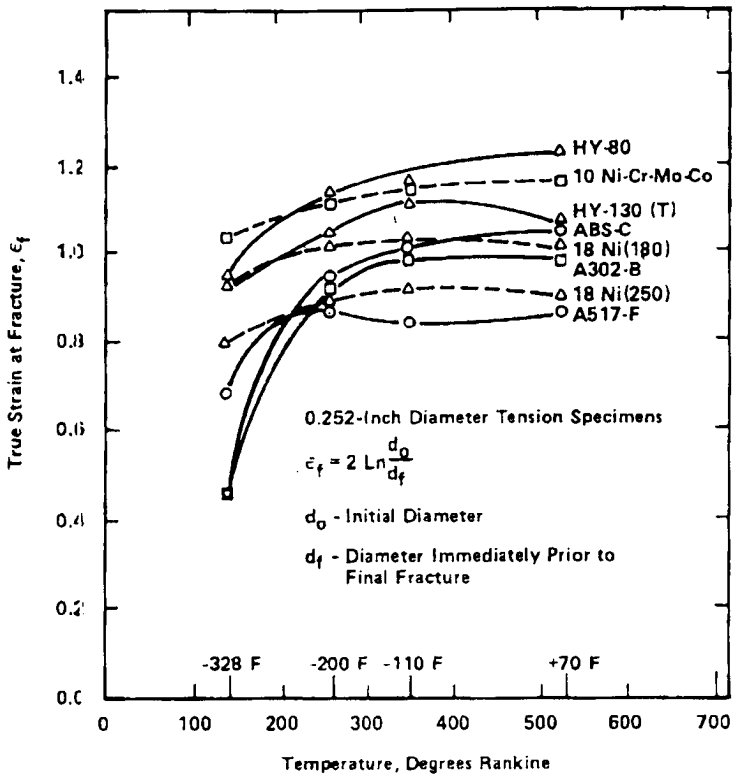

Figure 3-14 Fracture Strain of Eight Steels

3.2.3 Effects of Loading Rate on Ductility

Yield and ultimate strengths of steels under tension and compression loading are essentially identical. Because of testing difficulties, dynamic yield strength and ultimate strengths are usually obtained by testing axisymmetric specimens in compression. The ductility measures of percent elongation and reduction of area cannot be measured in these tests. Similarly, the test method for plane-strain ductility precludes the determination of dynamic plane-strain ductility. Despite the lack of data, all measures of ductility must decrease in value as the rate of loading increases. The relationship between plane-strain ductility and fracture toughness indicates that the effect of rate of loading on plane-strain fracture toughness is the same as its effect on fracture toughness. The effects of loading rate on fracture toughness are discussed in the following section.

3.3 Fracture Toughness

Most structural steels can fracture in either a ductile or a brittle manner. The fracture mode is governed by the temperature at fracture, the rate at which loads are applied and the magnitude of the constraints that prevent plastic deformation. The effects of these parameters on the mode of fracture are reflected in the fracture-toughness behavior of the material. In general, fracture toughness increases with increasing temperature, decreasing load rate, and decreasing constraint. Furthermore, there is no single unique fracture-toughness value for a given steel even at a fixed temperature and loading rate.

Traditionally, the fracture toughness for low- and intermediate-strength steels have been characterized, primarily by testing Charpy V-notch (CVN) specimens at different temperatures. However, fracture toughness for materials can be established best by using fracture-mechanics test methods. Following are a few characteristics of fracture toughness of steels by using CVN and fracture-mechanics test results.

3.3.1 Charpy V-Notch Fracture Toughness

The Charpy V-notch impact specimen has been the most widely used for characterizing fracture-toughness behavior of steels. These specimens may be tested at different temperatures, and impact fracture toughness at each test temperature may be determined from the energy absorbed during fracture, the percent shear (fibrous) fracture on the fracture surface, or the change in the width of the specimen (lateral expansion). At low temperatures, structural steels exhibit a low value of absorbed energy (about 5 ft-lb), and zero fibrous fracture and lateral expansion. The values of these fracture-toughness parameters increase as the test temperature increases until the specimens exhibit 100 percent fibrous fracture and reach a constant value of absorbed energy and of lateral expansion. This transition from brittle-to-ductile fracture behavior occurs at different temperatures for different steels and even for a given steel composition. The transition is also dependent upon the microstructure of the steel. Consequently, like other fracture-toughness tests, there is no single unique CVN value for a given steel, even at a fixed temperature and loading rate. Therefore, when fracture toughness is an important parameter, the design engineer must establish and specify the necessary level of fracture toughness for the material to be used in the particular structure or in a critical component within the structure.

3.3.2 Fracture Mechanics Concepts

Fracture mechanics concepts relate the applied nominal stresses and the tolerable crack size and shape to the fracture toughness of the material. Thus, by knowing the fracture toughness for a given material of a particular thickness and at a specific temperature and loading rate, the designer can determine the crack sizes that can be tolerated in structural members for a given design stress, without initiation of brittle fracture. Conversely, for a given design stress and a crack size in a structural component, the designer can specify a fracture-toughness value for the material that provides adequate structural safety and reliability.

This general relationship among material toughness, K_c, nominal stress, σ, and crack size, a, is shown schematically in Figure 3-15. Fracture occurs when the combination of stress and crack size reaches the K_c level. Thus, there are many combinations of stress and flaw size (e.g., σ_f and a_f) that may cause fracture in a structure fabricated from a steel with a particular value of K_c at a particular service temperature, loading rate, and plate thickness. Conversely, many combinations of stress and flaw size (e.g., σ_0 and a_0) will not cause failure of a particular structural material. Thus, material is only one of several parameters contributing to the safety and reliability of structures.

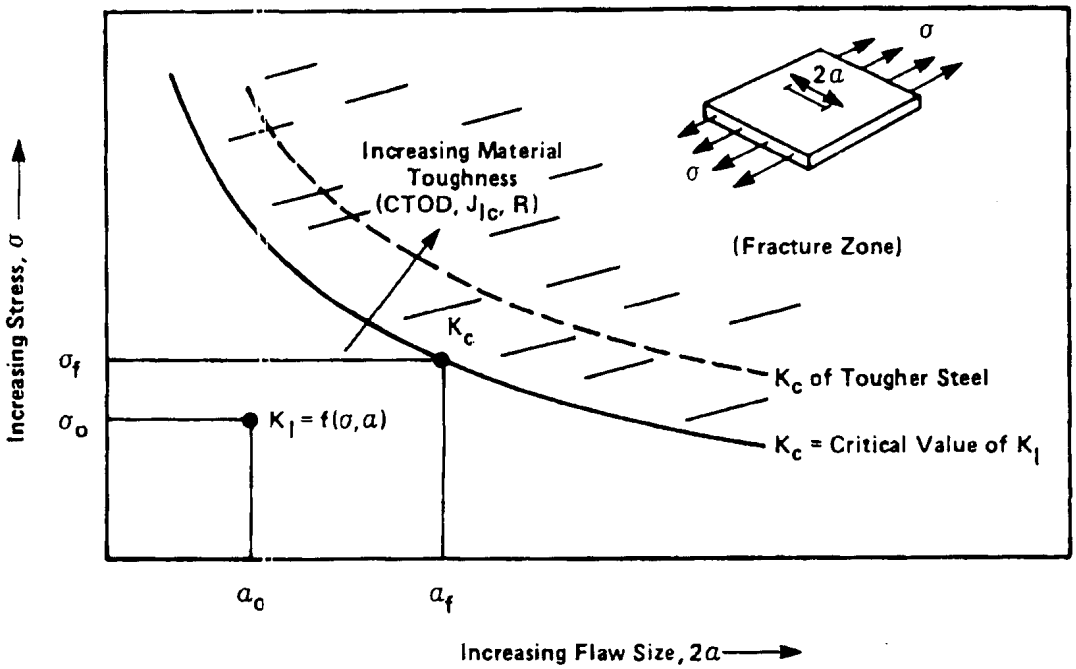

Figure 3-15 Schematic Illustration of Relationship Among Stress, Flaw Size and Material Toughness

The following is a brief discussion of some basic linear-elastic fracture mechanics concepts. Many structural details require elastic-plastic or plastic fracture mechanics analysis. Complete information on application of fracture mechanics is available in Barsom (1999).

3.3.2.1 Effect of Stress (Strain) State and Constraint on Fracture Toughness

Ahead of a sharp crack, the lateral constraint along the crack front is such that through-thickness stresses are present. Because these through-thickness stresses must be zero at each surface of a plate, they are less for thin plates compared with thick plates. For very thick plates, the through-thickness stresses are large, and a triaxial tensile state of stress occurs ahead of the crack. This triaxial state of stress restricts plastic deformation and reduces the apparent ductility and fracture toughness of the steel. This decrease in fracture toughness is controlled by the thickness of the plate, even though the inherent metallurgical properties of the material are unchanged. Thus, the fracture toughness decreases for thick plates, which represent a state of triaxial stress and linear-elastic plane-strain fracture behavior, compared with thin plates, which represent a state of plane stress and elastic-plastic or plastic fracture behavior of the same material. This behavior is shown schematically in Figure 3-16, which indicates that the minimum fracture toughness of a particular material, K_{Ic}, is reached when the thickness of the specimen is large enough so that the state of stress is plane strain. The minimum fracture toughness obtained from thick specimens is an inherent material property.

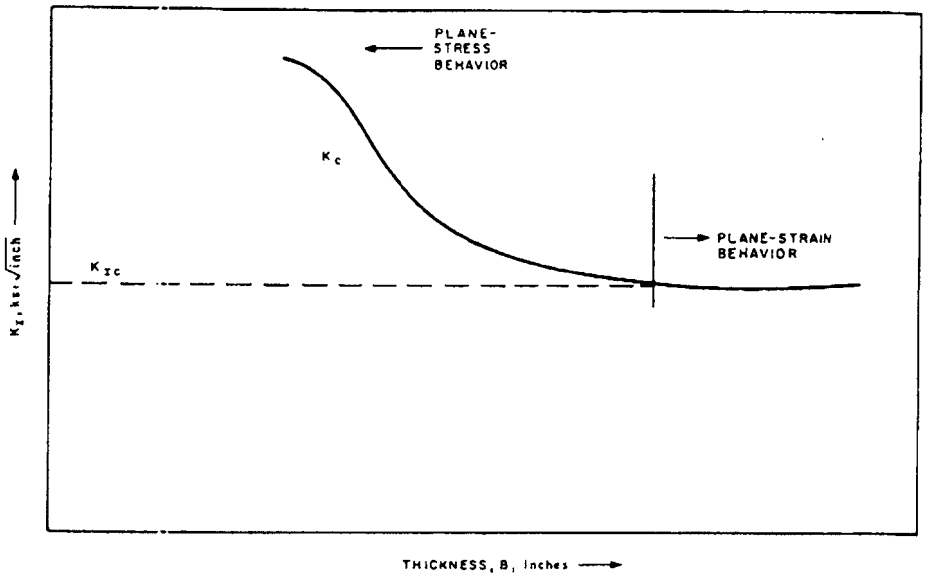

Figure 3-16 Effects of Thickness on K_c

3.3.2.2 Effect of Temperature on Linear-Elastic Fracture Toughness

Linear elastic fracture toughness, K_{Ic}, of structural steels under a constant rate of loading increases with increasing temperature. The rate of increase of K_{Ic} with temperature does not remain constant, but increases markedly above a given test temperature. An example of this behavior is shown in Figure 3-17 (Barsom, 1999) for an A517 steel plate tested at a slow loading rate. This transition in plane-strain fracture toughness is related to a change in the microscopic mode of crack initiation at the crack tip from cleavage to increasing amounts of ductile tearing.

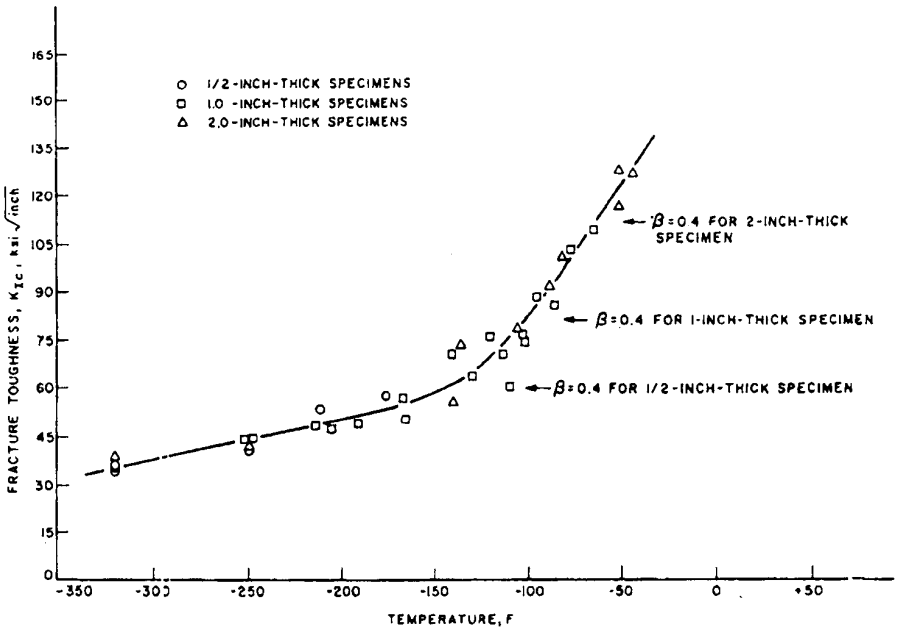

Figure 3-17 Plane-Strain Fracture-Toughness Transition Behavior as a Function of Temperature

3.3.2.3 Effect of Loading Rate on Linear-Elastic Fracture Toughness

An analysis of plane-strain fracture toughness data obtained for structural steels—valid according to ASTM E399 standard test procedures—shows that the fracture toughness transition curve is translated (shifted) to higher temperature values as the loading rate increases. Figure 3-18 (Barsom, 1999) demonstrates this behavior for an A36 steel plate. Thus, at a given temperature, fracture toughness values measured at high loading rates are lower than those measured at slower loading rates. Also, the fracture-toughness values for structural steels decrease with decreasing test temperature to a minimum K_{Ic} value equal to about 25 ksi $\sqrt{in}$. This minimum fracture-toughness value is independent of the loading rate used to obtain the fracture-toughness transition curve.

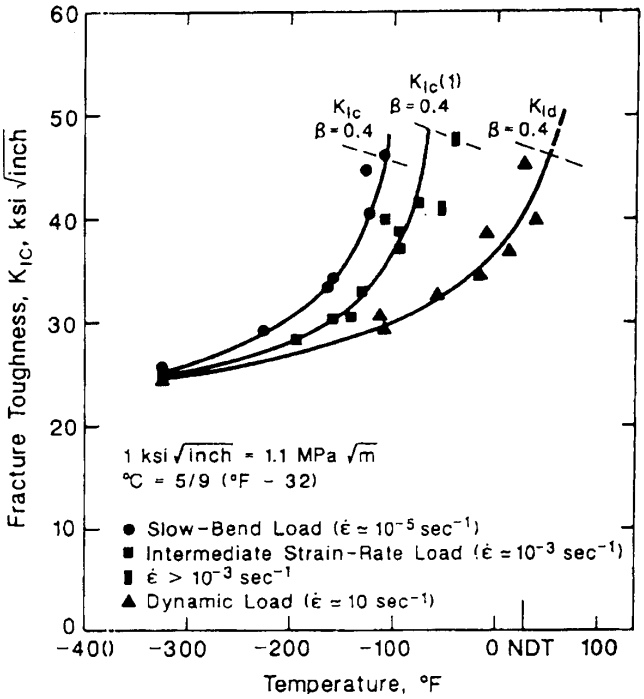

Figure 3-18 Effect of Temperature and Strain Rate on Plane-Strain Fracture-Toughness Behavior of ASTM A36 Type Steel

Data for steels having yield strengths between 36 and 250 ksi, (Figure 3-19 (Barsom, 1999)), show the shift between static and impact plane-strain fracture-toughness curves is given by the relationship

$$T_{shift} = 215 - 1.5\sigma_{ys} \text{ for } 28 \text{ ksi} < \sigma_{ys} \leq 130 \text{ ksi} \quad (3\text{-}4a)$$

and

$$T_{shift} = 0 \text{ for } \sigma_{ys} > 130 \text{ ksi} \quad (3\text{-}4b)$$

where T is temperature in degrees Fahrenheit, and σ_{ys} is room-temperature yield strength. The data indicate that the temperature shift is a direct consequence of the relative increase in yield strength with increasing load rate.

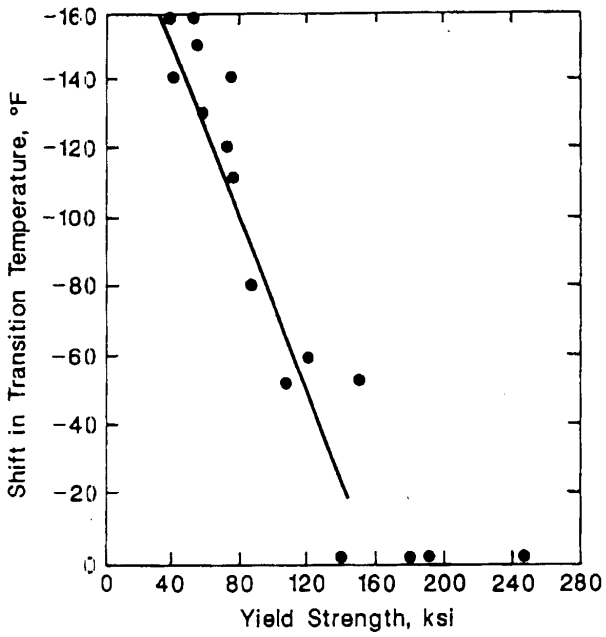

Figure 3-19 Effect of Yield Strength on Shift in Transition Temperature Between Impact and Static Plane-Strain Fracture-Toughness Curve

As stated earlier, the response time of most structures subjected to very rapid (impact) loads is about 1 to 2 seconds to maximum load. Thus, the characteristic fracture toughness curve for these structures is closer to the static curve than to the impact curve. The shift between the static fracture toughness curve and the dynamic fracture toughness curve corresponding to one-second loading to fracture is about 25% the temperature shift value calculated from Equation 3-4a (Barsom, 1999).

Proper use of fracture mechanics methodology for fracture control of structures necessitates determination of fracture toughness for the material at the temperature and loading rate representative of the intended application.

3.4 Effects of Plastic Deformation on Steel Properties

During production, fabrication, and erection, steel components may be flattened, straightened, bent, and cyclically loaded. These operations induce plastic deformations that may change the properties of the plastically deformed volume. Examples of such regions include the k-area of roller straightened structural shapes and the beam-to-column weldment in welded moment resisting frames. The effects of plastic deformations on the strength and ductility of steels may be illustrated by a simplified behavior of plastically deformed tensile specimens (Barsom, 1991).

Figure 3-20 shows loading and unloading behavior of a carbon steel tensile specimen. Loading path ABCDE is a schematic illustration of the stress-strain behavior for a specimen loaded monotonically to failure. Loading and unloading a specimen in the elastic region (line AB, Figure 3-20) is not accompanied by plastic deformation, and the specimen does not experience any change in geometry or properties.

The unloading path for specimens subjected to plastic deformation is parallel to the original elastic loading line. Consequently, a specimen loaded into the inelastic region along ABC path, unloads along the path CC′ and, when unloaded, will be longer and smaller in diameter. The magnitude of the change in the geometry of the unloaded specimen is governed by the magnitude of the residual strain, AC′. Upon reloading to failure, the specimen will exhibit the same yield and tensile strengths as the original material, except that the ductility at fracture will be decreased by an amount dictated by the magnitude of the residual strain. Similar conclusions may be made for specimens loaded into the strain hardening region, except that if the specimen is reloaded along path C′CD soon after unloading, the yield strength exhibited by the reloaded specimen will be higher than for the original loading. This increase is caused by the strain hardening characteristics of steels.

A specimen strained into the strain hardening region, which is then unloaded and allowed to age in the unloaded condition for several days at room temperature, or for shorter times at moderately higher temperatures, may follow the reloading curve shown in Figure 3-21. This phenomenon, known as strain aging, has the effect of increasing the yield strength, increasing the tensile strength, and decreasing the ductility at fracture.

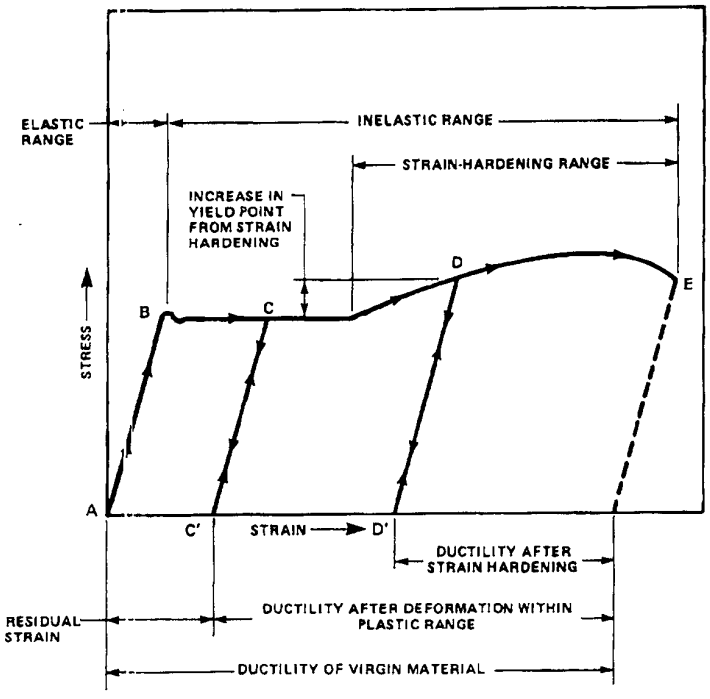

Figure 3-20 Effects of Strain Hardening

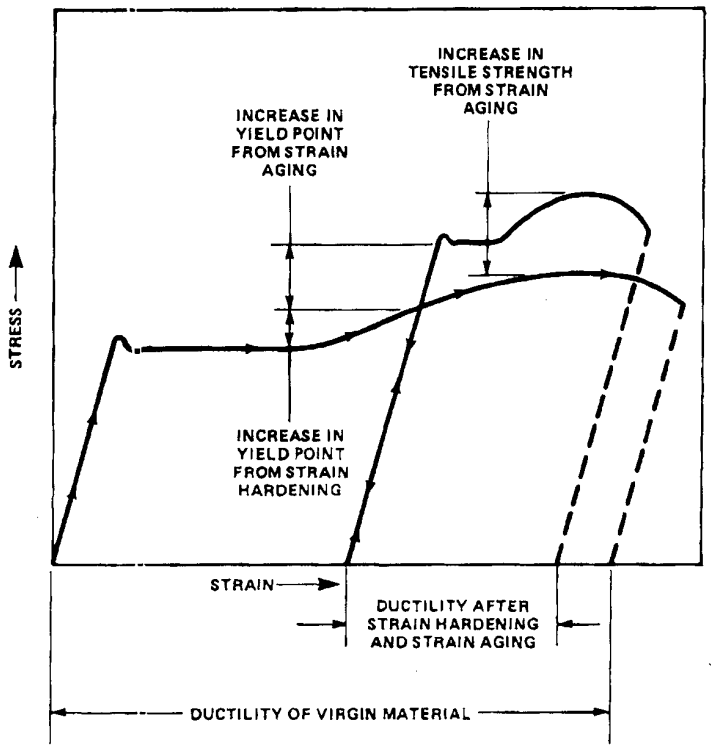

Figure 3-21 Effects of Strain Aging

Tensile and compressive strengths of steels are approximately identical. However, when a steel is deformed in tension, and subsequently deformed in compression, the compressive yield strength exhibited by the steel may be lower than would be expected had the virgin steel been initially loaded in compression. Similarly, the tensile yield strength of a steel first loaded in compression, then in tension, may be lower than the tensile yield strength of the virgin steel. This lowering of yield strength exhibited when deformation in one direction is followed by deformation in the opposite direction is known as the Bauschinger effect.

The Bauschinger effect may also occur in specimens deformed in one direction, then subsequently deformed under biaxial or triaxial strains. This effect may be of interest when large cyclic deflections or buckling are being considered.

4. TENSILE PROPERTIES OF STRUCTURAL STEELS

4.1 General

This Chapter summarizes information on the tensile properties of structural steel. It includes discussion of standard practice of the rolling mills for reporting these properties, information on the known variation of these properties for various grades of structural steel and within individual structural shapes both for contemporary steels and those produced in the past.

4.2 Mill Practice

In the United States, structural steel shape and plate is typically provided in accordance with ASTM A6 (ASTM, 1999). Under this standard general delivery specification, the strength of structural steels is determined from test coupons cut from the sections after rolling of the sections. The producer performs the tests and reports the results on the mill test report (MTR). Typically, the yield point, tensile strength, and percent elongation are reported on the MTR to provide evidence of the conformance of the steel to the applicable material specification. The test specimen may either be a machined round specimen taken from the quarter thickness location or a full thickness plate type specimen. In the U.S., coupons for mill tensile tests have traditionally been extracted from the web of the section. This location was selected since the flanges of "S" and "C" shapes are tapered, making extraction of rectangular coupons of uniform thickness difficult, without additional machining, while the web has uniform thickness. In 1996, ASTM A6 was changed, revising the location of the test specimen to the flange for wide-flange W shapes with flanges 6 in. or wider. The flange strength provides a more meaningful indication of the strength of a section since the flange comprises a larger area then the web and is the primary part of the section resisting bending moments.

Section 4.3 presents a summary of an investigation of the tensile properties of currently available rolled shapes. Investigations reported herein were performed as part of the research under the FEMA/SAC Program to Reduce Earthquake Hazards in Moment-Resisting Frames. The variation of the properties is presented, and the results are compared with the mill tests. Later sections cover earlier industry surveys of mill test reports.

4.3 Tensile Properties of Currently Produced Rolled Shapes

A sampling of current rolled shape production was undertaken to determine the tensile properties of these shapes, and to determine the variability of the properties within and among the shapes, and relationship between the results reported in typical mill reports and the laboratory tests. The properties measured during the tension test are depicted in Figure 4-1 and defined in the list below the figure.

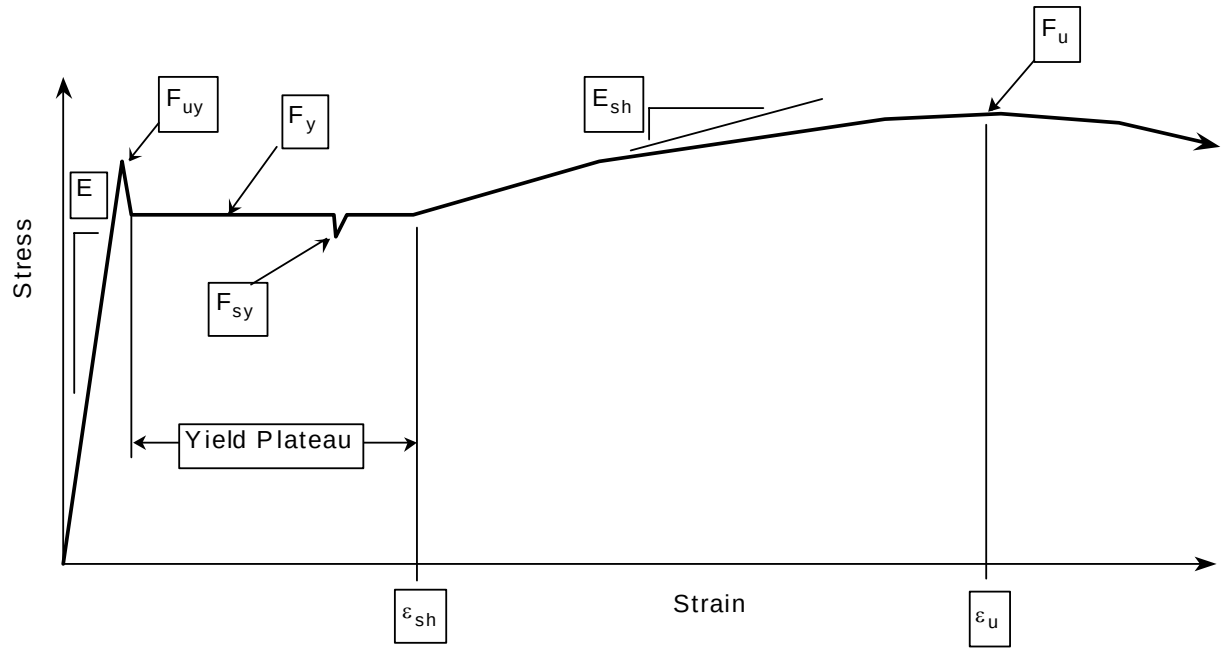

Figure 4-1 Idealized Stress-Strain Curve

The parameters indicated in the figure are:

E= elastic modulus assumed as 29,000 ksi

F_{uy} = upper yield point, ksi

F_y = dynamic yield strength, ksi

F_{sy} = static yield strength, ksi

F_u = tensile strength, ksi

ε_{sh} = strain at strain hardening

ε_u = strain at maximum stress

E_{sh} = strain hardening modulus, ksi

ASTM A370 sets the standard procedures for performing tensile and other mechanical tests of structural steel products. Under A370, mills are permitted to report either the upper yield point, F_{uy}, or the dynamic yield strength, F_y. The value of the dynamic yield strength is dependent upon the strain rate of the test. As previously described, yield strength increases with increasing strain rate. Normally the point of measurement of the dynamic yield strength is specified using an offset strain such as 0.2% or a specified extension under load. A strain rate independent value defined as the static yield strength, F_{sy}, provides a lower bound and is indicative of the steel's response to slowly applied loads, such as gravity loading in a building.

Tensile strength is taken as the maximum test load divided by the original cross sectional area of the specimen. The ratio of the yield strength to the tensile strength of the steel provides one measure of the steel's reserve strength after yielding and ability of the steel to redistribute inelastic strains. This measure is particularly important for bolted connections in that steels with high yield to tensile ratios are more likely to fail by net section fracture through bolt holes as opposed to yielding of the gross section of perforated elements.

4.3.1 Effect of Coupon Location upon Yield Strength

Tensile properties of rolled steel shapes are known to vary depending on location within the specimen. The webs of rolled shapes undergo greater working during the rolling process and also cool more quickly than the flanges, resulting in a difference in the micro-structure. Earlier sections of this report have discussed the effects of working and thermal history on tensile properties.

Several investigations into the variation of tensile properties with position in rolled shapes have been conducted in the past (AISI, 1974 and Barsom, 1988). The webs of rolled sections normally have higher yield strengths than the flanges, due to greater hot working of the thinner web material during the rolling process. Beedle and Tall (1959) reported that, in typical wide flange shapes produced at that time, the yield strength in the web is 4-7% higher than in the flange. Modern shape producers may start with a near net shape cross-section that reduces the differences in hot working between the webs and flange, relative to that which was common in the past. In order to determine the variation of tensile strength across typical cross sections under current production methods, a series of investigations was performed in which tensile specimens were taken from both the web and the flanges of a series of sections and subjected to tensile tests. A total of 18 sections produced by four different mills were tested. Most of the sections were ordered to the requirements of A572, Grade 50; however, one mill also provided specimens conforming to ASTM A913 Grade 50. Many of the sections ordered to the ASTM A572, Grade 50 specification also met the requirements of ASTM A36 and the newer ASTM A992 specifications.

Seven specimens were taken from each section, three from the web and two from each flange, as shown in Figure 4-2. The multiple sampling allowed the variation of the strength within the cross section to be determined. In the tensile tests performed on these specimens, static yield strength was measured by stopping the loading of the test specimen during the tests and measuring the load after holding the deformation constant for at least three minutes. The static yield strength is labeled F_{sy} in Figure 4-1. Dynamic yield strength was taken as the value measured on the yield plateau and is labeled as F_y in the figure. Typically, these values as well as the static yield strength was measured three times in each test.

The effect of the coupon location was studied to find overall trends, as well as trends of individual producers. In addition, comparison of measured strengths to those reported on MTRs was investigated. Table 4-1 presents the results of these tests. The table indicates means and standard deviations for the ratio of yield strength in the flange to web $F_{yflange}/F_{yweb}$, measured dynamic yield strength of the flange to that reported in the MTR, and the ratio of the dynamic yield strength of the web to that reported in the MTR.

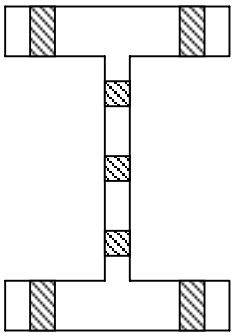

Figure 4-2 Location of Tensile Specimens

Table 4-1 Comparison of Web and Flange Tensile Properties – Contemporary Production

Mill	Number of Sections	Lab. Flange /Web	Location of Mill Test	Lab. Flange /Mill	Lab. Web /Mill
A	6	0.95, 0.05	Flange	0.94,0.03	0.98,0.06
	1		Web	0.94	0.99
B	4	0.98, 0.04	Web	0.97,0.03	0.99,0.05
C	1	0.95	Web	0.94	0.99
D	3	1.06,0.10	Flange (Full Thickness Lab. Tests)	0.97,0.03	0.92,0.10
D	3	0.97,0.02	Flange (½ in. Round at ¼ Thickness Lab. Test)	0.85,0.08	0.87, 0.10

The ratio of $F_{yflange}/F_{yweb}$ was calculated by dividing the mean value obtained from four flange specimens by the mean value obtained from the three web specimens for each section. The mean of the three dynamic yield strength measurements made for each specimen was used for this comparison.

The set of data from each producer was subdivided into two groups based upon the location of the mill test coupon. The results show for mills A and C that the relationship between the mill test results and laboratory tests did not depend upon the location of the mill test coupon. For the material from producer A, the flange yield strength was 95% of the web value, and the measured web yield strength was within 2% of the value reported on the MTR, regardless of mill test location. The sections from mill B, which had all the MTRs taken from the web, agreed well

with the laboratory results. The average web strength was within 1% of the MTR results. Mill D, which supplied ASTM A913 material, took all the coupons from the flanges, and used full thickness coupons for its mill tests. MTR values for material from Mill D correlated reasonably well with the laboratory tests from full thickness plate specimens. The correlation with the laboratory tests with the ½ in. round specimens was very poor. This would be anticipated as the quenching and tempering process used to produce ASTM A913 material results in the surface of the shape being both harder and stronger than material within the section. Coupons that are representative of the full thickness of the shape will provide similar material to that reported by the mill, while coupons that exclude the hard surface material will show lower yield strengths.

4.3.2 Effect of Strain Rate upon Yield Strength

Table 4-2 compares the average static yield strength based upon three measurements for each coupon divided by the average dynamic yield strength of the specimen. The dynamic strain was approximately 150 μin/in/sec. Statistics are separately shown for the flange, the web, and for both flange and web (all) coupons. The standard deviation of the three static readings divided by the measured dynamic yield is also shown. The statistics are remarkably similar for both the web and flange. The value of 0.95 found in previous studies of the ratio of the static to dynamic yield strength of steels used in rolled sections would still appear to be a reasonable estimate. The actual increase in yield strength under dynamic loading is dependent upon the strain rate at which the dynamic yield strength is measured. As described in an earlier chapter, a faster strain rate would tend to increase the dynamic value.

Table 4-2 Ratio of Static to Dynamic Yield Strengths

	$F_{sy\ ave}/F_y$	Std. Dev/F_y
Flange Only	0.957	0.0037
Web Only	0.953	0.0038
All Coupons	0.956	0.0038

4.3.3 Yield to Tensile Strength Ratio

The frequency distribution of the yield-to-tensile ratio (F_y/F_u) for the flange coupons is shown in Figure 4-3. Under the new ASTM A992 specification, the maximum permissible yield to tensile ratio is 0.85. All of the specimens tested met this requirement. The mean values from each mill were similar. Mill D had the highest average value, and Mill C the lowest. Mill D also had the highest individual value, 0.839, but even it was below the maximum F_y/F_u ratio of 0.85 permitted under ASTM A992. It should be noted that the ratios shown in the figure are based upon laboratory results. The yield strength reported by the mills will often be larger than the dynamic laboratory value used to calculate the ratio in the figure, while the tensile strengths are usually comparable. Consequently, the yield to tensile ratio reported on MTRs will be somewhat larger than the values calculated from the laboratory data and shown in the figure.

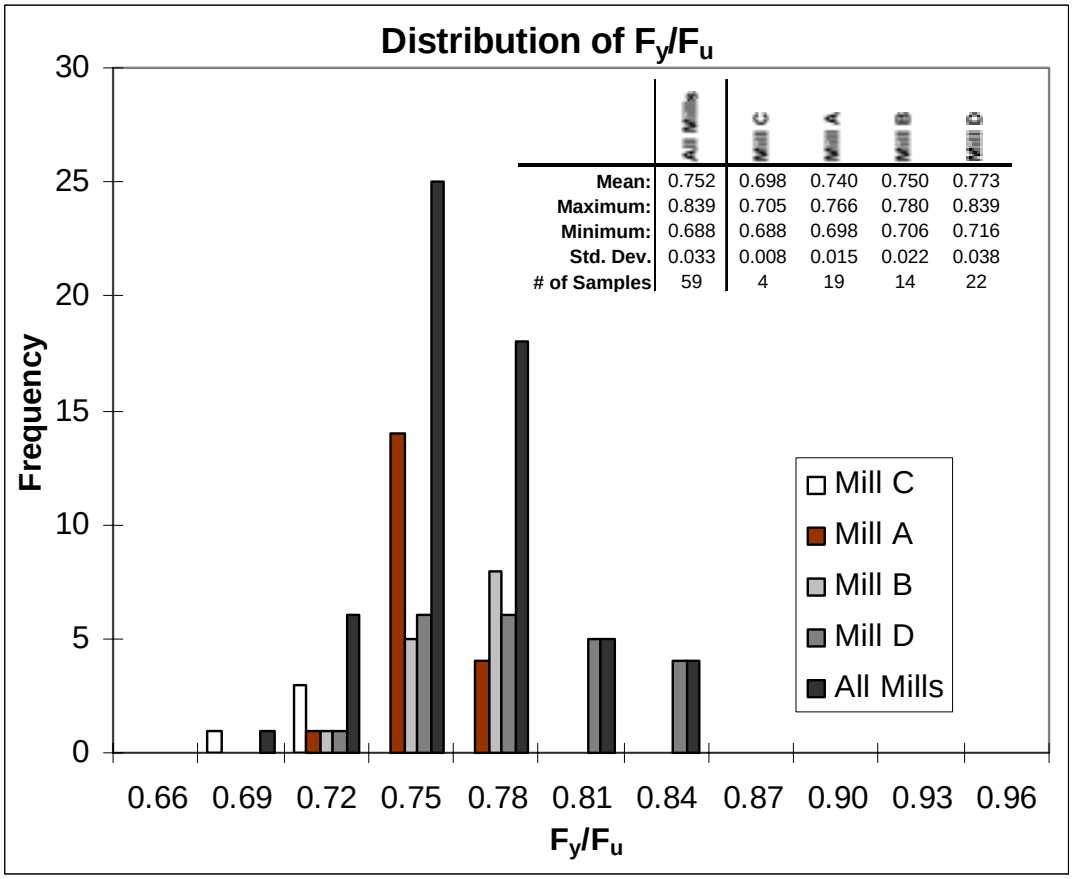

Figure 4-3 Distribution of Yield to Tensile Ratio F_y/F_u

4.3.4 Inelastic Stress-Strain Behavior of Steels

The inelastic portion of the stress strain curve for the steels tested was carefully measured during the tensile testing of the coupons removed from the rolled sections. Quantities recorded included the strain at initiation of strain hardening, the strain at the development of ultimate tensile strength, and the strain hardening modulus. In addition, the ratio of the yield to tensile strength of each specimen was calculated. This parameter provides an index of the degree of strain hardening. The purpose for these measurements was to provide a means for developing the complete stress-strain curve for these steels to be incorporated into computational studies. The data from the flange tests were analyzed to develop the average stress strain curve shown in Figure 4-4. The flange tests were used since the structural performance of a "W" section is primarily controlled by the flange behavior. The strength values shown in the curve are normalized to the nominal yield strength, $F_{yn,}$ of 50 ksi for both ASTM A572, Grade 50 and A913 steels, and the strain values by the nominal yield strain, ε_{yn}, of 50 ksi/29,000 ksi.

Table 4-3 presents the data used to generate the average flange stress-strain curve shown in Figure 4-4. The maximum and minimum values of each statistic as well as the standard deviation are indicated. The small scatter in the strain hardening modulus was surprising.

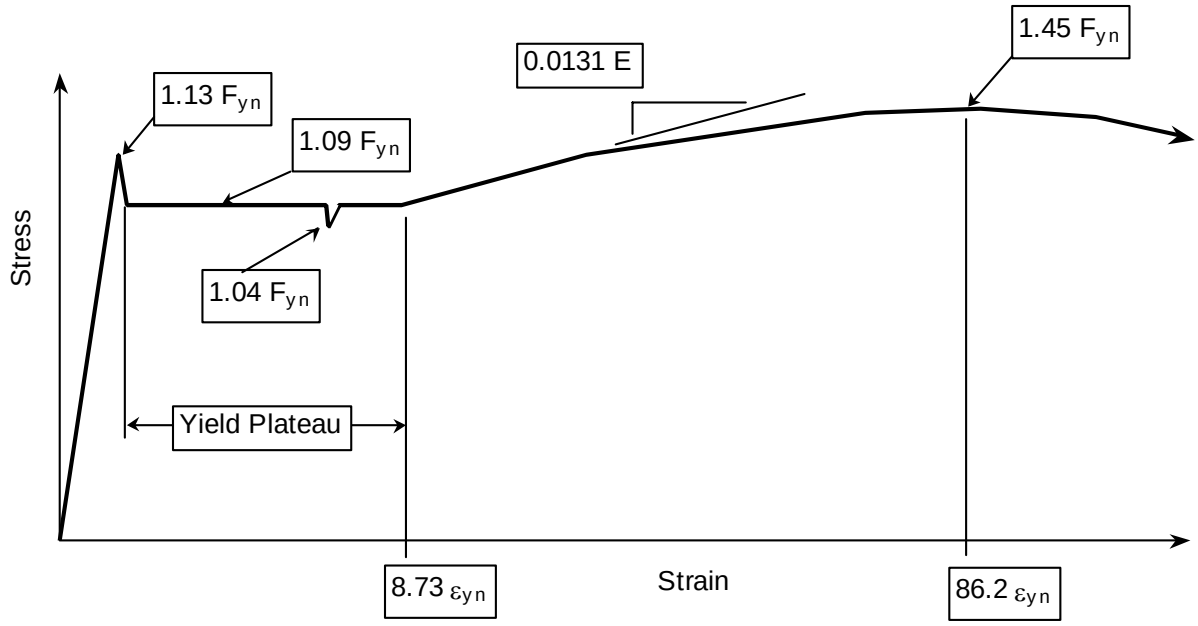

Figure 4-4 Average Flange Stress-Strain Curve

Table 4-3 Flange Test Values

	F_{uy}/F_{yn}	F_y/F_{yn}	F_{sy}/F_{yn}	$\varepsilon_{sh}/\varepsilon_{yn}$	E_{sh}/E	$\varepsilon_u/\varepsilon_{yn}$	F_u/F_{yn}
Mean:	1.13	1.09	1.04	8.73	0.0131	86.2	1.45
Maximum:	1.29	1.28	1.24	14.0	0.0165	117	1.55
Minimum:	0.96	0.96	0.91	4.29	0.0075	68.2	1.32
Std. Dev.:	0.09	0.08	0.08	2.90	0.0024	11.5	0.06
# of Specimens:	41	59	59	38	38	59	63

4.4 Strength of Historic Steels

Prior to 1960, ASTM A7 with a specified minimum yield point of 33 ksi was the only structural steel recognized in the AISC Specification for Buildings. The 1961 edition of the AISC Specification recognized the ASTM A373 specification, a weldable version of ASTM A7. In 1960, ASTM A36 replaced the A7 specification entirely, and three higher strength steels were simultaneously introduced: ASTM A242, A440, and A441. The yield point of steels conforming to A242, A440, and A441 was a function of the material thickness. Group III sections and plates thicker than 1-1/2 in. had a minimum specified yield point of 42 ksi. Group II sections and plates between ¾-1-1/2 in. had a minimum yield point of 46 ksi, while smaller sections and thinner plates had specified minimum yield point of 50 ksi. A440 was not intended for welded

construction. A242 was a weathering steel. ASTM A572 and ASTM A588, which were introduced in 1966 and 1968, replaced these higher strength steels in the 1970s.

Beedle and Tall summarize the results of early industry and laboratory tests of yield strengths for steels produced in the 1950s. The data is applicable to structural shapes produced to the ASTM A7 and A373 specifications, and is shown in Table 4-4. The statistics shown in the table are the mean strengths based on mill test data obtained for steels from different mills, the standard deviation of the reported data for each mill, the number of samples included in the population, and the ratio of the mean value to the minimum permitted by the applicable ASTM specification. The simulated mill tests are tests of coupons taken from the web of the same sections reported in the mill tests for Mill 3, and independently tested at a rapid load rate to simulate the testing performed at the mill. The simulated tests corresponded quite well with the mill tests. Beedle and Tall reported that the mill test yield point was 10-15% higher than the static yield strength of the web, and that the flange had strength approximately 4-7% less than the web. These are comparable to the differences found in the study of contemporary steels reported in the previous section.

Table 4-4 1950 Shape Test Data (A7, A373)

Data Source	Mean (ksi)	Standard Deviation (ksi)	Number of Samples	Mean/ Specified
Mill 1	39.96	3.13	3,127	1.21
Mill 2	44.1	NA	3,010	1.33
Mill 3	42.9	4.4	35	1.30
Simulated Mill 3	41.2	4.2	35	1.25

The American Iron and Steel Institute performed a survey (AISI SU/19) that covered shapes produced between August, 1967 and November, 1968. The population contained in this survey included 361 mill tests. The survey included both carbon (A36) and high strength low alloy (A440) sections. The data on high strength low alloy shapes was not reported since the number of tests was insufficient to justify data analysis. It is assumed that the data reported would reflect the results from A36 steel produced during this period. The report indicates that 364 mill reports were submitted for the study from 7 mills. Three of the results were from rimmed or capped steels and were deleted from the survey. The majority of the steels, 356 reports, were semi-killed, and the remainder were killed hot top deoxidation. Open-hearth steel making was used for 302 of the reports, and 62 were from a basic oxygen furnace produced steel. No electric furnace steels are included in the survey. A histogram of the results is shown in the Figure 4-5. The mean yield and tensile strength are 1.22 and 1.17 of the minimum yield point of 36 ksi and minimum tensile strength of 58 ksi specified in ASTM A36.

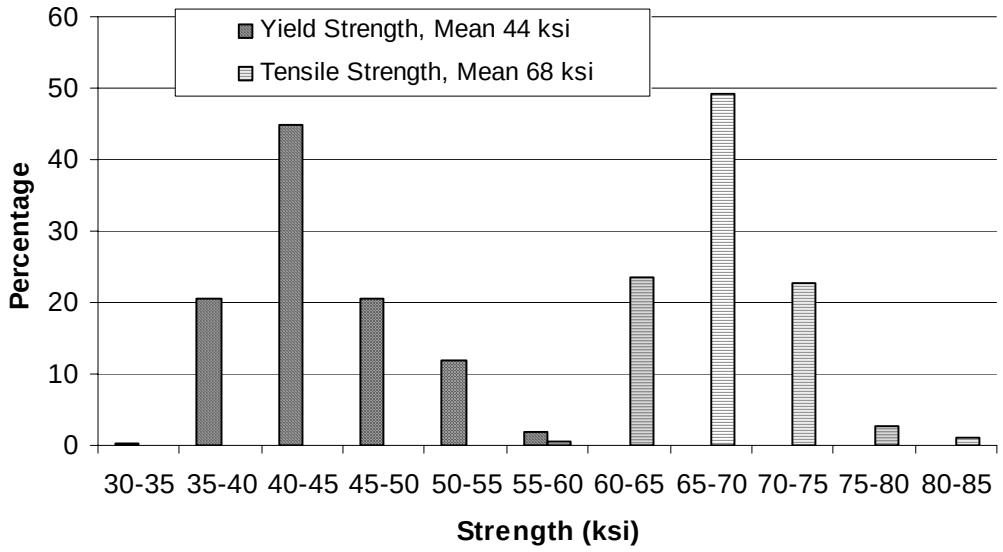

Figure 4-5 Results of AISI SU/19 Survey, A36 Steel

4.5 Influence of Dual Graded Steels upon Expected Strength

In the 1980s and 90s, the domestic steel industry underwent a major transition with many of the traditional producers leaving the structural market and several new producers entering the market. Whereas the traditional producers of structural steel generally produced steel in integrated mills from iron, as described in Chapter 2, the new producers generally used scrap based processes. Steels produced by these more modern processes tended to have residual elements from ferrous scrap, may have had microalloying elements, and therefore tended to have higher strength than the steels from earlier traditional producers. Many of these producers found that much of the structural steel they produced would meet the minimum requirements of both ASTM A36 and A572 Grade 50, and in the early 1990s, several of these mills began a process of dual-certifying steel as meeting both specifications. In essence, these mills produced only a single grade of steel but sold it either as A36 or A572 Grade 50, as the customer required. These steels are commonly referred to as dual grade.

Dual grade steel reduced inventory, which resulted in reduced costs. The warehouse or producer no longer had to maintain separate inventory for each grade. The user benefited from a reduced cost for the higher strength steel. However, the effect upon the strength distribution of rolled shapes was not as beneficial. In practice, the producers segregated the steel into lots, based upon the mill test results. Steel with yield strength less than 50 ksi was classified as A36. Steel with a yield strength greater then 50 ksi and tensile strength greater then 65 ksi but less than 80 ksi was classified as a dual grade steel since it met the physical strength requirements of both A36 and A572 Grade 50. Steel with a yield strength greater than 50 ksi but with a tensile strength greater than 80 ksi was classified as A572 Grade 50. Steels that met the dual grade requirements are also sold as either A36 or A572 Grade 50 rather than dual certified steel. The result of this sorting of steel grades is a skewed distribution of yield strength as shown in Figure 4-6.

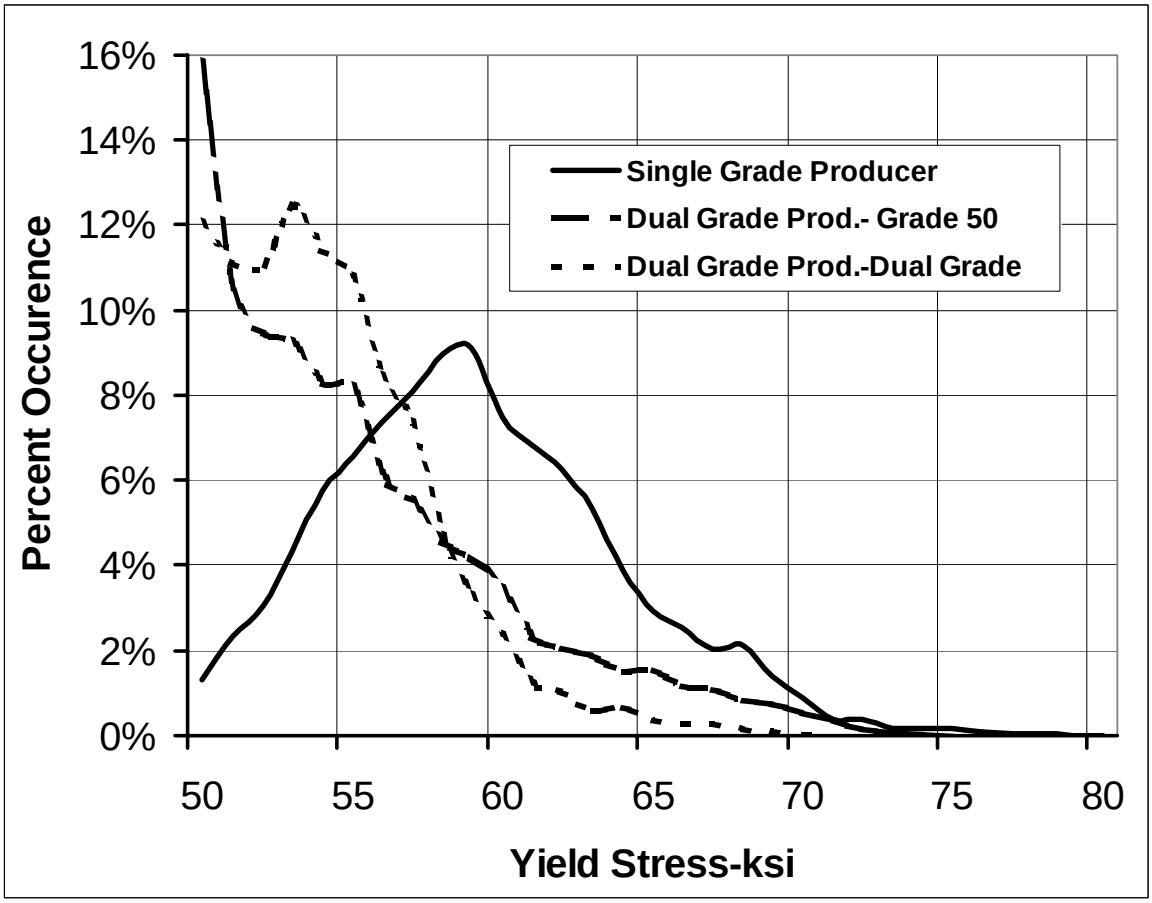

Figure 4-6 Histogram of Yield Strength for Grade 50 Material

The distribution of yield strength for dual and Grade 50 steel from mills selling dual grade steel was skewed towards the minimum specified yield strength of 50 ksi. The distribution of yield strength from the mills only producing single graded steels had a more normal distribution and a higher average. The skewed distribution of yield strength for the mills producing dual grade is illustrated in Table 4-5. The average yield stress is lower for the dual grade producers, and about ¼ of their dual and grade 50 steel has a yield stress within 2 ksi of the minimum specified. The single grade producers had only about 4% of their production within 2 ksi of the limit, with the rest being stronger. Therefore, Grade 50 steels and dual grade steels produced by dual grade producers during the period 1990-1998 should be assumed to have the distribution of the dual grade producers. Most of the production of dual grade material from these two mills for most of this time period was smaller shapes, classified in shape groups 1 and 2. The steels from the other producers will have a distribution of strengths similar to that for the single grade producers with a higher average strength.

Table 4-5 Distribution of Steel Strength, Dual and Single Grade Producers

Producer Type-Steel	Average ksi	Standard Deviation ksi	$50 \le \% \le 52$ ksi	$50 \le \% \le 55$ ksi
Single Grade-Grade 50	59.6	4.7	3.6%	16.8%
Dual Grade-Dual Grade	55.8	3.4	26.3%	53.3%
Dual Grade-Grade 50	54.8	4.9	23.2%	58.1%

The truncation of the histogram for yield strength exhibited by the dual grade producers also produced a skewed distribution of yield strengths for material sold as A36. Dual grade producers classified steel not meeting the 50 ksi minimum yield point of grade 50 steel as A36. This is the steel on the tail of the curve below 50 ksi. The result is that dual grade producers tend to produce A36 steel that has a higher strength than the single grade producers. This is shown in Figure 4-7. All of the steels included in the histogram were sold as single grade A36 steel.

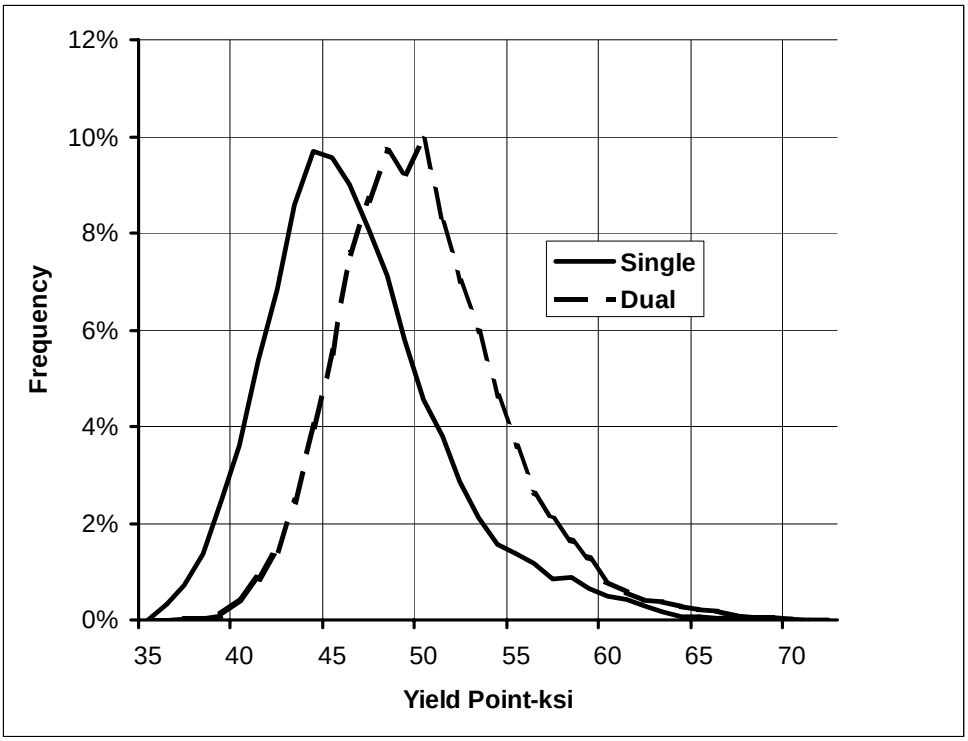

Figure 4-7 Yield Point Histogram of A36 Grade Material

The mean yield point of the dual grade producers is 50.4 ksi, with a standard deviation of 4.53. The mean yield point of the single grade producers is 46.8 ksi, with a standard deviation of 4.84 ksi. The distribution of yield points is approximately normally distributed about the mean value for both sets of producers. It must be noted that, under the condition of dual grade steel in the market place, steel specified as A36 material may have substantially higher yield strength. Therefore, A36 material should not be specified for applications in which predictability of the yield level is important.

4.5.1 Recommended Changes to ASTM Specification

The investigations indicate that the yield point reported in the mill test reports over-estimates the static (gravity) and dynamic yield strengths of the steel. The yield strength of these steels is sensitive to the strain rate of the test. The static yield strength, which is measured after the specimen has been held at fixed strain for a period of time, is independent of the test machine and test protocol. However, this test is not suitable for mill useage due to the length of time required to perform the measurement. A correlation with the more rapid mill test procedures must be used to estimate the true yield strength of the steel. Present ASTM specifications allow mills to report the upper yield point rather then the dynamic yield strength of the steel. Some mills follow this procedure while others do not. As a result, different mills would report somewhat different yield values for the same piece of material. Correlation of true yield strengths with the mill test values could be improved if the applicable ASTM specifications were changed to require reporting of specified yield strength, rather than yield point, for the structural steels. The yield strength should be determined using an offset method, which will reduce the scatter in reported yield strength/yield point and provide a statistic which has a better correlation with the actual yield strength of the steel.

4.6 Summary

Table 4-6 summarizes the results of the various surveys performed, and provides a means of estimating the strength of steel in both older and new construction. The values indicated are yield point values obtained from the webs of rolled shapes.

It appears from this data that, for earlier carbon steels, the mean yield point is approximately 1.2 the minimum specified. The value of 1.2 is also suitable for estimating the mean yield strength of grade 50 steel from single grade steel producers. Consequently, it seems reasonable to assume that until about 1993, the ratio of the mean yield point of the mill tests to the minimum specified in the specification is 1.2. This value applies to A7, A36, and A572 Grade 50. It could also be used for the other high strength steels such as A242, A440, and A441. Since 1995, the strength of the A36 and dual grade A36 is likely to be about 1.5 times the specified value of 36 ksi. The ratio for A572 would appear to be about 1.10 for shapes from producers of dual grade and 1.2 for single grade producers. The mean flange dynamic yield strength of the steels would be 90% of the mean mill test web values. The influence of the new ASTM requirements for testing tensile strength using coupons extracted from shape flanges upon these statistics should be evaluated when adequate production statistics are available.

Table 4-6 Summary of Mill Yield Point Statistics

Steel	Years	Specified Yield Point (ksi)	Mean/ Specified	Standard Deviation (ksi)
A7-Shape	1950's Prior to A36 Steel	33	1.21	3.13
A7-Shape	1950's Prior to A36 Steel	33	1.33	NA
A36	1967-68	36	1.22	NA
Single Grade Producers-Grade 50	1992	50	1.19	4.7
Dual Grade Producers - Dual Grade	1992	36 and 50	1.55 and 1.12	3.4
Dual Grade Producers-Grade 50	1992	50	1.09	4.9

5. THROUGH-THICKNESS STRENGTH OF ROLLED SECTION FLANGES

5.1 Introduction

In the 1970s, lamellar tearing of thick plates and column flanges in highly restrained welded joints due to weld shrinkage stresses was identified as an issue. Fracture surfaces in material that has failed through lamellar tearing appears to have a wood-like texture and a series of stair stepped fracture surfaces aligned parallel to the plate surface and extending in the direction in which the plate (or shape) was rolled. Observation of failed column flanges in a few welded moment resisting connections damaged by the Northridge earthquake had a similar appearance. Since it is known that large through-thickness tensile stresses are imposed on column flanges at the beam flange to column flange joint in unreinforced, welded moment resisting connections, the ability of column material to resist the tensile stress through the column flange was investigated. Therefore an extensive series of investigations was performed to determine the through-thickness behavior of heavy column shapes (Dexter, 2000). These investigations were jointly funded under the FEMA/SAC Program to Reduce Earthquake Hazards in Moment Resisting Steel Frames, by TradeArbed and the American Institute of Steel Construction.

The through-thickness direction, or "Z" direction of hot rolled steel product typically has a lower ductility, fracture toughness, and tensile strength than does the same material when strained in either the longitudinal "X" or transverse "Y" directions. Figure 5-1 illustrates this nomenclature.

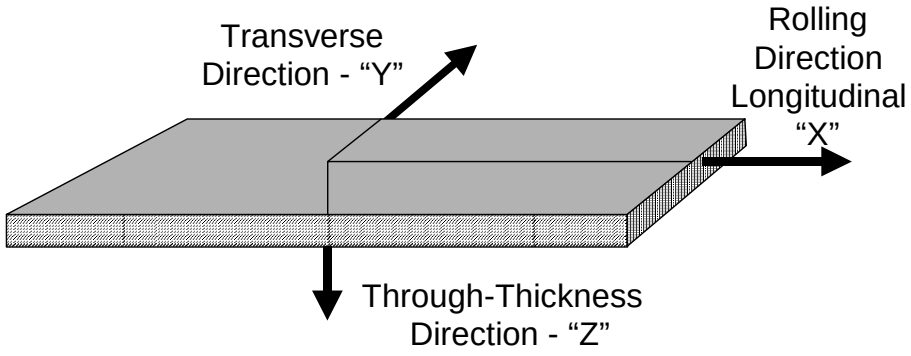

Figure 5-1 Reference Axes for Steel

5.2 Causes of Anisotropic Behavior of Steel

The reduction in through-thickness properties relative to longitudinal and transverse properties in steel occurs primarily from the heterogeneous distribution of the shape of non-metallic inclusions. The size, distribution, and shape of manganese and silicon sulfide inclusions in particular are the primary variables controlling the through-thickness behavior of steels. These inclusions start out as globular discontinuities located at the grain boundaries of the solidified steel in ingots and castings. During the rolling process, they are flattened and

elongated, forming flat planes of discontinuity aligned parallel to the X-Y plane and generally extending in the rolling direction. The degree of geometric change in these inclusions is a function of the amount of thickness reduction that occurs in the product during the hot rolling process. The degree of anisotropy is dependent upon the cross section of the flattened inclusions, the distribution of the inclusions, and the toughness of the surrounding steel matrix. Reduction in ductility and strength in the through-thickness direction occurs due to the low strength of the deformed manganese sulfide inclusions. The flattened inclusions debond and behave like very small cracks in the steel. Under some conditions of applied stress, steel toughness, and inclusion size and distribution, these small cracks may join up and form a fracture plane. The resulting fracture is termed a lamellar tear and, as noted earlier, often has a woody appearance. The fracture is similar to one in which a piece of wood is loaded perpendicular to the growth axis. The fracture between the flattened inclusions produces the characteristic fracture appearance.

The steel maker can improve the through-thickness performance of steel by reducing the number and size of the inclusions, and controlling the shape of the remaining inclusions. Lower sulfur content not only reduces the anisotropy of the steel, but also increases the fracture toughness of the steel in all directions. Steels with enhanced through-thickness properties or "Z" steels are available in plate material and are often specified for critical applications with large through-thickness stress, such as the joint cans of tubular offshore structures.

Through-thickness properties of steel plate one inch and greater in thickness are evaluated using a through-thickness tensile specimen in accordance with ASTM A770. A common requirement in the offshore industry is for the material to be capable of a minimum reduction in area under tension of 35%, although a reduction in area of 25% or less is often quoted as sufficient to provide a low risk of lamellar tearing. Often, low maximum permissible sulfur content of 0.005% is also specified. This level of sulfur is one-tenth the limit of most structural steel specifications.

An example of the influence of sulfur content upon through-thickness reduction in area is shown in Figure 5-2, which summarizes some results from Dexter's SAC sponsored tests. This figure shows the reduction of area obtained from a series of through-thickness specimens removed from column flanges of structural sections having different sulfur contents. A clear trend is observed with steels having lower sulfur content exhibiting greater reduction in area and higher through-thickness ductility than steels with higher sulfur content. In this testing program, samples were removed from the core area of wide flange specimens as well as from locations within the flange, outboard of the core area. It can also be seen that specimens taken from the core area exhibit lower through-thickness ductility than do the other specimens. This is due to the segregation effects described in Chapter 2.

5.3 Typical Through-Thickness Properties

Barsom and Korvink (1997) presented data based on extensive through-thickness testing conducted on structural plates and shapes produced in the 1970s. Data on the ratio of through-thickness tensile strength and elongation to longitudinal and transverse strengths and elongations are presented. This data indicates that the mean value of the ratio of through-thickness strength

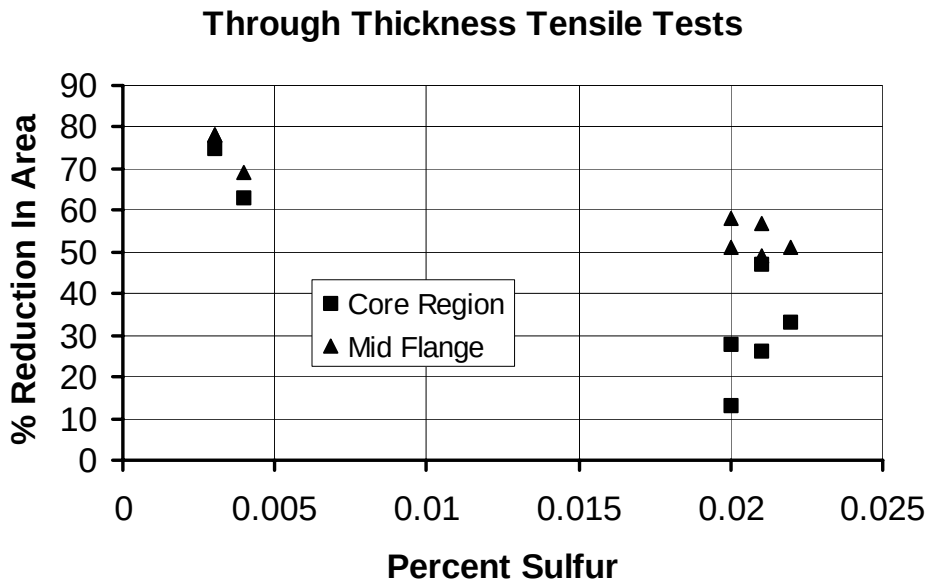

Figure 5-2 Reduction in Area as a Function of Sulfur Content

to longitudinal strength is about 1.0, meaning that the expected value of through-thickness strength is comparable to that for longitudinal strength. However, this data also showed significant variation in the through-thickness tensile strength, with a probable lower bound value for the ratio of through thickness to longitudinal strength of about 0.8. In a limited series of tests conducted on contemporary steels by Dexter and Melerdrez (1998), a similar relationship was found. Figure 5-3 presents the data from Dexter's comparisons of through thickness to longitudinal strengths. As can be seen from this data, both yield and tensile strength are approximately equal in the through thickness and longitudinal directions, and in many specimens, the through-thickness strength properties actually exceed the longitudinal properties. In one case, however, the through-thickness properties are markedly lower, at about 90% of the longitudinal values.

Older steels, particularly those with sulfur contents above 0.030%, may exhibit the reduction in strength reported by Barsom. The sulfur content of older steels was evaluated from the data in a survey (SU/17) conducted by the American Iron and Steel Institute. That survey included 592 mill tests of carbon steel plate produced from 1967 through 1969. Three hundred and thirty of the plates were made by the open-hearth method, 165 in basic oxygen furnaces, and 97 in electric furnaces. All were produced from ingots, with 252 from semi-killed steel, 64 from killed open-top, and 276 from killed hot-topped steels. The sulfur content of these steels is shown in Figure 5-4. A comparison of the sulfur content of these older steels with that from the shapes included in evaluations of contemporary steels shown in Figure 5-5 does not show a significant difference. However, other factors such as control of the inclusion shape size and distribution must also be considered. Modern practice using near net shape continuous casting processes is likely to produce steels with better through-thickness properties than the processes used at the time of Barsom's survey.

Based upon this limited comparison and considering only sulfur content, older shapes may have through-thickness strength comparable to the sections tested in Dexter's research. Lamellar tearing during welding may occur. The sulfur content as well as the other elements of the base metal should be checked prior to making repair in both old and new steels. A welding procedure that reduces strains in the through-thickness directions should be employed, and the column flange should be ultrasonically inspected after welding is completed.

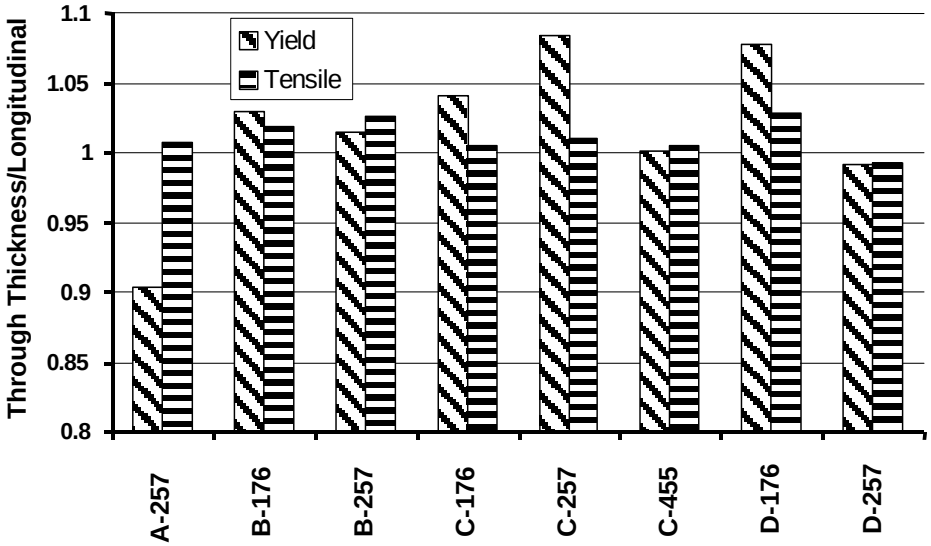

Figure 5-3 Comparison of Through-Thickness and Longitudinal Properties

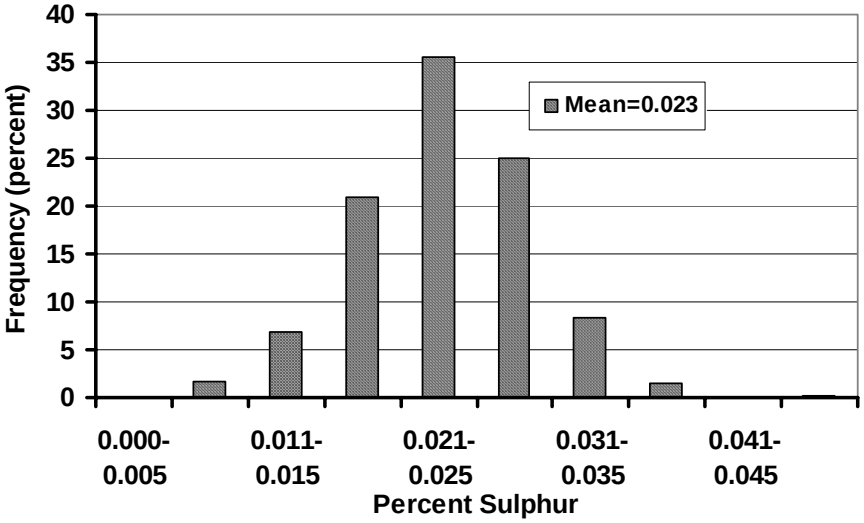

Figure 5-4 Sulfur Content From Survey SU/17

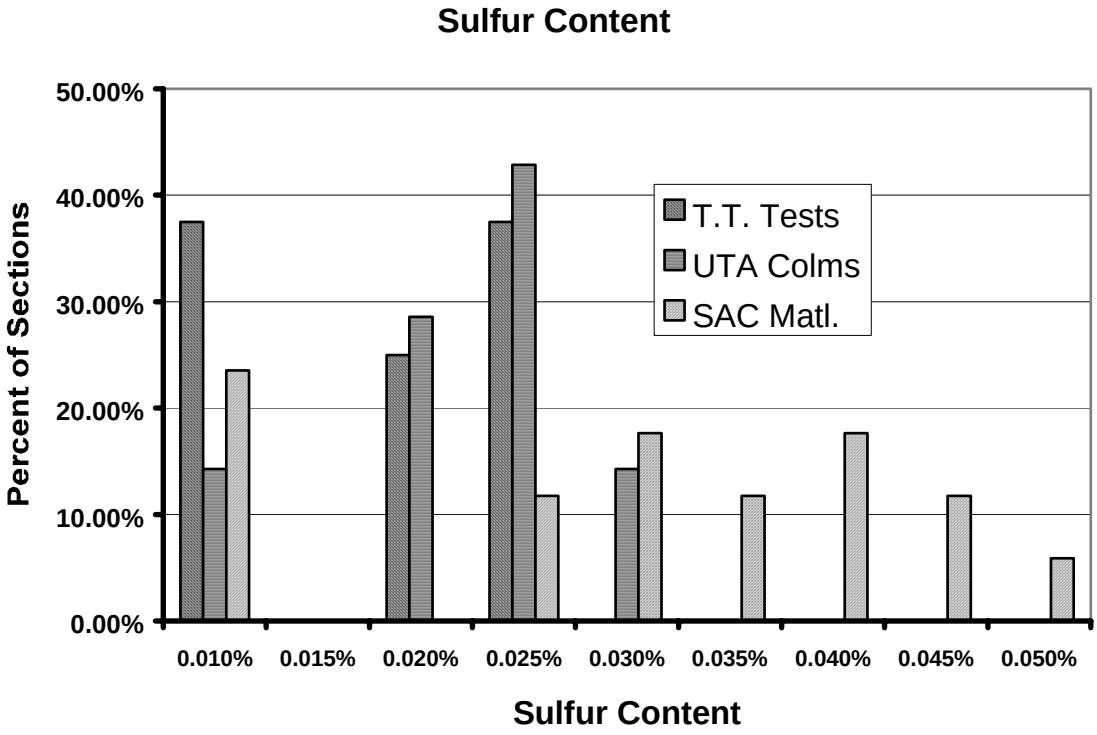

Figure 5-5 Sulfur Content of Recent Steels

5.4 Evaluation of Welded T-Joint Connections

The influence of through-thickness ductility and sulfur content upon potential performance of moment frame connections was evaluated using a series of simulated beam flange to column flange welded connections (Dexter and Melendrez, 1999). High strength, one inch thick plate with 100 ksi yield strength was welded to a series of column sections to simulate the typical welded beam flange to column flange joint in a moment-resisting connection. The high strength plate was welded with matching high strength, high notch toughness electrodes. These assemblies were then tested by applying a tensile loading onto the high strength plate simulating a beam flange. The purpose of using the higher strength flange and weld metal was to force a failure into the column flange material so that the effect of through-thickness strength properties on such connections could be evaluated. Figure 5-6 shows a typical specimen used in the testing program. Figure 5-7 shows a specimen mounted in a universal testing machine.

Two types of specimens were used. One type specimen, with a 4-inch wide simulated flange plate, was tested at both quasi-static and higher strain rates, with cross head displacements of 0.20 inch/second, to simulate earthquake loading. A second type specimen had 12-inch wide flange plates to more closely simulate the configuration of larger welded moment resisting connections. These larger specimens could only be tested at a quasi-static loading rate.

Figure 5-6 Typical Column Flange Through-Thickness Test Specimen

In addition to flange plate width and strain rate, other variables explored in the test program included material producer, material specification, column section dimensions, influence of beam flange continuity plates, welding heat input, weld filler metal toughness and joint detailing. Both ASTM A572 Grade 50 and A913, Grade 65 column sections were tested. Column section foot weights varied from 175 to 605 pounds per foot.

In initial tests, no failures occurred in the column flange. All specimens failed by necking and eventual fracture of the high strength pull plates. In later tests, weld reinforcement was removed to increase the effective through-thickness stress on the column flange. In the entire program, all specimens failed by ductile fracture of the pull plates except several specimens with welds that were intentionally made with low notch toughness weld metal, high heat input, and root defects, and without continuity plates. The specimen without the continuity plates produced a divot type fracture, in which a portion of the column flange was pulled loose from the rest of the column at a 92 ksi weld stress. This divot type fracture is shown in Figure 5-8. No evidence of lamellar tearing is observable on the fracture surface.

Figure 5-7 Typical Tee-Joint Test Setup in the 2670 kN Capacity Universal Testing Machine Showing Location of Strain Gages and LVDTs

Figure 5-8 View of Divot-Type Fracture of Column Flange in Specimen with No Continuity Plates

In addition to the tests performed on new sections, one test was performed on a W14x455 section removed from a building that suffered damage in the Northridge earthquake. The result was again a failure in the high strength pull plate.

5.5 Conclusions

The results of this experimental study indicate that welded T-joints of the type found in beam flange to column flange joints in welded moment resisting connections can resist very large tensile demands without inducing lamellar tearing type failures. Due to inherent conditions of restraint in these joints, yield and tensile strength of column flange material in these joints is significantly elevated and unlikely to initiate a failure under stresses that can be imposed by materials of similar strength. Further, failures of the type found in many moment resisting connections following the 1994 Northridge earthquake can be initiated in these weldments if low notch toughness weld filler metals and joint defects are introduced.

6. CHARPY V-NOTCH TOUGHNESS OF ROLLED SHAPES AND PLATE

6.1 Introduction

Notch toughness is a measure of a material's ability to tolerate sharp crack-like defects. The tougher the material, the larger the defect the steel can tolerate before unstable crack extension occurs as a brittle fracture.

The Charpy V-Notch (CVN) test is a simple method of estimating the dynamic fracture toughness of steels. The test measures the energy required to fracture a notched plate specimen loaded in single-point bending. The specimen size and notch dimensions are specified in ASTM 370. A pendulum applies a dynamic load to the specimen. The results of the test are the energy required to fracture the specimen. Other parameters such as the percent shear evident on the fracture surface and the lateral expansion on the compression side of the specimen are also used to characterize the behavior of the steel.

The notch toughness of a particular steel is dependent upon the temperature of the steel when it is tested. The measured notch toughness increases at higher temperatures. Typically, the notch toughness of a steel is characterized by a CVN curve that is a plot of the measured energy to produce fracture at various temperatures. Figure 6-1 presents a typical CVN curve. The results are typically divided into three regions of behavior termed lower shelf, transition, and upper shelf. The lower shelf is the region of low notch toughness at low temperature in which the specimen fractures in a cleavage mode with no significant plastic deformation occurring. The fracture surface is flat, and exhibits no shear lips on the side. The upper shelf occurs at higher temperatures. More energy is required to fracture the specimen at the upper shelf temperature. Fractures of steel in the upper shelf region usually exhibit large plastic deformation and considerable shear lip formation.

Between the two shelves on the CVN curve is a region of change in notch toughness with temperature. This region is labeled the transition zone, and is often characterized by determining the temperature at which the steel attains a certain energy level. The 15 ft.-lb. energy level is often used to fix the transition temperature of low-strength steel. Steel specimens meeting the same material specification but obtained from different heats or even different portions of a rolled shape will generally exhibit a curve with the shape shown in the figure. The transition temperature and the upper shelf energy are often used to characterize the difference in the test values from one steel or location to another.

6.2 Toughness Surveys

6.2.1 Plate

In 1979, the American Iron and Steel Institute (AISI, 1979) published the results of a survey of the Charpy V-Notch properties of various grades of steel plate. Data contained in the survey for A572 Gr. 50 plate are of interest. The data includes samples from five producers and was collected during the period 1972-1973. A total of 52 plate samples were included in the survey. Thickness ranged from ¾ inches to 1-1/2 in. All of the plate was produced to killed fine grain

practice, a method of improving notch toughness properties. Controlled rolled A572 plates as well as strand cast material were not included.

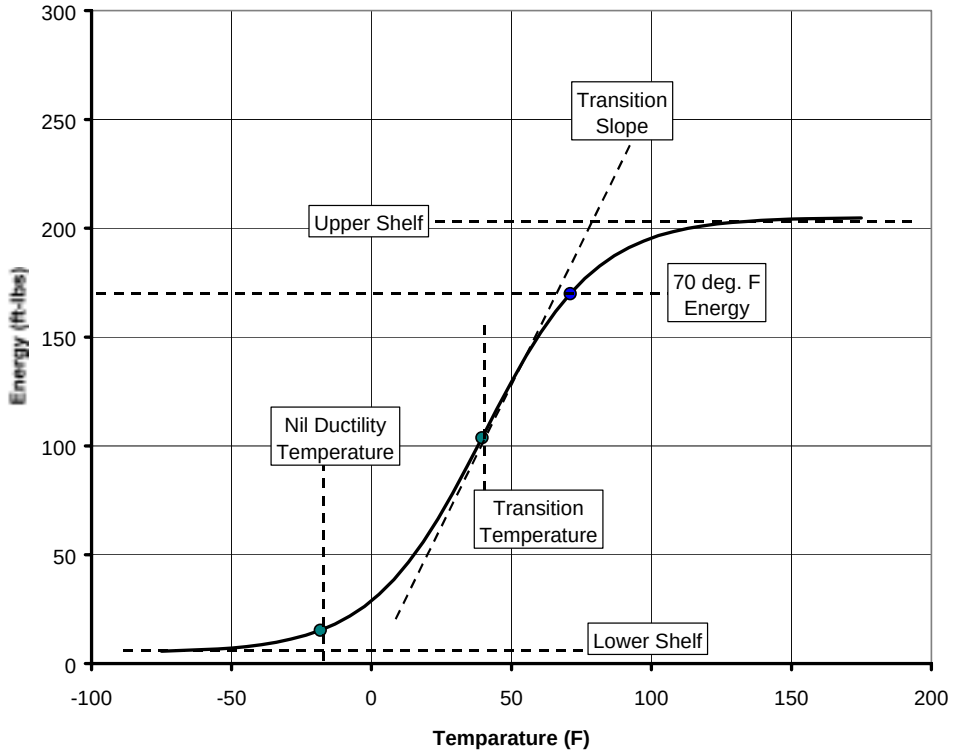

Figure 6-1 Typical CVN Curve

Samples were taken from seven locations in each plate. One location was designated as the reference location. The results of the other six locations were compared with this simulated mill test location. Three longitudinal and three transverse specimens, LT and TL orientation shown in Figure 2-4, were removed from each location and tested. The longitudinal direction specimens are the specimens normally used to measure the notch toughness of plate and rolled shapes. The long dimension of the Charpy specimen is in the direction of rolling, and the direction of fracture extension is perpendicular to the rolling direction, across the plate. Transverse specimens have their long dimension across the plate, transverse to the rolling direction, and the direction of fracture extension is parallel to the rolling direction of the plate. The reported statistics were based upon the average of the three results at each location. The frequency distribution for these average values is shown in the Figures 6-2 and 6-3. The reduction in notch toughness with decreasing temperature is evident. Comparing the two histograms, the lower toughness of the plate in the direction transverse to the rolling direction is evident. The lower toughness of the plate in the transverse direction is not unusual, and indicates the importance of the marking of pieces cut from plates to indicate the direction of rolling when notch toughness of the material is important. Stresses transverse to the rolling direction that would cause crack propagation in the direction measured by transverse Charpy tests are unusual, although they can occur in dual axis framing connections.

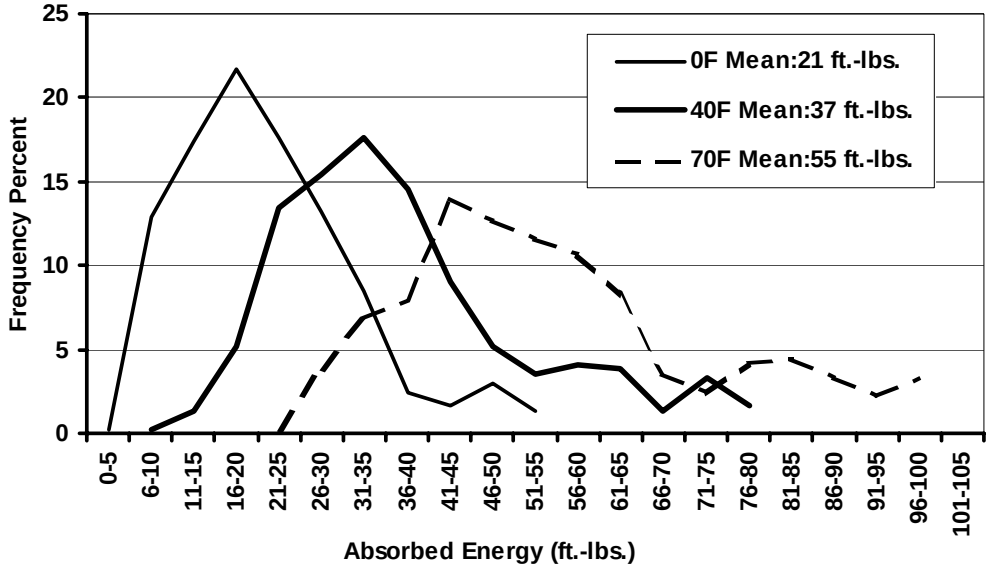

Figure 6-2 Longitudinal CVN A572 Plate 1972-73

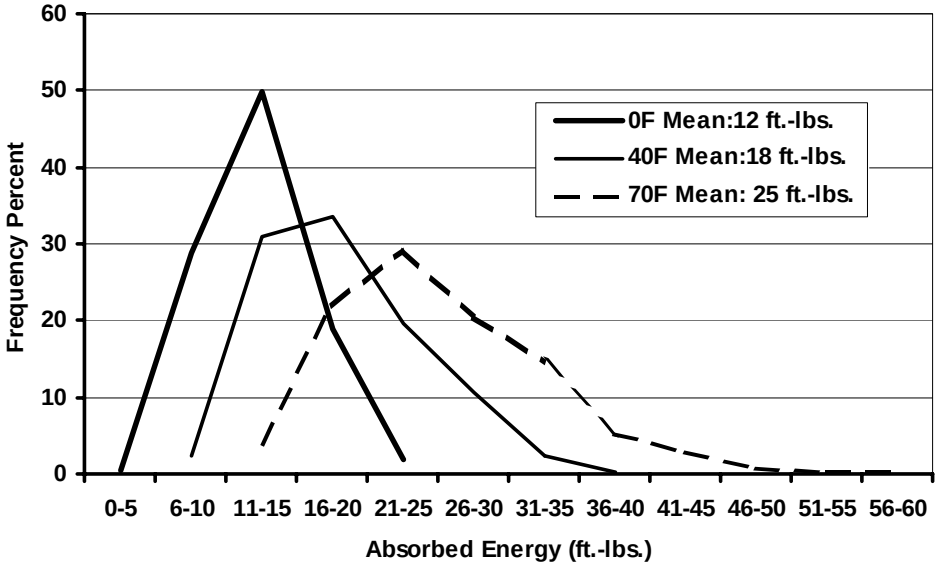

Figure 6-3 Transverse CVN A572 Plate 1972-73

6.2.2 Wide Flange Shape

Barsom and Reisdorf (1988) investigated the microstructure, mechanical properties, and CVN fracture toughness of A36, A572 Grade 50, and A588 Grade A structural shapes produced in the 1970s. These were W14 shapes weighing from 342 to 730 lb/ft. The CVN tests were conducted at the web-quarterthickness, flange quarterthickness, and flange midthickness. The CVN data show, among other things, that for the flange-quarterthickness location, the average

15 ft-lb. transition temperature (V_{15}) of the twenty-eight A36 steel samples tested was about 40° F and ranged from -30 to 105 °F. For the same test location, the average V_{15} of the twenty-seven A572 Grade 50 steel samples investigated was 50° F and ranged from 10 to 80 °F. For the eight A588 Grade A steel samples tested at the same location, the average V_{15} was 10 °F and ranged from –30 to 55 °F.

In 1995, the American Institute of Steel Construction (AISC, 1995) conducted a survey of the CVN toughness of wide flange shapes. The survey consisted of Charpy V-Notch tests from rolled wide flange shapes produced by six producers during the period 1994-1995. According to the report, "The sample consisted of an unidentified mix of heats ordered with CVN toughness requirements and heats tested for internal quality control programs." The majority of the data was for steel conforming either to ASTM A36 or A572 Grade 50. Temperatures at which the steel was tested ranged from 40 °F to 70 °F, with the majority of testing conducted at 40 °F. A total of 2,489 sets of data were presented for A36 material, and 4,471 for A572 material. Each data set consisted of the mean value of three tests taken for a specific heat. The majority of the data for shape groups 4 and 5 was obtained from the core region, while the data from the other shape groups were taken from the flange. All results were from standard longitudinal specimens.

The results of the survey are summarized in Figure 6-4 for A36 steel and Figure 6-5 for A572, Grade 50 steel. The results are somewhat surprising; the higher test temperature of 70 °F has a greater frequency of lower CVN toughness values than the 40 °F temperature. The frequency distributions of the data from some of the individual shape groups are varied. Some are bimodal, some are flat, and others have skewed distributions. Combining these differing distributions may have resulted in the unexpected higher CVN toughness shown in the histograms for the tests performed at 40 °F. The CVN toughness of the steels included in this survey is very good. At a test temperature of 70 °F, only 22% of the A36 steel and 23% of the A572 steel had a CVN toughness less than 30 ft.-lbs. The AISC study also included data on Quenched Self Tempered steels conforming to ASTM A913. These A913 steels had very high toughness at 32 °F. The A913 steels had minimum CVN toughness values over 90 ft.-lbs. The A36 and A572 steels also had high CVN toughness with a lowest CVN toughness of 33 ft.-lbs. at 70° F.

Under the FEMA/SAC program to reduce the seismic hazards in moment resisting steel frames, additional CVN toughness testing of structural wide flange shapes was conducted. The CVN toughness of the shapes was measured in the flange, the web, the core at the junction of the web and flange, and in some sections at the so called k-area, the intersection of the flange to web fillet and the web.

The core region of the rolled shapes was investigated by measuring the hardness in the region of the web-flange juncture and also by performing tensile and CVN tests in the core area. The purpose of this investigation was to determine if the mechanical properties of the shapes in this region differ significantly from those in the web and flange away from the core. The AISC Specifications require supplemental testing to determine the notch toughness of the core region for Group 4 and 5 shapes when they are used in applications subjected to tensile loading and spliced with complete joint penetration welds. This requirement came about due to a series of service fractures that occurred in structures incorporating these "jumbo" shapes. The failed

sections exhibited low fracture toughness in the core region due to segregation of the steel in the ingot that caused the region of the core to have chemical and mechanical properties different from the flange and web. Other factors that produce lower notch toughness in this region of the shape include reduced amount of hot working during the rolling process and the slower cooling rate for this region of the shape, resulting in grain size growth.

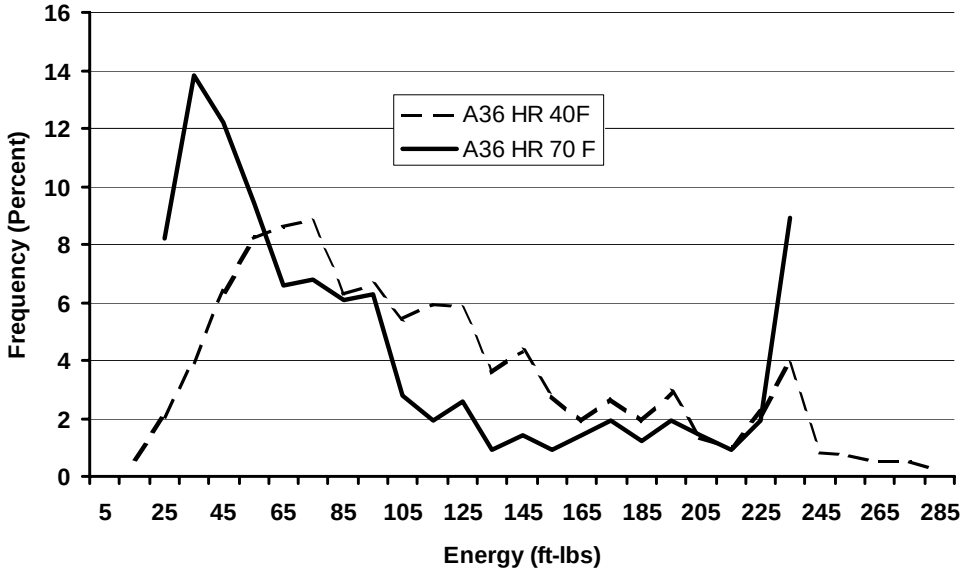

Figure 6-4 Distribution of CVN Toughness Values A36 Shape (AISC, 1995)

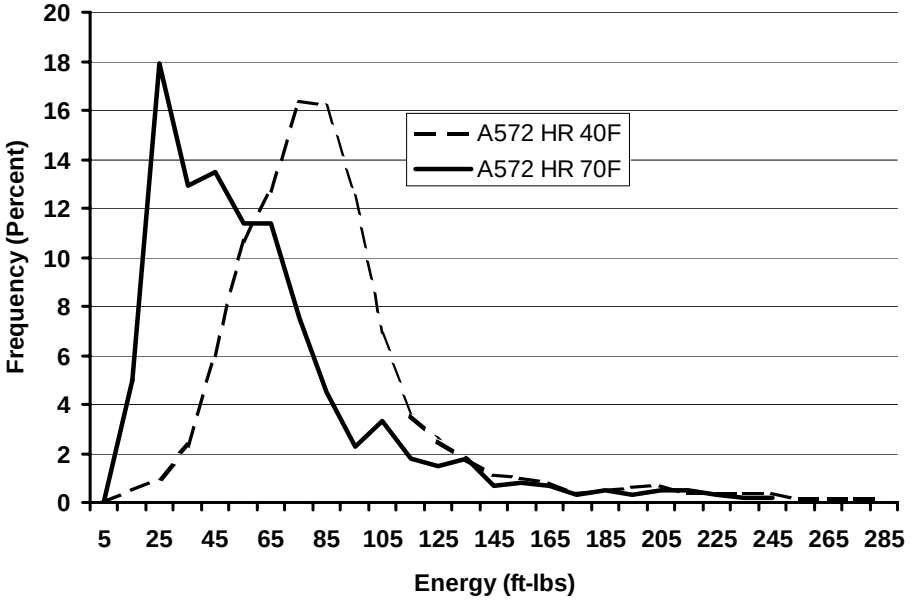

Figure 6-5 Distribution of CVN Toughness Values, A572, Grade 50 Shape (AISC, 1995)

Typical results for one of the sections tested is shown in the Figures 6-6, 6-7, and 6-8. The flange region exhibited a gradual transition, with an estimated transition temperature below -50 ^{o}F. The upper shelf energy is about 200 ft.-lbs. The core region exhibited a very abrupt transition with a transition temperature of approximately 10 ^{o}F. The upper shelf energy of the core region was 230 ft.-lbs. The web also exhibited an abrupt transition in notch toughness with a transition temperature similar to the flange. The upper shelf of the web was higher than the flange, but comparable to the core. The results from most of the sections tested were similar; the notch toughness was different in each of these three locations. The upper shelf notch toughness of the core was often equal to the web or flange notch toughness. The transition temperature, defined as the temperature corresponding to an absorbed energy of 15 ft.-lbs., and the upper shelf energy were used to compare the results. A lower transition temperature and higher upper shelf energy are desirable. Table 6-1 summarizes key statistics for upper shelf energy obtained from all of the tests. A histogram showing the distribution of upper shelf values for material extracted from the shape flanges, web, and core is shown in Figure 6-9.

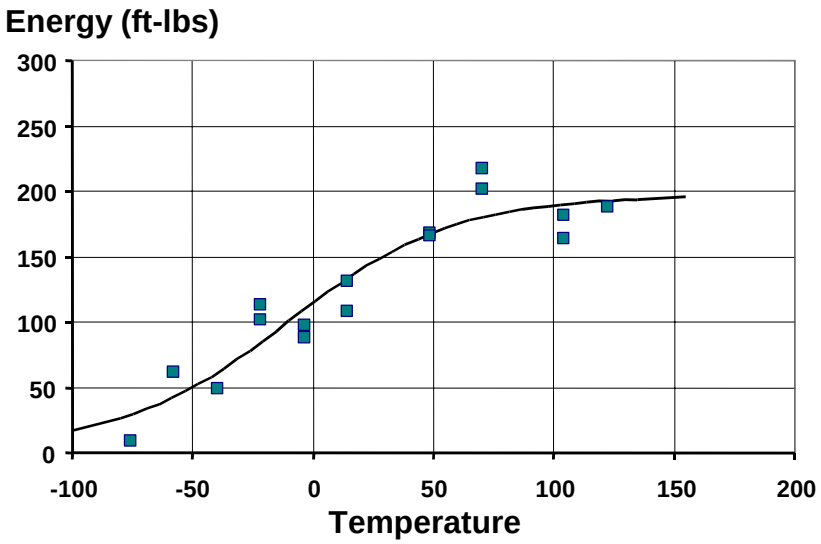

Figure 6-6 Transition Curve for Flange Material, A572, Grade 50 W24x162 Shape

The average upper-shelf value was around 200 ft.-lbs. at all three locations. The core region showed the highest mean upper-shelf value, but it was only slightly higher than the flange and web regions. The distribution of the core region shows a definite peak between 210 and 240 ft.-lbs.

The test results showed that, unlike upper shelf energy, transition temperature was very much dependent on the specimen location as shown in Table 6-2 and Figure 6-10.

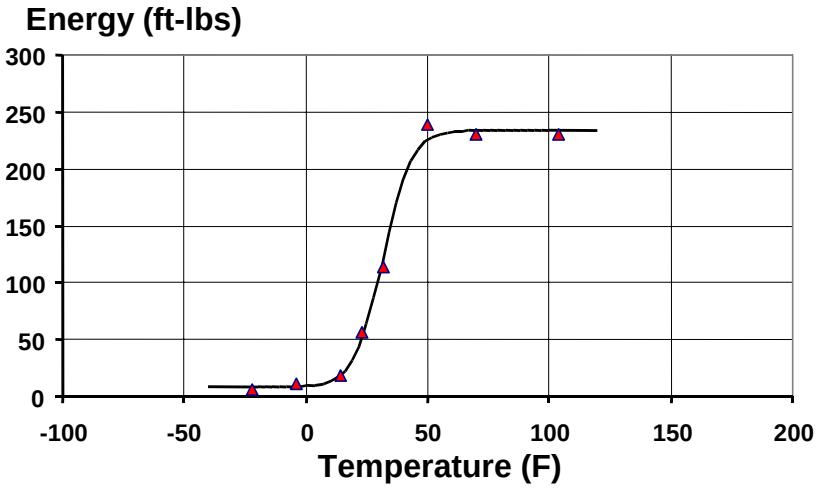

Figure 6-7 Transition Curve for Core Material, A572, Grade 50 W24x162 Shape

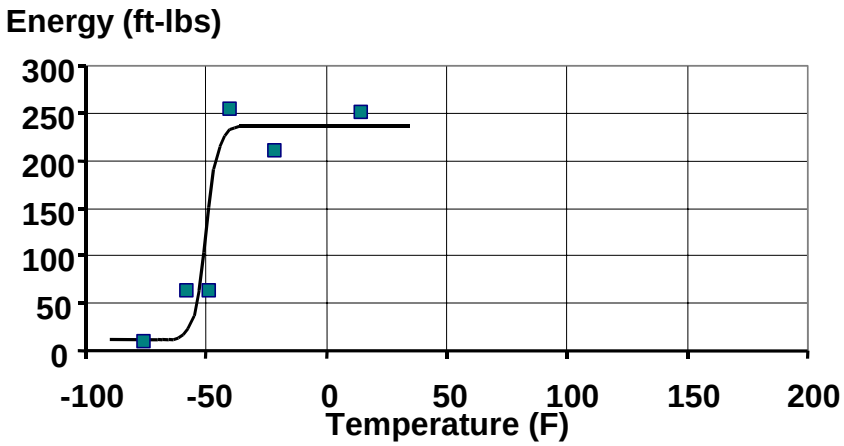

Figure 6-8 Transition Curve for Web Material, A572, Grade 50 W24x162 Shape

Table 6-1 Statistics on Upper Shelf CVN Energy for A572, Grade 50 Structural Shape

	Flange	Web	Core	All
Mean:	196	187	203	196
Maximum:	264	264	264	264
Minimum:	99	67	70	67
Std. Dev.:	60	61	59	59
# of Samples:	17	15	17	49

Units: ft-lbs

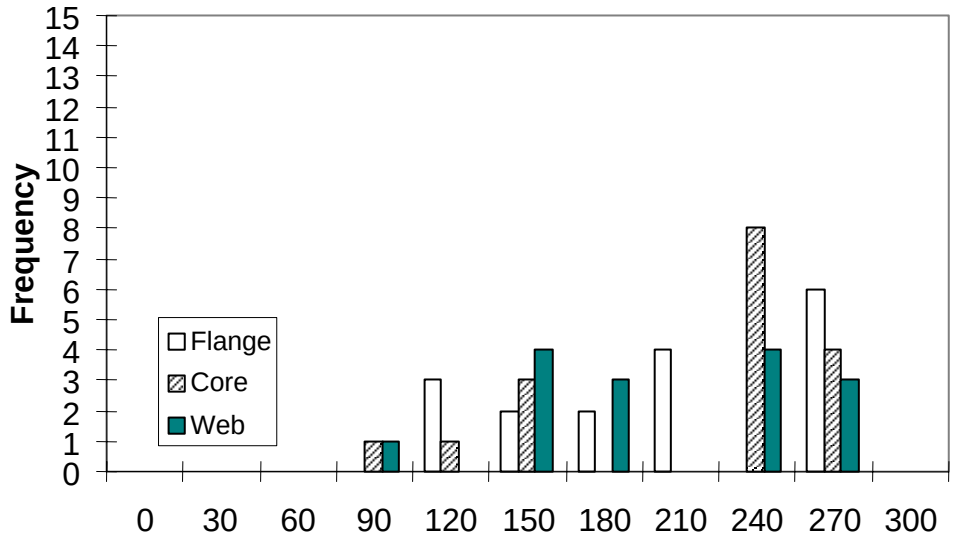

Figure 6-9 Distribution of Upper-Shelf CVN Values

Table 6-2 Statistics for Transition Temperature (^{o}F), A572, Grade 50 Shape

	Flange	Web	Core	All
Mean:	-51	-41	-20	-37
Maximum:	39	22	47	47
Minimum:	-75	-75	-75	-75
Std. Dev.:	36	29	39	37
# of Samples:	17	15	17	49

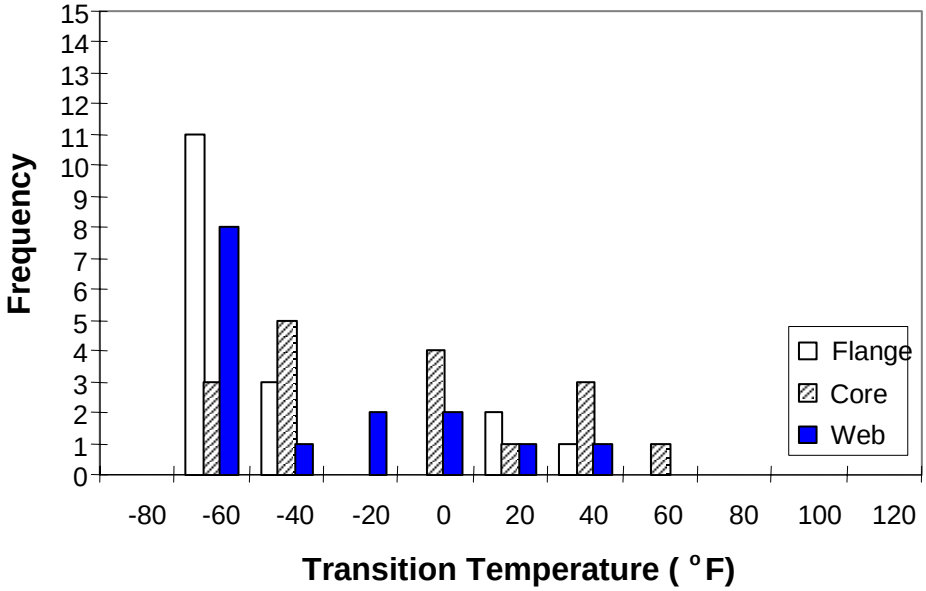

Figure 6-10 Distribution of CVN Transition Temperature, A572, Grade 50 Shape

The distributions for the flange and web regions show a definite skew to the left. This is in part because, in many cases, the temperature at 15 ft.-lbs. could only be estimated as it was not possible to bring the methanol bath to a low enough temperature to achieve brittle behavior. In these cases, the transition temperature was taken as the minimum temperature attained in that set of Charpy specimens. For example, the transition curve for the flange specimens from the W24x162 shown previously do not reflect a 15 ft.-lbs. temperature, because the lowest recorded specimen energy was greater than 15 ft.-lbs. at -76 °F. Experience shows that notch toughness continues to decrease with temperature until a lower shelf of around 2 ft.-lbs. is reached. Since it was impossible to attain a temperature that low with the available equipment, the transition temperature is reported as -76 °F.

The core region showed the highest average transition temperature, and the flange the lowest. This trend is consistent with results from individual members. In 10 of 17 members, the core transition temperature was higher than in both the flanges and webs.

Data suggest that the core regions of members have higher upper shelf energy, more abrupt transitions, and higher transition temperatures, relative to the flange and web regions. Typically, CVN toughness specifications are intended to assure a suitably low transition temperature. For example, a specification of minimum toughness of 20 ft.-lbs. at 70 ^{o}F has the effect of assuring that transition temperature is below 70 ^{o}F. Since the core region tends to have the highest transition temperature, it appears that the core location should be specified to measure the CVN toughness of sections to insure that all areas of the section have adequate notch toughness. The only exception to this being material in the k-area region of roller-straightened sections. This is discussed in the next chapter.

6.3 Summary and Comparison of CVN Toughness Surveys

Table 6-3 summarizes the data from the available surveys discussed above. The table shows the mean CVN energy for tests at 0 ^{o}F, 40 ^{o}F, and 70 ^{o}F, as well as the frequency of values below 15 and 30 ft.-lbs. at each temperature. The difference in the two surveys between the frequency of tests less than 15 ft.-lbs. is not significant. The modern steels display a much smaller frequency below 30 ft.-lbs. at 40 ^{o}F, and a much larger value at 70 ^{o}F. The mean CVN toughness of the modern A572 shape steel is much higher at 40 ^{o}F, and comparable to the earlier plate steel at 70 ^{o}F. The 1988 survey of W14 column shapes indicates that their toughness was more variable than comparable plates. Some sections had good toughness and others had low toughness even at room temperature.

Based upon these most current surveys, it appears reasonable to conservatively assume that less than 5% of steel product will have CVN toughness less than 15 ft.-lbs. at 70 ^{o}F, and less than 20% of steel products will have a CVN toughness of 30 ft.-lbs. or less at 70 ^{o}F. The percentage is reduced at the lower temperature of 40 ^{o}F, which is very puzzling and contrary to the expected behavior of a reduction in CVN toughness with a lower test temperature. This may be because the population of steels tested at the two temperatures is not the same. The early plate survey is probably more representative of typical steels with a 2 and 36% probability of CVN toughness less than 15 and 30 ft.-lbs. respectively. Earlier steels not produced to fine grain practice may have lower CVN toughness.

Table 6-3 Summary of Toughness Data 1973 - Present

Survey Years	Steel, Product, and Specimen	0 °F Test Temperature	40 °F Test Temperature	70 °F Test Temperature
1973-74	A572, Plate, Transverse	Mean 12 ft.-lbs. <15 ft.-lbs.: 79.1% <30 ft.-lbs.: 100%	Mean 18 ft.-lbs. <15 ft.-lbs.: 33.5% <30 ft.-lbs.: 97.3%	Mean 25 ft.-lbs. <15 ft.-lbs.: 4.1% <30 ft.-lbs.: 76.1%
1973-74	A572, Plate, Longitudinal	Mean 21 ft.-lbs. <15 ft.-lbs.: 30.5% <30 ft.-lbs.: 83.0%	Mean 37 ft.-lbs. <15 ft.-lbs.: 1.6% <30 ft.-lbs.: 35.7%	Mean 55 ft.-lbs. <15 ft.-lbs.: 0% <30 ft.-lbs.: 4.1%
1994-95	A572, Shape, Longitudinal	No Data	Mean 91 ft.-lbs. <15 ft.-lbs.: 0.5% <30 ft.-lbs.: 1.5%	Mean 61 ft.-lbs. <15 ft.-lbs.: 5% <30 ft.-lbs.: 22.9%
1994-95	A36, Shape, Longitudinal	No Data	Mean 112 ft.-lbs. <15 ft.-lbs.: 0.6% <30 ft.-lbs.: 2.7%	Mean 95 ft.-lbs. <15 ft.-lbs.: 0% <30 ft.-lbs.: 8.2%

Based upon the various surveys and the results of testing conducted in support of the FEMA/SAC program, it seems very likely that most hot rolled structural shapes will have a fracture toughness of at least 15 ft.-lbs. at room temperature. The CVN toughness of core region of large shapes may not attain this CVN toughness level without special treatment at the mill. It is suggested that the current recommendations contained in FEMA-267, that core regions of large shapes be at least 20 ft.-lbs. at 70 °F, be retained. Steel for structures such as exterior frames, open stadiums, and open and unheated parking garages need to be tested to insure that they have adequate notch toughness at their lower service temperatures. Testing temperatures should be selected depending on the anticipated service conditions.

7. MATERIAL PROPERTIES AT k-AREA REGION OF WIDE FLANGE SHAPES

7.1 Introduction

Welded moment resisting connections often incorporate details including web doubler plates and beam flange continuity plates that may require welding to the web of the section, near its juncture with the column flange. This region of the wide flange shape is typically termed the k-area region, due to the use of the symbol k, in the AISC manual, to designate the dimension from the outside face of the shape flange to the toe of the fillet at the juncture of the flange and web. In the period 1995-1997, several projects using details that required welding in the k-area region of the shape experienced problems with fabrication induced fractures of the section (Tide, 2000). These fractures typically extended from the toe of the fillet between the section flange, and web and ran into the web, away from the flange. Other types of unanticipated fractures were also reported to occur in this k-area region. For example, in some full-scale tests of welded moment-resisting beam column connections, the specimens failed when fractures extended between the column web and flange, running along the k-area. Due to concern that low notch toughness in the k-area region had the potential to cause poor behavior both during fabrication and in service, the FEMA/SAC program to reduce seismic hazards in moment resisting steel frames included a series of investigations into the notch toughness and strength properties of material in the k-area region of heavy shapes of the type commonly used as columns in moment-resisting frames intended for seismic applications.

As part of these investigations, the variation of tensile and notch toughness properties within a section was evaluated and the fracture properties in the web along the k-area of roller-straightened sections were investigated. The toughness, hardness, and strength at k-area were investigated, and the results are summarized below.

7.2 k-Area Properties of Rolled Shapes

Service fractures at the end of continuity plate welds and web doubler plates have occurred in the region of the k-area. The location of these fractures had high hardness and low fracture toughness. The change in the properties relative to other areas of the section has been attributed to roller imposed contact forces on the web during cold roller straightening of the sections. As wide flange shapes cool down, after hot rolling, they often take on bows that are outside the tolerances permitted by the ASTM A6. Therefore, they must be straightened. One of the most common methods of straightening these sections is termed roller straightening. Roller straightening is accomplished by passing the section thorough a series of offset rollers, which plastically deform the section about the y-y axis. The rollers contact the web in the vicinity of the k-area. It is believed that, through the processes of strain hardening and strain aging described in Chapter 2, the contact stresses from the rollers cause the mechanical properties at this location to change, the steel becoming stronger, harder, and more brittle.

The roller straightening method has been used for many years on light sections with a weight less than 150 lbs./ft. Heavier sections have typically been gag straightened by deforming the section as simple beams. The failures described above occurred on heavy column sections with a weight in excess of 150 lbs./ft. The rolled sections examined by Jaquess and Frank (1999) were evaluated to determine if they were roller straightened, and the properties of the sections at the k-area were examined.

As an initial method of characterizing the distribution of properties in a wide flange shape, hardness surveys were performed on the web-flange juncture of typical rolled sections using the Rockwell B scale. The sample included a considerable portion of the web and flange as shown in Figure 7-1 below. The hardness approximately 1/8 in. in from the surface of the sections was measured around the sample as shown in Figure 7-2. Typical results are shown in Figures 7-3 and 7-4 respectively for the web and flanges of W24x62 shape obtained from two producers. These sections were roller straightened. Figure 7-3 shows the average of the two web lines of the top and bottom T section. The vertical solid line in the figure is the location of the inside of the flange. The dashed line is the location of the k-area. The web line has considerable hardness variation with the highest hardness occurring in the region of the k-area. The shapes from the two producers displayed very similar hardness. Figure 7-4 shows the average hardness variation in the flange. No significant hardness gradients were found in the flanges. The hardness of two additional roller straightened sections was also determined. They were found to have similar hardness variations. The thickness of the web at the k-area was measured with a micrometer in all of these sections. One section displayed a thickness reduction of 0.009 in. in the web at the k-area. The other sections had no measurable reduction in thickness.

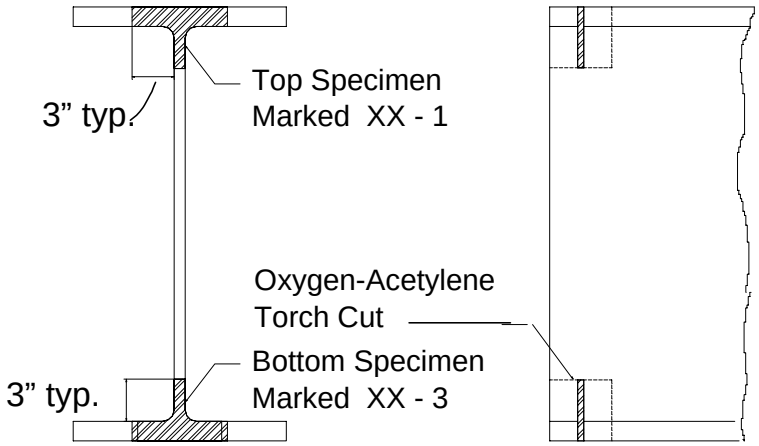

Figure 7-1 Locations of k-Area Samples

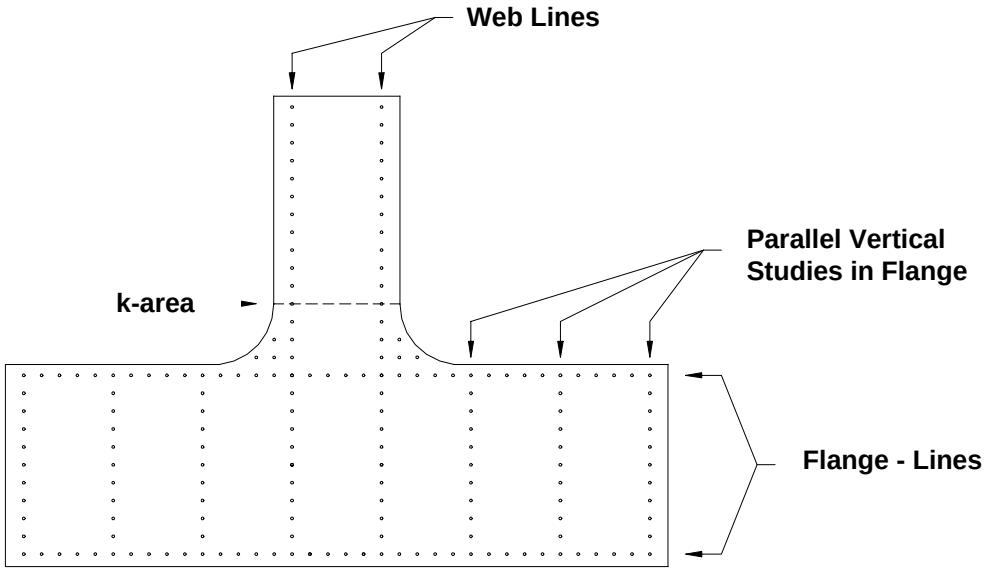

Figure 7-2 Locations of Hardness Tests

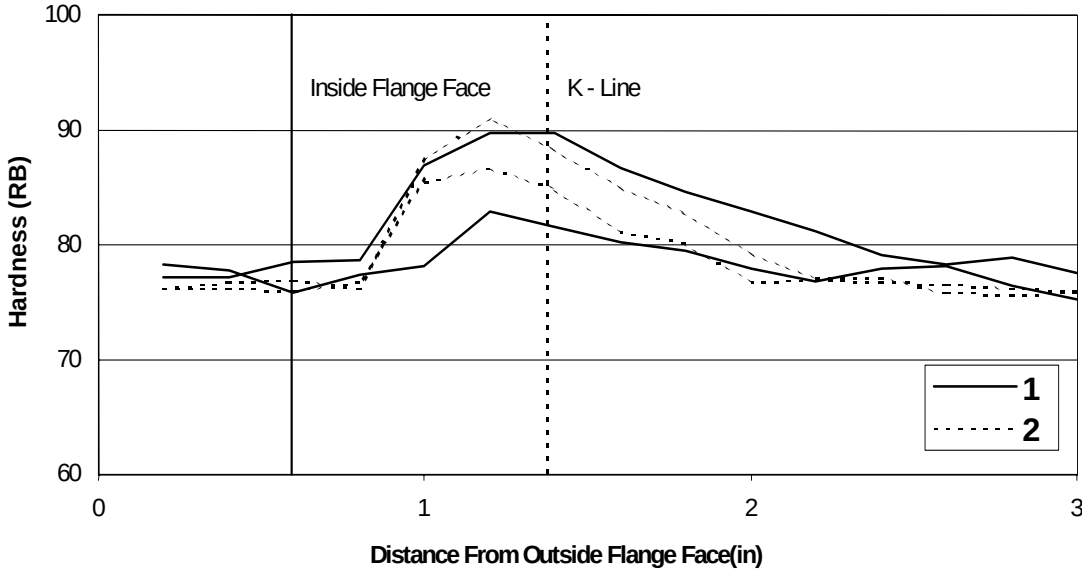

Figure 7-3 Hardness Profile of Web – W24x62

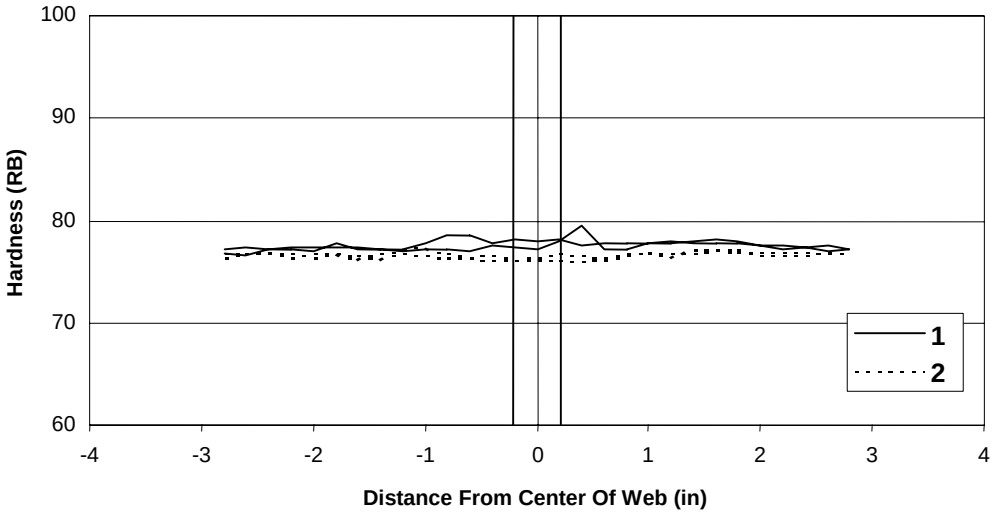

Figure 7-4 Hardness Profile of Flange – W24x62

For the sections tested, the CVN toughness of the material in the k-area region was compared to the CVN toughness measured in the web away from this region. The results are shown in Figures 7-5 and 7-6, respectively, for the two W24x62 sections previously discussed. The results are for Charpy specimens oriented vertically in the web with the notch oriented to produce fracture propagation in the longitudinal direction of the section. This direction is the called the T-L direction. It is not the L-T direction normally used to measure the CVN toughness of steel. T-L specimens from the mid-depth or center of the web were tested to compare with the results at the k-area.

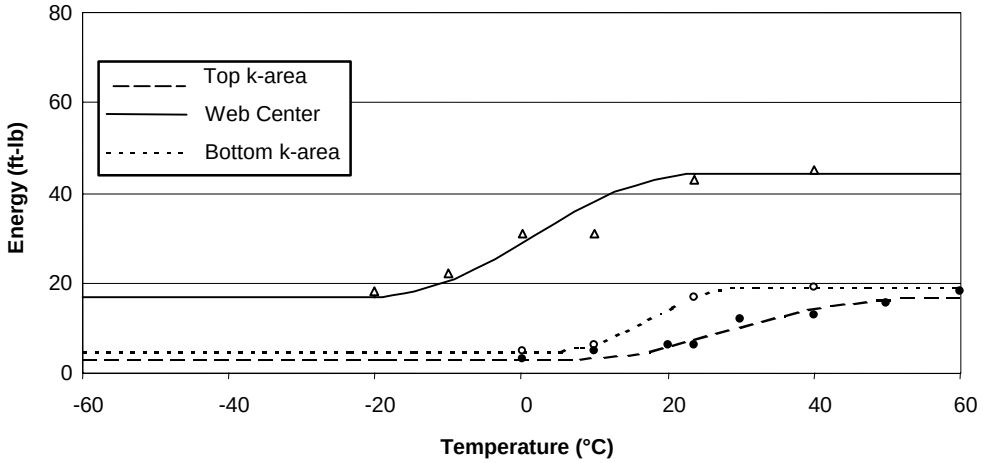

Figure 7-5 Charpy V-Notch Toughness Results of W24x62 from Producer 1

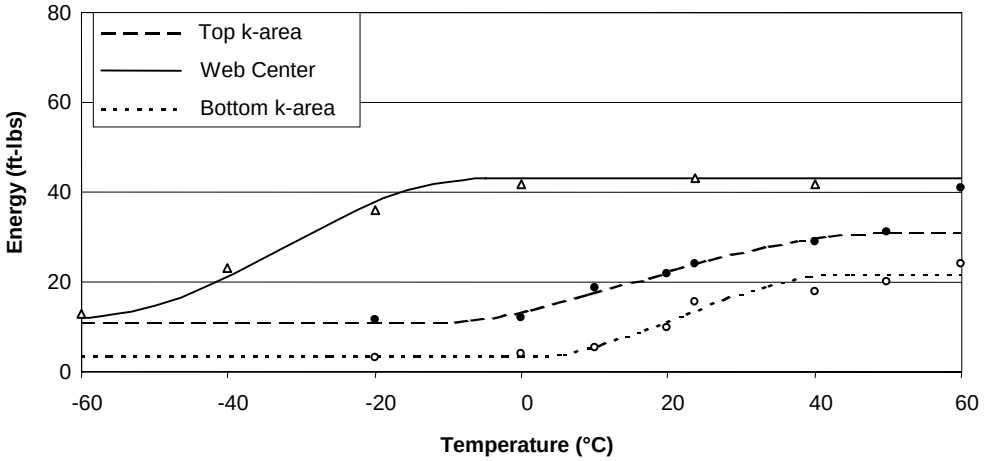

Figure 7-6 Charpy V-Notch Toughness Results of W24x62 from Producer 2

The k-area material exhibited a dramatic reduction in CVN toughness relative to the center of the web. The 15 ft.-lbs. transition temperature was at or above room temperature, and the upper shelf values were 40 to 80% of the values from the center of the web. The results confirm the observations from other investigations of the k-area of roller-straightened sections. These k-area regions will have a high hardness, higher yield and tensile strength, and lower notch toughness.

7.3 Conclusions

The results for this light beam section from two producers are similar to what has been found in heavier sections that have been roller straightened. The high hardness and low toughness makes the k-area susceptible to cracking. Welding in the k-area of roller-straightened sections should be avoided.

8. STRENGTH VARIATION IN A913 STEEL

ASTM A913 is a specification for structural steel shapes produced by the Quenching and Self-Tempering (QST) heat-treating process. This process consists of hot rolling the sections to the final geometry and then quenching the section within the rolling line and allowing the hot core region of the section to temper the cooler and more rapidly cooled exterior surfaces. The process requires precise control of the steel temperature at the time of quenching, which may require cooling hot regions such as the junction of the flange and web. The quenching and self-tempering process produces harder and higher-strength steel on the surface and a lower-strength steel in the interior of the section. Currently, only a single producer can supply material conforming to this specification. That producer has licensed the process to other producers, but they do not currently produce material to this specification.

Steel meeting the A913 specification is available in Grade 50 and Grade 65. It is reported by the producer as having very desirable properties for welding. As it may become advantageous for designers to use this material in the future, a series of investigations was conducted to evaluate the properties of this material. In addition to the notch toughness and through-thickness tensile testing reported in other chapters of this report, additional investigations were performed to evaluate the distribution of strength within the section.

8.1 Hardness Survey of Shapes

Hardness readings were taken in the same survey pattern used in the k-area evaluation, reported in Chapter 7. Typical results are shown in Figures 8-1 and 8-2. The results of an as-rolled section of the same size are shown for comparison.

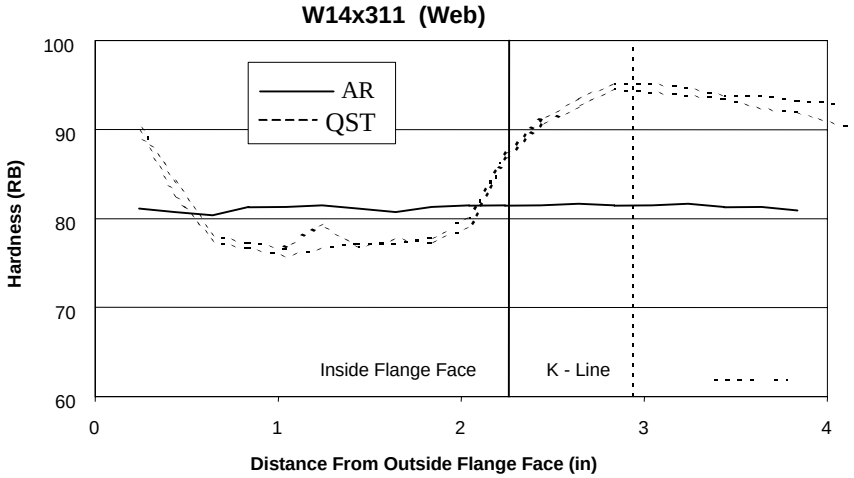

Figure 8-1 Hardness Testing in Web of ASTM A913 Material

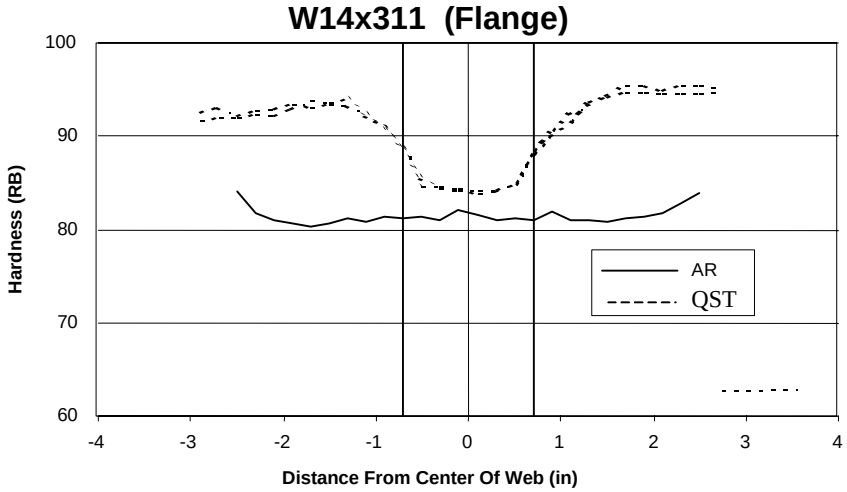

Figure 8-2 Hardness Testing in Flange of ASTM A913 Material

Both figures show the results of hardness testing of W14x311 sections. The specimen indicated as section QST is an ASTM A913, Grade 50 steel, while the specimen indicated as AR is a section conforming to ASTM A572, Grade 50 in the as rolled condition. The two lines shown for each section are the average results of the top and bottom flange or web. The A913 specimens displayed high hardness, Rockwell B 92-95, on the outside surface of the flanges away from the web and near the k-area in the web. The center of the flange has a lower hardness, Rockwell B 75-78, than the conventionally rolled section. The conventionally rolled section shows almost no hardness variation within the cross section. These results were typical of all the specimens tested.

8.2 Notch Toughness

The areas of high hardness in the web were investigated to determine the notch toughness of the region. The purpose of this investigation was to determine if the high hardness of the k-area region was also a region of low notch toughness similar to the roller straightened A572, Grade 50 sections discussed in Chapter 7. The notch toughness results for one section are shown in Figure 8-3.

The CVN toughness of the center of the web was comparable to the CVN toughness along both the top and bottom k-area of the section. The specimens were oriented in the T-L direction. Similar results were found for the other shapes that were produced to the A913 process.

8.3 Strength Variations

The variation in strength in the thickness direction of the flanges was evaluated by using ½ in. round tensile specimens centered at depths of ¼ and ½ the thickness of the flange from the flange surface. The results of the tests are summarized in Figure 8-4. The center thickness results shown on the right of the paired results have a lower yield and ultimate strength. The

results of a conventionally produced shape, B1, are shown for comparison. The results for the mid and quarter thickness locations for shape B1 are almost identical. The thicker flanges on the heavier shapes show a larger difference in the strength of the two locations. It should be noted on the thinner flanges that the material sampled by the two specimens actually overlapped.

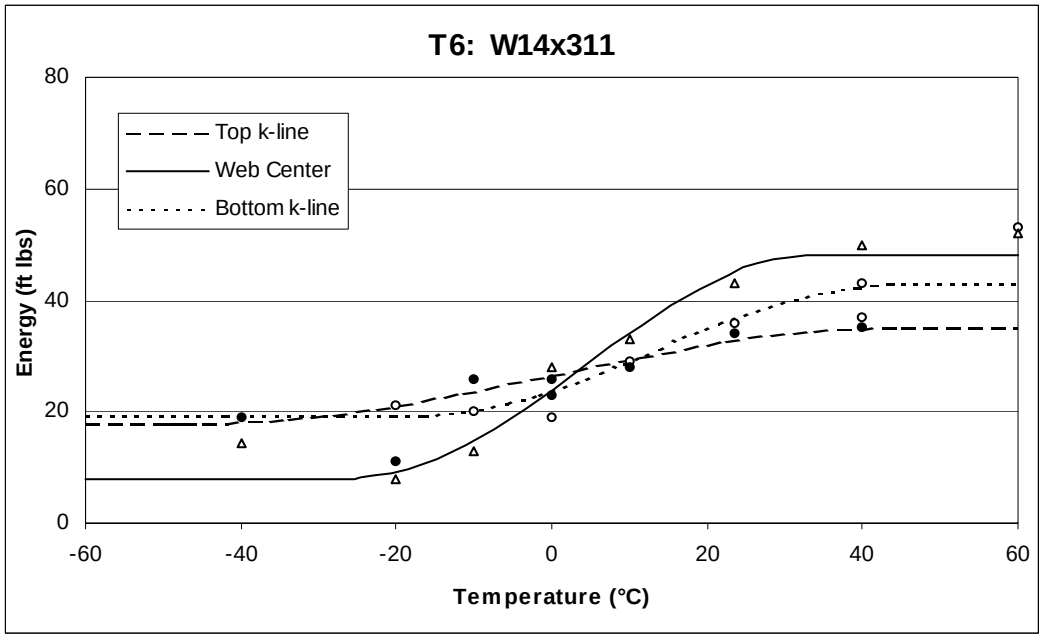

Figure 8-3 Transition Curve for k-Area Material, ASTM A913 Section

8.4 Conclusions

The CVN toughness of the A913 shapes was not significantly different at the k-area than at the center of the web. The high hardness of this region was not due to roller straightening, and did not indicate degradation in notch toughness. The beams supplied for the testing were not roller straightened and it can be expected that beams from the QST process that are roller straightened would exhibit elevated hardening in the k-areas. The low hardness in the central part of the flange was correlated with a significant reduction in strength measured in the tensile specimens. The reduced strength of the central part of the flange is due to the reduced cooling rate during the quenching of the steel. Full flange thickness tensile specimens should be used to characterize the strength of these sections.

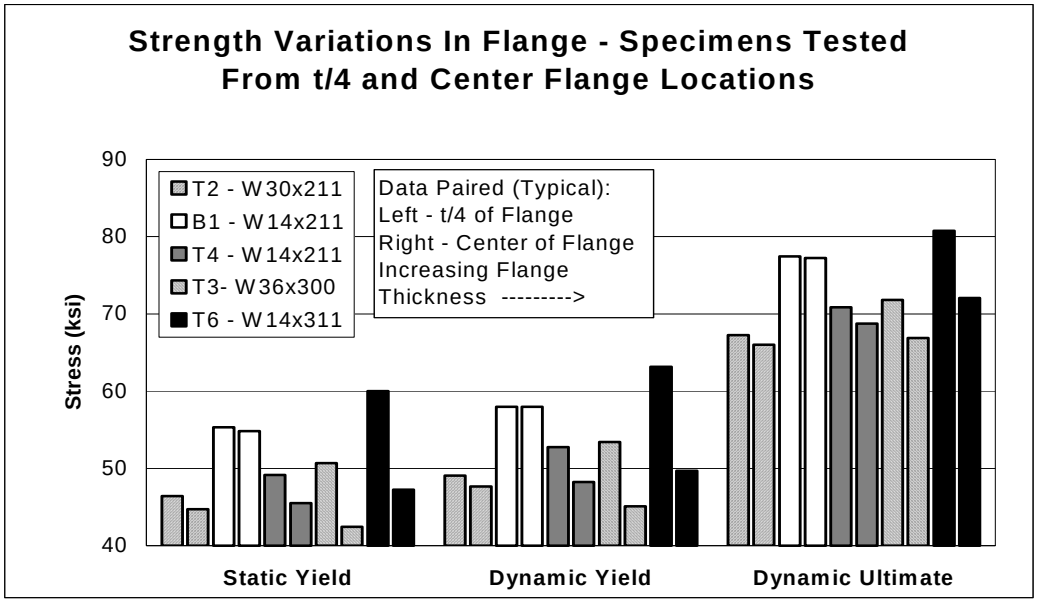

Figure 8-4 Variations in Flange Strength of QST Shapes

REFERENCES, FEMA REPORTS, SAC REPORTS, AND ACRONYMS

References.

AISI, 1974, *The Variation of Product Analysis and Tensile Properties—Carbon Steel Plates and Wide Flange Shapes*, American Iron and Steel Institute, Washington, DC.

AISI, 1979, *The Variations of Charpy V-Notch Impact Test Properties in Steel Plates*, American Iron and Steel Institute, Washington, DC.

AISI, 1985, *Steel Products Manual, Plates; Rolled Floor Plates: Carbon, High Strength Low Alloy, and Alloy Steel*, American Iron and Steel Institute, Washington, DC.

ASM, 1978, *Properties and Selection: Iron and Steel, Metals Handbook*, American Society of Metals, Vol. 1, Metals Park, OH.

ASM, 1985, *Carbon and Steels, Metals Handbook-Desk Edition*, American Society of Metals, Metals Park, OH.

ASTM, 1999, *Standard Specification for General Requirements for Rolled Steel Plates, Shapes, Sheet Piling, and Bars for Structural Use, ASTM A6*, American Society for Testing and Materials, Philadelphia, PA.

ASTM, 1997, *Standard Specification for Structural Steel, ASTM A36*, American Society for Testing and Materials, Philadelphia, PA.

ASTM, 1997, *Standard Specification for Methods and Definitions for Mechanical Testing of Steel Products, ASTM A370*, American Society for Testing and Materials, Philadelphia, PA.

ASTM, 1985, *Standard Specification for High Strength Low-alloy Columbium-Vanadium Steels of Structural Quality, ASTM A572*, American Society for Testing and Materials, Philadelphia, PA.

ASTM, 1985, *Standard Specification for ASTM 770*, American Society for Testing and Materials, Philadelphia, PA.

Barsom, J.M., 1971, "Relation Between Plane-Strain Ductility and K_{Ic} for Various Steels," *Journal of Engineering for Industry-Transactions of the ASM*.

Barsom, J.M., and Reisdorf, B.G., 1988, "Characteristics of Heavy-Weight Wide-Flange Structural Shapes," *Welding Research Council Bulletin, No. 332*, Welding Research Council, New York, NY.

Barsom, J.M., 1991, "Properties of Bridge Steels, Vol. I, Chap. 3", *Highway Structures Design Handbook*, Steel Bridge Alliance, Chicago, IL.

Barsom, J.M., 1996, "Steel Properties-Effects of Constraint, Temperature, and Rate of Loading," *Seismic Design, Evaluation and Retrofit of Steel Bridges—Proceedings of the Second U.S. Seminar*, A. Astaneh-Asl, and J. Roberts, Eds., Report No. UBC/CTE-STEEL-96/09, University of California, Berkeley.

Barsom, J.M., and Korvink, S.D., 1997, *Through Thickness Properties of Structural Steels*, SAC Joint Venture, SAC/BD-97/01.

Barsom, J.M., and Korvink, S.D., 1998, "*Effects of Strain Hardening and Strain Aging on the K-region of Structural Shapes*, SAC Joint Venture, SAC/BD-98/02.

Barsom, J.M., and Rolfe, S.T., 1999, *Fracture and Fatigue Control in Structures - Applications of Fracture Mechanics*, Third Edition, American Society for Testing and Materials, West Conshohocken, PA.

Beedle, L.S., and Tall, L., 1960, "Basic Column Strength," *Proceedings*, American Society of Civil Engineers, 86 (ST-7), p.139.

Cattan, J., 1995, *Statistical Analysis of Charpy V-Notch Toughness for Steel Wide Flange Structural Shapes*, AISC, Chicago, IL.

Clausing, D.P., 1969, "Tensile Properties of Eight Constructional Steels Between 70 and -320 F," *Journal of Materials*.

Clausing, D.P., 1970, "Effect of Plastic-Strain on Ductility and Toughness," *International Journal of Fracture Mechanics*, Vol. 6, No. 1.

Dexter, R.M., and Melendrez, M., 1999, *Through-Thickness Strength and Ductility of Column Flanges in Moment Connections*, SAC Joint Venture, SAC/BD-99/02.

Frank, K.H., and Read, D.R., 1993, *Statistical Analysis of Tensile Data for Wide-Flange Structural Shapes*, AISI/AISC Report.

Jaquess, T.K., and Frank, K.H., 1999, *Characterization of the Material Properties of Rolled Sections*, SAC Joint Venture, SAC/BD-99/07-1.

Lankford, W.T. Jr., et al., 1985, *The Making, Shaping and Treating of Steel*, Association of Iron and Steel Engineers, Pittsburgh, PA.

Miller, K.R. and Frank, K.H., 1999, *Study of the Material Properties of the Web-Flange Intersection of Rolled Shapes*, SAC Joint Venture, SAC/BD-99/08-1.

Pellini, W.S., 1973, "Design Options for Selection of Fracture Control Procedures in the Modernization of Codes, Rules, and Standards," *Proceedings: Joint United States - Japan Symposium on Application of Pressure Component Codes*, Tokyo, Japan.

Tide, R.H.R., 2000, "Evaluation of Steel Properties and Cracking in k-area of W shapes," *Engineering Structures*, Vol. 22 (2), pp. 128-134, Elsevier Science Ltd.

FEMA Reports.

FEMA reports are listed by report number.

FEMA-178, 1992, *NEHRP Handbook for the Seismic Evaluation of Existing Buildings*, developed by the Building Seismic Safety Council for the Federal Emergency Management Agency, Washington, DC.

FEMA-267, 1995, *Interim Guidelines, Inspection, Evaluation, Repair, Upgrade and Design of Welded Moment Resisting Steel Structures*, prepared by the SAC Joint Venture for the Federal Emergency Management Agency, Washington, DC. Superseded by FEMA 350 to 353.

FEMA-267A, 1996, *Interim Guidelines Advisory No. 1*, prepared by the SAC Joint Venture for the Federal Emergency Management Agency, Washington, DC. Superseded by FEMA 350 to 353.

FEMA-267B, 1999, *Interim Guidelines Advisory No. 2*, prepared by the SAC Joint Venture for the Federal Emergency Management Agency, Washington, DC. Superseded by FEMA 350 to 353.

FEMA-273, 1997, *NEHRP Guidelines for the Seismic Rehabilitation of Buildings*, prepared by the Applied Technology Council for the Building Seismic Safety Council, published by the Federal Emergency Management Agency, Washington, DC.

FEMA-274, 1997, *NEHRP Commentary on the Guidelines for the Seismic Rehabilitation of Buildings*, prepared by the Applied Technology Council for the Building Seismic Safety Council, published by the Federal Emergency Management Agency, Washington, DC.

FEMA-302, 1997, *NEHRP Recommended Provisions for Seismic Regulations for New Buildings and Other Structures, Part 1 – Provisions*, prepared by the Building Seismic Safety Council for the Federal Emergency Management Agency, Washington, DC.

FEMA-303, 1997, *NEHRP Recommended Provisions for Seismic Regulations for New Buildings and Other Structures, Part 2 – Commentary*, prepared by the Building Seismic Safety Council for the Federal Emergency Management Agency, Washington, DC.

FEMA-310, 1998, *Handbook for the Seismic Evaluation of Buildings – A Prestandard*, prepared by the American Society of Civil Engineers for the Federal Emergency Management Agency, Washington, DC.

FEMA-350, 2000, *Recommended Seismic Design Criteria for New Steel Moment-Frame Buildings*, prepared by the SAC Joint Venture for the Federal Emergency Management Agency, Washington, DC.

FEMA-351, 2000, *Recommended Seismic Evaluation and Upgrade Criteria for Existing Welded Steel Moment-Frame Buildings*, prepared by the SAC Joint Venture for the Federal Emergency Management Agency, Washington, DC.

FEMA-352, 2000, *Recommended Postearthquake Evaluation and Repair Criteria for Welded Steel Moment-Frame Buildings*, prepared by the SAC Joint Venture for the Federal Emergency Management Agency, Washington, DC.

FEMA-353, 2000, *Recommended Specifications and Quality Assurance Guidelines for Steel Moment-Frame Construction for Seismic Applications*, prepared by the SAC Joint Venture for the Federal Emergency Management Agency, Washington, DC.

FEMA-354, 2000, *A Policy Guide to Steel Moment-Frame Construction*, prepared by the SAC Joint Venture for the Federal Emergency Management Agency, Washington, DC.

FEMA-355A, 2000, *State of the Art Report on Base Metals and Fracture*, prepared by the SAC Joint Venture for the Federal Emergency Management Agency, Washington, DC.

FEMA-355B, 2000, *State of the Art Report on Welding and Inspection*, prepared by the SAC Joint Venture for the Federal Emergency Management Agency, Washington, DC.

FEMA-355C, 2000, *State of the Art Report on Systems Performance of Steel Moment Frames Subject to Earthquake Ground Shaking*, prepared by the SAC Joint Venture for the Federal Emergency Management Agency, Washington, DC.

FEMA-355D, 2000, *State of the Art Report on Connection Performance*, prepared by the SAC Joint Venture for the Federal Emergency Management Agency, Washington, DC.

FEMA-355E, 2000, *State of the Art Report on Past Performance of Steel Moment-Frame Buildings in Earthquakes*, prepared by the SAC Joint Venture for the Federal Emergency Management Agency, Washington, DC.

FEMA-355F, 2000, *State of the Art Report on Performance Prediction and Evaluation of Steel Moment-Frame Buildings*, prepared by the SAC Joint Venture for the Federal Emergency Management Agency, Washington, DC.

SAC Joint Venture Reports.

SAC Joint Venture reports are listed by report number, except for SAC 2000a through 2000k; those entries that do not include a FEMA report number are published by the SAC Joint Venture.

SAC 94-01, 1994, *Proceedings of the Invitational Workshop on Steel Seismic Issues, Los Angeles,* September 1994, prepared by the SAC Joint Venture for the Federal Emergency Management Agency, Washington, DC.

SAC 94-01, 1994b, *Proceedings of the International Workshop on Steel Moment Frames, Sacramento,* December, 1994, prepared by the SAC Joint Venture for the Federal Emergency Management Agency, Washington, DC.

SAC 95-01, 1995, *Steel Moment Frame Connection Advisory No. 3*, prepared by the SAC Joint Venture for the Federal Emergency Management Agency, Washington, DC.

SAC 95-02, 1995, *Interim Guidelines: Evaluation, Repair, Modification and Design of Welded Steel Moment Frame Structures,* prepared by the SAC Joint Venture for the Federal Emergency Management Agency, Report No. FEMA-267, Washington, DC.

SAC 95-03, 1995, *Characterization of Ground Motions During the Northridge Earthquake of January 17, 1994*, prepared by the SAC Joint Venture for the Federal Emergency Management Agency, Washington, DC.

SAC 95-04, 1995, *Analytical and Field Investigations of Buildings Affected by the Northridge Earthquake of January 17, 1994*, prepared by the SAC Joint Venture for the Federal Emergency Management Agency, Washington, DC.

SAC 95-05, 1995, *Parametric Analytic Investigations of Ground Motion and Structural Response, Northridge Earthquake of January 17, 1994,* prepared by the SAC Joint Venture for the Federal Emergency Management Agency, Washington, DC.

SAC 95-06, 1995, *Technical Report: Surveys and Assessment of Damage to Buildings Affected by the Northridge Earthquake of January 17, 1994*, prepared by the SAC Joint Venture for the Federal Emergency Management Agency, Washington, DC.

SAC 95-07, 1995, *Technical Report: Case Studies of Steel Moment-Frame Building Performance in the Northridge Earthquake of January 17, 1994*, prepared by the SAC Joint Venture for the Federal Emergency Management Agency, Washington, DC.

SAC 95-08, 1995, *Experimental Investigations of Materials, Weldments and Nondestructive Examination Techniques*, prepared by the SAC Joint Venture for the Federal Emergency Management Agency, Washington, DC.

SAC 95-09, 1995, *Background Reports: Metallurgy, Fracture Mechanics, Welding, Moment Connections and Frame Systems Behavior*, prepared by the SAC Joint Venture for the Federal Emergency Management Agency, Report No. FEMA-288, Washington, DC.

SAC 96-01, 1996, *Experimental Investigations of Beam-Column Subassemblages, Part 1 and 2*, prepared by the SAC Joint Venture for the Federal Emergency Management Agency, Washington, DC.

SAC 96-02, 1996, *Connection Test Summaries*, prepared by the SAC Joint Venture for the Federal Emergency Management Agency, Report No. FEMA-289, Washington, DC.

SAC 96-03, 1997, *Interim Guidelines Advisory No. 1 Supplement to FEMA-267 Interim Guidelines*, prepared by the SAC Joint Venture for the Federal Emergency Management Agency, Report No. FEMA-267A, Washington, DC.

SAC 98-PG, *Update on the Seismic Safety of Steel Buildings – A Guide for Policy Makers*, prepared by the SAC Joint Venture for the Federal Emergency Management Agency, Washington, DC.

SAC 99-01, 1999, *Interim Guidelines Advisory No. 2 Supplement to FEMA-267 Interim Guidelines*, prepared by the SAC Joint Venture, for the Federal Emergency Management Agency, Report No. FEMA-267B, Washington, DC.

SAC, 2000a, *Recommended Seismic Design Criteria for New Steel Moment-Frame Buildings*, prepared by the SAC Joint Venture for the Federal Emergency Management Agency, Report No. FEMA-350, Washington, DC.

SAC, 2000b, *Recommended Seismic Evaluation and Upgrade Criteria for Existing Welded Steel Moment-Frame Buildings*, prepared by the SAC Joint Venture for the Federal Emergency Management Agency, Report No. FEMA-351, Washington, DC.

SAC, 2000c, *Recommended Postearthquake Evaluation and Repair Criteria for Welded Steel Moment-Frame Buildings*, prepared by the SAC Joint Venture for the Federal Emergency Management Agency, Report No. FEMA-352, Washington, DC.

SAC, 2000d, *Recommended Specifications and Quality Assurance Guidelines for Steel Moment-Frame Construction for Seismic Applications*, prepared by the SAC Joint Venture for the Federal Emergency Management Agency, Report No. FEMA-353, Washington, DC.

SAC, 2000e, *A Policy Guide to Steel Moment-Frame Construction*, prepared by the SAC Joint Venture for the Federal Emergency Management Agency, Report No. FEMA-354, Washington, DC.

SAC, 2000f, *State of the Art Report on Base Metals and Fracture*, prepared by the SAC Joint Venture for the Federal Emergency Management Agency, Report No. FEMA-355A, Washington, DC.

SAC, 2000g, *State of the Art Report on Welding and Inspection*, prepared by the SAC Joint Venture for the Federal Emergency Management Agency, Report No. FEMA-355B, Washington, DC.

SAC, 2000h, *State of the Art Report on Systems Performance*, prepared by the SAC Joint Venture for the Federal Emergency Management Agency, Report No. FEMA-355C, Washington, DC.

SAC, 2000i, *State of the Art Report on Connection Performance*, prepared by the SAC Joint Venture for the Federal Emergency Management Agency, Report No. FEMA-355D, Washington, DC.

SAC, 2000j, *State of the Art Report on Past Performance of Steel Moment-Frame Buildings in Earthquakes*, prepared by the SAC Joint Venture for the Federal Emergency Management Agency, Report No. FEMA-355E, Washington, DC.

SAC, 2000k, *State of the Art Report on Performance Prediction and Evaluation*, prepared by the SAC Joint Venture for the Federal Emergency Management Agency, Report No. FEMA-355F, Washington, DC.

SAC/BD-96/01, *Selected Results from the SAC Phase 1 Beam-Column Connection Pre-Test Analyses*, submissions from B. Maison, K. Kasai, and R. Dexter; and A. Ingraffea and G. Deierlein.

SAC/BD-96/02, *Summary Report on SAC Phase 1 - Task 7 Experimental Studies*, by C. Roeder (a revised version of this document is published in Report No. SAC 96-01; the original is no longer available).

SAC/BD-96/03, *Selected Documents from the U.S.-Japan Workshop on Steel Fracture Issues*.

SAC/BD-96/04, *Survey of Computer Programs for the Nonlinear Analysis of Steel Moment Frame Structures*.

SAC/BD-97/01, *Through-Thickness Properties of Structural Steels*, by J. Barsom and S. Korvink.

SAC/BD-97/02, *Protocol for Fabrication, Inspection, Testing, and Documentation of Beam-Column Connection Tests and Other Experimental Specimens*, by P. Clark, K. Frank, H. Krawinkler, and R. Shaw.

SAC/BD-97/03, *Proposed Statistical and Reliability Framework for Comparing and Evaluating Predictive Models for Evaluation and Design*, by Y.-K. Wen.

SAC/BD-97/04, *Development of Ground Motion Time Histories for Phase 2 of the FEMA/SAC Steel Project*, by. P. Somerville, N. Smith, S. Punyamurthula, and J. Sun.

SAC/BD-97/05, *Finite Element Fracture Mechanics Investigation of Welded Beam-Column Connections*, by W.-M. Chi, G. Deierlein, and A. Ingraffea.

SAC/BD-98/01, *Strength and Ductility of FR Welded-Bolted Connections*, by S. El-Tawil, T. Mikesell, E. Vidarsson, and S. K. Kunnath.

SAC/BD-98/02, *Effects of Strain Hardening and Strain Aging on the K-Region of Structural Shapes*, by J. Barsom and S. Korvink

SAC/BD-98/03, *Implementation Issues for Improved Seismic Design Criteria: Report on the Social, Economic, Policy and Political Issues Workshop* by L. T. Tobin.

SAC/BD-99/01, *Parametric Study on the Effect of Ground Motion Intensity and Dynamic Characteristics on Seismic Demands in Steel Moment Resisting Frames* by G. A. MacRae.

SAC/BD-99/01A, *Appendix to: Parametric Study on the Effect of Ground Motion Intensity and Dynamic Characteristics on Seismic Demands in Steel Moment Resisting Frames* by G. A. MacRae.

SAC/BD-99/02, *Through-Thickness Strength and Ductility of Column Flange in Moment Connections*, by R. Dexter and M. Melendrez.

SAC/BD-99/03, *The Effects of Connection Fractures on Steel Moment Resisting Frame Seismic Demands and Safety*, by C. A. Cornell and N. Luco.

SAC/BD-99/04, *Effects of Strength/Toughness Mismatch on Structural and Fracture Behaviors in Weldments*, by P. Dong, T. Kilinski, J. Zhang, and F.W. Brust.

SAC/BD-99/05, *Assessment of the Reliability of Available NDE Methods for Welded Joint and the Development of Improved UT Procedures*, by G. Gruber and G. Light.

SAC/BD-99/06, *Prediction of Seismic Demands for SMRFs with Ductile Connections and Elements*, by A. Gupta and H. Krawinkler.

SAC/BD-99/07, *Characterization of the Material Properties of Rolled Sections*, by T. K. Jaquess and K. Frank.

SAC/BD-99/08, *Study of the Material Properties of the Web-Flange Intersection of Rolled Shapes*, by K. R. Miller and K. Frank.

SAC/BD-99/09, *Investigation of Damage to WSMF Earthquakes other than Northridge*, by M. Phipps.

SAC/BD-99/10, *Clarifying the Extent of Northridge Induced Weld Fracturing and Examining the Related Issue of UT Reliability*, by T. Paret.

SAC/BD-99/11, *The Impact of Earthquakes on Welded Steel Moment Frame Buildings: Experience in Past Earthquakes*, by P. Weinburg and J. Goltz.

SAC/BD-99/12, *Assessment of the Benefits of Implementing the New Seismic Design Criteria and Inspection Procedures*, by H. A. Seligson and R. Eguchi.

SAC/BD-99/13, *Earthquake Loss Estimation for WSMF Buildings*, by C. A. Kircher.

SAC/BD-99/14, *Simplified Loss Estimation for Pre-Northridge WSMF Buildings*, by B. F. Maison and D. Bonowitz.

SAC/BD-99/15, *Integrative Analytical Investigations on the Fracture Behavior of Welded Moment Resisting Connections*, by G. G. Deierlein and W.-M. Chi.

SAC/BD-99/16, *Seismic Performance of 3- and 9- Story Partially Restrained Moment Frame Buildings*, by B. F. Maison and K. Kasai.

SAC/BD-99/17, *Effects of Partially-Restrained Connection Stiffness and Strength on Frame Seismic Performance*, by K. Kasai, B. F. Maison, and A. Mayangarum.

SAC/BD-99/18, *Effects of Hysteretic Deterioration Characteristics on Seismic Response of Moment Resisting Steel Structures*, by F. Naeim, K. Skliros, A. M. Reinhorn, and M. V. Sivaselvan.

SAC/BD-99/19, *Cyclic Instability of Steel Moment Connections with Reduced Beam Section*, by C.-M. Uang and C.-C. Fan.

SAC/BD-99/20, *Local and Lateral-Torsion Buckling of Wide Flange Beams*, by L. Kwasniewski, B. Stojadinovic, and S. C. Goel.

SAC/BD-99/21, *Elastic Models for Predicting Building Performance*, by X. Duan and J. C. Anderson.

SAC/BD-99/22, *Reliability-Based Seismic Performance Evaluation of Steel Frame Buildings Using Nonlinear Static Analysis Methods*, by G. C. Hart and M. J. Skokan.

SAC/BD-99/23, *Failure Analysis of Welded Beam to Column Connections*, by J. M. Barsom and J. V. Pellegrino.

SAC/BD-99/24, *Weld Acceptance Criteria for Seismically-Loaded Welded Connections*, by W. Mohr.

SAC/BD-00/01, *Parametric Tests on Unreinforced Connections, Volume I – Final Report*, by K.-H. Lee, B. Stojadinovic, S. C. Goel, A. G. Margarian, J. Choi, A. Wongkaew, B. P. Reyher, and D.-Y, Lee.

SAC/BD-00/01A, *Parametric Tests on Unreinforced Connections, Volume II – Appendices*, by K.-H. Lee, B. Stojadinovic, S. C. Goel, A. G. Margarian, J. Choi, A. Wongkaew, B. P. Reyher, and D.-Y, Lee.

SAC/BD-00/02, *Parametric Tests on the Free Flange Connections*, by J. Choi, B. Stojadinovic, and S. C. Goel.

SAC/BD-00/03, *Cyclic Tests on Simple Connections Including Effects of the Slab*, by J. Liu and A. Astaneh-Asl.

SAC/BD-00/04, *Tests on Bolted Connections, Part I: Technical Report*, by J. Swanson, R. Leon, and J. Smallridge.

SAC/BD-00/04A, *Tests on Bolted Connections, Part II: Appendices*, by J. Swanson, R. Leon, and J. Smallridge.

SAC/BD-00/05, *Bolted Flange Plate Connections*, by S. P. Schneider and I. Teeraparbwong.

SAC/BD-00/06, *Round Robin Testing of Ultrasonic Testing Technicians*, by R. E. Shaw, Jr.

SAC/BD-00/07, *Dynamic Tension Tests of Simulated Welded Beam Flange Connections*, by J. M. Ricles, C. Mao, E. J. Kaufmann, L.-W. Lu, and J. W. Fisher.

SAC/BD-00/08, *Design of Steel Moment Frame Model Buildings in Los Angeles, Seattle and Boston*, by P. Clark.

SAC/BD-00/09, *Benchmarking of Analysis Programs for SMRF System Performance Studies*, by A. Gupta and H. Krawinkler.

SAC/BD-00/10, *Loading Histories for Seismic Performance Testing of SMRF Components and Assemblies*, by H. Krawinkler, A. Gupta, R. Medina, and N. Luco.

SAC/BD-00/11, *Development of Improved Post-Earthquake Inspection Procedures for Steel Moment Frame Buildings*, by P. Clark.

SAC/BD-00/12, *Evaluation of the Effect of Welding Procedure on the Mechanical Properties of FCAW-S and SMAW Weld Metal Used in the Construction of Seismic Moment Frames*, by M. Q. Johnson.

SAC/BD-00/13, *Preliminary Evaluation of Heat Affected Zone Toughness in Structural Shapes Used in the Construction of Seismic Moment Frames*, by M. Q. Johnson and J. E. Ramirez.

SAC/BD-00/14, *Evaluation of Mechanical Properties in Full-Scale Connections and Recommended Minimum Weld Toughness for Moment Resisting Frames*, by M. Q. Johnson, W. Mohr, and J. Barsom.

SAC/BD-00/15, *Simplified Design Models for Predicting the Seismic Performance of Steel Moment Frame Connections*, by C. Roeder, R. G. Coons, and M. Hoit.

SAC/BD-00/16, *SAC Phase 2 Test Plan*, by C. Roeder.

SAC/ BD-00/17, *Behavior and Design of Radius-Cut, Reduced Beam Section Connections*, by M. Engelhardt, G. Fry, S. Jones, M. Venti, and S. Holliday.

SAC/BD-00/18, *Test of a Free Flange Connection with a Composite Floor Slab*, by M. Venti and M. Engelhardt.

SAC/BD-00/19, *Cyclic Testing of a Free Flange Moment Connection*, by C. Gilton, B. Chi, and C. M. Uang.

SAC/BD-00/20, *Improvement of Welded Connections Using Fracture Tough Overlays*, by James Anderson, J. Duan, P. Maranian, and Y. Xiao.

SAC/BD-00/21, *Cyclic Testing of Bolted Moment End-Plate Connections*, by T. Murray, E. Sumner, and T. Mays.

SAC/BD-00/22, *Cyclic Response of RBS Moment Connections: Loading Sequence and Lateral Bracing Effects*, by Q. S. Yu, C. Gilton, and C. M. Uang.

SAC/BD-00/23, *Cyclic Response of RBS Moment Connections: Weak Axis Configuration and Deep Column Effects*, by C. Gilton, B. Chi, and C. M. Uang.

SAC/BD-00/24, *Development and Evaluation of Improved Details for Ductile Welded Unreinforced Flange Connections*, by J. M. Ricles, C. Mao, L.-W. Lu, and J. Fisher.

SAC/BD-00/25, *Performance Prediction and Evaluation of Steel Special Moment Frames for Seismic Loads*, by K. Lee and D. A. Foutch.

SAC/BD-00/26, *Performance Prediction and Evaluation of Low Ductility Steel Moment Frames for Seismic Loads*, by S. Yun and D. A. Foutch.

SAC/BD-00/27, *Steel Moment Resisting Connections Reinforced with Cover and Flange Plates*, by T. Kim, A. S. Whittaker, V. V. Bertero, A. S. J. Gilani, and S. M. Takhirov.

SAC/BD-00/28, *Failure of a Column K-Area Fracture*, by J. M. Barsom and J. V. Pellegrino.

SAC/BD-00/29, *Inspection Technology Workshop*, by R. E. Shaw, Jr.

SAC/BD-00/30, *Preliminary Assessment of the Impact of the Northridge Earthquake on Construction Costs of Steel Moment Frame Buildings*, by Davis Langdon Adamson.

Acronyms.

2-D, two-dimensional
3-D, three-dimensional
A, acceleration response, amps
A2LA, American Association for Laboratory Accreditation
ACAG, air carbon arc gouging
ACIL, American Council of Independent Laboratories
AE, acoustic emission (testing)
AISC, American Institute for Steel Construction
AISI, American Iron and Steel Institute
AL, aluminum
ANSI, American National Standards Institute
API, American Petroleum Institute
ARCO, Atlantic-Richfield Company
As, arsenic
ASD, allowable stress design
ASME, American Society of Mechanical Engineers
ASNT, American Society for Nondestructive Testing
ASTM, American Society for Testing and Materials
ATC, Applied Technology Council
AWS, American Welding Society
B, boron
BB, Bolted Bracket (connection)
BD, background document
BF, bias factor
BFO, bottom flange only (fracture)
BFP, Bolted Flange Plates (connection)
BM, base metal
BO, Boston, Massachusetts
BOCA, Building Officials and Code Administrators
BOF, basic oxygen furnace
BSEP, Bolted Stiffened End Plate (connection)
BSSC, Building Seismic Safety Council
BUEP, Bolted Unstiffened End Plate (connection)
C, carbon
CA, California
CAC-A, air carbon arc cutting
CAWI, Certified Associate Welding Inspector
CGHAZ, coarse-grained HAZ
CJP, complete joint penetration (weld)
CMU, concrete masonry unit, concrete block
COD, crack opening displacement
"COV," modified coefficient of variation, or dispersion
CP, Collapse Prevention (performance level)
Connection Performance (team)
Cr, chromium
CSM, Capacity Spectrum Method
CTOD, crack tip opening dimension or displacement
CTS, controlled thermal severity (test)
Cu, copper

CUREe, California Universities for Research in Earthquake Engineering
CVN, Charpy V-notch
CWI, Certified Welding Inspector
D, displacement response, dead load
DMRSF, ductile, moment-resisting, space frame
DNV, Det Norske Veritas
DRAIN-2DX, analysis program
DRAIN-3DX, analysis program
DRI, direct reduced iron
DST, Double Split Tee (connection)
DTI, Direct Tension Indicator
EAF, electric-arc furnace
EBT, eccentric bottom tapping
EE, electrode extension
EERC, Earthquake Engineering Research Center, UC Berkeley
EGW, electrogas welding
ELF, equivalent lateral force
EMS, electromagnetic stirring
ENR, Engineering News Record
ESW, electroslag welding
EWI, Edison Welding Institute
FATT, fracture appearance transition temperature
fb, fusion boundary
FCAW-G, flux-cored arc welding – gas-shielded
FCAW-S or FCAW-SS, flux-cored arc welding – self-shielded
FEMA, Federal Emergency Management Agency
FF, Free Flange (connection)
FGHAZ, fine-grained HAZ
FL, fusion line
FR, fully restrained (connection)
GBOP, gapped bead on plate (test)
gl, gage length
GMAW, gas metal arc welding
GTAW, gas tungsten arc welding
HAC, hydrogen-assisted cracking
HAZ, heat-affected zone
HBI, hot briquetted iron
HSLA, high strength, low alloy
IBC, *International Building Code*
ICBO, International Conference of Building Officials
ICC, International Code Council
ICCGHAZ, intercritically reheated CGHAZ
ICHAZ, intercritical HAZ
ID, identification
IDA, Incremental Dynamic Analysis
IMF, Intermediate Moment Frame
IO, Immediate Occupancy (performance level)
IOA, Incremental Dynamic Analysis
ISO, International Standardization Organization
IWURF, Improved Welded Unreinforced Flange (connection)
L, longitudinal, live load
LA, Los Angeles, California
LACOTAP, Los Angeles County Technical Advisory Panel
LAX, Los Angeles International Airport
LB, lower bound (building)
LBZ, local brittlezone
LDP, Linear Dynamic Procedure
LEC, Lincoln Electric Company
LMF, ladle metallurgy furnace
LRFD, load and resistance-factor design
LS, Life Safety (performance level)
LSP, Linear Static Procedure
LTH, linear time history (analysis)
LU, Lehigh University
M, moment
MAP, modal analysis procedure
MAR, microalloyed rutile (consumables)
MCE, Maximum Considered Earthquake
MDOF, multidegree of freedom
MMI, Modified Mercalli Intensity
Mn, manganese
Mo, molybdenum
MRF, steel moment frame
MRS, modal response spectrum
MRSF, steel moment frame
MT, magnetic particle testing
N, nitrogen
Nb, niobium
NBC, *National Building Code*
NDE, nondestructive examination

NDP, Nonlinear Dynamic Procedure
NDT, nondestructive testing
NEHRP, National Earthquake Hazards Reduction Program
NES, National Evaluation Services
NF, near-fault, near-field
Ni, nickel
NLP, nonlinear procedure
NLTH, nonlinear time history (analysis)
NS, north-south (direction)
NSP, Nonlinear Static Procedure
NTH, nonlinear time history (analysis)
NVLAP, National Volunteer Laboratory Accreditation Program
O, oxygen
OHF, open hearth furnace
OMF, Ordinary Moment Frame
OTM, overturning moment
P, axial load
P, axial load, phosphorus
Pb, lead
PGA, peak ground acceleration
PGV, peak ground velocity
PIDR, pseudo interstory drift ratio
PJP, partial joint penetration (weld)
PPE, Performance, Prediction, and Evaluation (team)
PQR, Performance Qualification Record
PR, partially restrained (connection)
PR-CC, partially restrained, composite connection
PT, liquid dye penetrant testing
PWHT, postweld heat treatment
PZ, panel zone
QA, quality assurance
QC, quality control
QCP, Quality Control Plan, Quality Certification Program
QST, Quenching and Self-Tempering (process)
RB, Rockwell B scale (of hardness)
RBS, Reduced Beam Section (connection)
RCSC, Research Council for Structural Connections
RT, radiographic testing
S, sulphur, shearwave (probe)
SAC, the SAC Joint Venture; a partnership of SEAOC, ATC, and CUREe
SAV, sum of absolute values
SAW, submerged arc welding
SBC, *Standard Building Code*
SBCCI, Southern Building Code Congress International
SCCGHAZ, subcritically reheated CGHAZ
SCHAZ, subcritical HAZ
SCWB, strong column, weak beam
SCWI, Senior Certified Welding Inspector
SDC, Seismic Design Category
SDOF, single degree of freedom
SE, Seattle, Washington
SEAOC, Structural Engineers Association of California
SFRS, seismic-force-resisting system
Si, silicon
SMAW, shielded metal arc welding
SMF, Special Moment Frame
SMRF, special moment-resisting frame (in 1991 UBC)
SMRF, Steel Moment Frame
SMRSF, special moment-resisting space frame (in 1988 UBC)
SN, strike-normal, fault-normal
Sn, tin
SP, Side Plate (connection)
SP, strike-parallel, fault-parallel
SP, Systems Performance (team)
SPC, Seismic Performance Category
SRSS, square root of the sum of the squares
SSPC, Steel Shape Producers Council
SSRC, Structural Stability Research Council
SUG, Seismic Use Group
SW, Slotted Web (connection)
SwRI, Southwest Research Institute
T, transverse
TBF, top and bottom flange (fracture)
Ti, titanium
TIGW, tungsten inert gas welding
TMCP, Thermo-Mechanical Processing
TN, Tennessee
TT, through-thickness
TWI, The Welding Institute
UB, upper bound (building)

UBC, *Uniform Building Code*
UCLA, University of California, Los Angeles
UM, University of Michigan
URM, unreinforced masonry
US, United States of America
USC, University of Southern California
USGS, US Geological Survey
UT, ultrasonic testing
UTA, University of Texas at Austin
UTAM, Texas A & M University
V, vanadium
VI, visual inspection
w/o, without
WBH, Welded Bottom Haunch (connection)
WCPF, Welded Cover Plate Flange (connection)
WCSB, weak column, strong beam
WF, wide flange
WFP, Welded Flange Plate (connection)
WFS, wire feed speed
WPQR, Welding Performance Qualification Record
WPS, Welding Procedure Specification
WSMF, welded steel moment frame
WT, Welded Top Haunch (connection)
WTBH, Welded Top and Bottom Haunch (connection)
WUF-B, Welded Unreinforced Flanges – Bolted Web (connection)
WUF-W, Welded Unreinforced Flanges – Welded Web (connection)

SAC PHASE II PROJECT PARTICIPANTS

FEMA Project Officer

Michael Mahoney
Federal Emergency Management Agency
500 C St. SW, Room 404
Washington, DC 20472

FEMA Technical Advisor

Robert D. Hanson
Federal Emergency Management Agency
DFO Room 353
P.O. Box 6020
Pasadena, CA 91102-6020

Joint Venture Management Committee (JVMC)

William T. Holmes, Chair
Rutherford and Chekene
427 Thirteenth Street
Oakland, CA 94612

Christopher Rojahn
Applied Technology Council
555 Twin Dolphin Dr., Suite 550
Redwood City, CA 94065

Edwin T. Huston
Smith & Huston, Inc.
8618 Roosevelt Way NE
Seattle, WA 98115

Arthur E. Ross
Cole/Yee/Shubert & Associates
2500 Venture Oaks Way, Suite 100
Sacramento, CA 95833

Robert Reitherman
California Universities for Research in Earthquake Engineering
1301 South 46th St.
Richmond, CA 94804

Robin Shepherd
Earthquake Damage Analysis Corporation
40585 Lakeview Drive, Suite 1B
P.O. Box 1967
Big Bear Lake, CA 92315

Project Management Committee (PMC)

Stephen A. Mahin, Project Manager
Pacific Earthquake Engr. Research Center
University of California
Berkeley, CA 94720

William T. Holmes, JVMC
Rutherford and Chekene
427 Thirteenth Street
Oakland, CA 94612

Ronald O. Hamburger, Project Director for Project Development
EQE International
1111 Broadway, 10th Floor
Oakland, CA 94607-5500

Christopher Rojahn, JVMC
Applied Technology Council
555 Twin Dolphin Dr., Suite 550
Redwood City, CA 94065

James O. Malley, Project Director for Topical Investigations
Degenkolb Engineers
225 Bush St., Suite 1000
San Francisco, CA 94104-1737

Robin Shepherd, JVMC
Earthquake Damage Analysis Corporation
40585 Lakeview Drive, Suite 1B
P.O. Box 1967
Big Bear Lake, CA 92315

Peter W. Clark, Technical Assistant to PMC
SAC Steel Project Technical Office
1301 South 46th St.
Richmond, CA 94804

Project Administration

Allen Paul Goldstein, Project Administrator
Allen Paul Goldstein and Associates
1621B 13th Street
Sacramento, CA 95814

Lori Campbell, Assistant to the Project Administrator
4804 Polo Court
Fair Oaks, CA 95628

Project Oversight Committee (POC)

William J. Hall, Chair
3105 Valley Brook Dr.
Champaign, IL 61821

Shirin Ader
International Conference of Building Officials
5360 Workman Mill Rd.
Whittier, CA 90601-2298

John M. Barsom
Barsom Consulting, Ltd.
1316 Murray Ave, Suite 300
Pittsburgh, PA 15217

Roger Ferch
Herrick Corporation
7021 Koll Center Parkway
P.O Box 9125
Pleasanton, CA 94566-9125

Theodore V. Galambos
University of Minnesota
122 CE Building, 500 Pillsbury Dr. SE
Minnneapolis, MN 55455

John L. Gross
National Institute of Stds. & Technology
Building and Fire Research Lab,
Building 226, Room B158
Gaithersburg, MD 20899

James R. Harris
J.R. Harris and Co.
1580 Lincoln St., Suite 550
Denver, CO 80203-1509

Richard Holguin
520 Kathryn Ct.
Nipomo, CA 93444

Nestor Iwankiw
American Institute of Steel Construction
One East Wacker Dr., Suite 3100
Chicago, IL 60601-2001

Roy Johnston
Brandow & Johnston Associates
1600 West 3rd St.
Los Angeles, CA 90017

Leonard Joseph
Thornton-Tomassetti Engineers
641 6th Ave., 7th Floor
New York, NY 10011

Duane K. Miller
The Lincoln Electric Company
22801 St. Clair Ave.
Cleveland, OH 44117-1194

John Theiss
EQE/Theiss Engineers
1848 Lackland Hills Parkway
St. Louis, MO 63146-3572

John H. Wiggins
J.H. Wiggins Company
1650 South Pacific Coast Hwy, Suite 311
Redondo Beach, CA 90277

Team Leaders for Topical Investigations

Douglas A. Foutch
University of Illinois
MC-250, 205 N. Mathews Ave.
3129 Newmark Civil Engineering Lab
Urbana, IL 61801

Karl H. Frank
University of Texas at Austin
10100 Bornet Rd.
Ferguson Lab, P.R.C. #177
Austin, TX 78758

Matthew Johnson
Edison Welding Institute
1250 Arthur E. Adams Drive
Columbus, OH 43221

Helmut Krawinkler
Department of Civil Engineering
Stanford University
Stanford, CA 94305

Charles W. Roeder
University of Washington
233-B More Hall FX-10
Dept. of Building and Safety
Seattle, WA 98195-2700

L. Thomas Tobin
Tobin and Associates
134 California Ave.
Mill Valley, CA 94941

Lead Guideline Writers

John D. Hooper
Skilling Ward Magnusson Barkshire, Inc.
1301 Fifth Avenue, Suite 3200
Seattle, WA 98101-2699

Lawrence D. Reaveley
University of Utah
Civil Engineering Dept.
3220 Merrill Engineering Building
Salt Lake City, UT 84112

Thomas A. Sabol
Englekirk & Sabol Consulting Engineers
P.O. Box 77-D
Los Angeles, CA 90007

C. Mark Saunders
Rutherford & Chekene
303 Second St., Suite 800 North
San Francisco, CA 94107

Robert E. Shaw
Steel Structures Technology Center, Inc.
42400 W Nine Mile Road
Novi, MI 48375-4132

Raymond H. R. Tide
Wiss, Janney, Elstner Associates, Inc.
330 Pfingsten Road
Northbrook, IL 60062-2095

C. Allin Cornell, Associate Guideline Writer
Stanford University
Terman Engineering Center
Stanford, CA 94305-4020

Technical Advisory Panel (TAP) for Materials and Fracture

John M. Barsom, POC
Barsom Consulting, Ltd.
1316 Murray Ave, Suite 300
Pittsburgh, PA 15217

Serge Bouchard*
TradeARBED
825 Third Avenue, 35th Floor
New York, NY 10022

Michael F. Engestrom*
Nucor-Yamato Steel
P.O. Box 678
Frederick, MD 21705-0678

Karl H. Frank, Team Leader
University of Texas at Austin
10100 Bornet Rd.
Ferguson Lab, P.R.C. #177
Austin, TX 78758

Nestor Iwankiw, POC*
American Institute of Steel Construction
One East Wacker Dr., Suite 3100
Chicago, IL 60601-2001

Dean C. Krouse*
705 Pine Top Drive
Bethelem, PA 18017

Frederick V. Lawrence
University of Illinois at Urbana-Champaign
205 N. Mathews Ave.
Room 2129 Newmark Lab
Urbana, IL 61801

Robert F. Preece
Preece, Goudie & Associates
100 Bush St., Suite 410
San Francisco, CA 94104

Raymond H. R. Tide, Guideline Writer
Wiss, Janney, Elstner Associates, Inc.
330 Pfingsten Road
Northbrook, IL 60062-2095

TAP for Welding and Inspection

John M. Barsom, POC
Barsom Consulting, Ltd.
1316 Murray Ave, Suite 300
Pittsburgh, PA 15217

John W. Fisher
Lehigh University
117 ATLSS Drive
Bethlehem, PA 18015-4729

J. Ernesto Indacochea
University of Illinois at Chicago
Civil and Materials Engineering (mc 246)
842 West Taylor Street
Chicago, IL 60607

Matthew Johnson, Team Leader
Edison Welding Institute
1250 Arthur E. Adams Drive
Columbus, OH 43221

David Long
PDM Strocal, Inc.
2324 Navy Drive
Stockton, CA 95206

Duane K. Miller, POC
The Lincoln Electric Company
22801 St. Clair Ave.
Cleveland, OH 44117-1194

Robert Pyle*
AISC Marketing
10101 South State Street
Sandy, Utah 84070

Douglas Rees-Evans*
Steel Dynamics, Inc.
Structural Mill Division
2601 County Road 700 East
Columbia City, IN 46725

Richard I. Seals
P.O. Box 11327
Berkeley, CA 94712-2327

Robert E. Shaw, Guideline Writer
Steel Structures Technology Center, Inc.
42400 W Nine Mile Road
Novi, MI 48375-4132

TAP for Connection Performance

Charlie Carter*
American Institute of Steel Construction
One East Wacker Drive, Suite 3100
Chicago, IL 60601-2001

Robert H. Dodds
University of Illinois at Urbana-Champaign
205 N. Mathews Ave.
2129 Newmark Lab
Urbana, IL 61801

Roger Ferch, POC
Herrick Corporation
7021 Koll Center Parkway
P.O Box 9125
Pleasanton, CA 94566-9125

John D. Hooper, Guideline Writer
Skilling Ward Magnusson Barkshire, Inc.
1301 Fifth Avenue, Suite 3200
Seattle, WA 98101-2699

Egor Popov
University of California at Berkeley
Department of Civil and Environmental
Engineering, Davis Hall
Berkeley, CA 94720

Steve Powell*
SME Steel Contractors
5955 W. Wells Park Rd.
West Jordan, UT 84088

Charles W. Roeder, Team Leader
University of Washington
233-B More Hall FX-10
Dept. of Building and Safety
Seattle, WA 98195-2700

Stanley T. Rolfe
University of Kansas
Civil Engineering Department
2006 Learned Hall
Lawrence, KS 66045-2225

Rick Wilkinson*
Gayle Manufacturing Company
1455 East Kentucky
Woodland, CA 95695

TAP for System Performance

Jacques Cattan*
American Institute of Steel Construction
One East Wacker Drive, Suite 3100
Chicago, IL 60601-2001

Gary C. Hart
Hart Consultant Group
The Water Garden, Ste. 670E
2425 Olympic Blvd.
Santa Monica, CA 90404-4030

Y. Henry Huang*
Los Angeles County Dept. of Public Works
900 S. Fremont Avenue, 8th Floor
Alhambra, CA 91803

Helmut Krawinkler, Team Leader
Department of Civil Engineering
Stanford University
Stanford, CA 94305

Dennis Randall*
SME Steel Contractors
5955 West Wells Park Road
West Jordan, UT 84088

Andrei M. Reinhorn
State University of New York at Buffalo
Civil Engineering Department
231 Ketter Hall
Buffalo, NY 14260

Arthur E. Ross, JVMC
Cole/Yee/Shubert & Associates
2500 Venture Oaks Way, Suite 100
Sacramento, CA 95833

C. Mark Saunders, Guideline Writer
Rutherford & Chekene
303 Second St., Suite 800 North
San Francisco, CA 94107

W. Lee Shoemaker*
Metal Building Manufacturers Association
1300 Summer Avenue
Cleveland, OH 44115

John Theiss, POC
EQE/Theiss Engineers
1848 Lackland Hills Parkway
St. Louis, MO 63146-3572

TAP for Performance Prediction and Evaluation

Vitelmo V. Bertero
University of California at Berkeley
Pacific Earthquake Engr. Research Center
1301 S. 46th St.
Richmond, CA 94804

Bruce R. Ellingwood
Johns Hopkins University
Department of Civil Engineering
3400 N. Charles St.
Baltimore, MD 21218

Douglas A. Foutch, Team Leader
University of Illinois
MC-250, 205 N. Mathews Ave.
3129 Newmark Civil Engineering Lab
Urbana, IL 61801

Theodore V. Galambos, POC
University of Minnesota
122 CE Building, 500 Pillsbury Dr. SE
Minnneapolis, MN 55455

Lawrence G. Griffis
Walter P. Moore & Associates
3131 Eastside, Second Floor
Houston, TX 77098

Edwin T. Huston, JVMC
Smith & Huston, Inc.
8618 Roosevelt Way NE
Seattle, WA 98115

Harry Martin*
American Iron and Steel Institute
11899 Edgewood Road, Suite G
Auburn, CA 95603

Thomas A. Sabol, Guideline Writer
Englekirk & Sabol Consulting Engineers
P.O. Box 77-D
Los Angeles, CA 90007

Tom Schlafly*
American Institute of Steel Construction
One East Wacker Drive, Suite 3100
Chicago, IL 60601-2001

Technical Advisors

NormAbrahamson
Pacific Gas & Electric
P.O. Box 770000, MC N4C
San Francisco, CA 94177

C.B. Crouse
URS – Dames and Moore
2025 First Avenue, Suite 500
Seattle, WA 98121

Robert Kennedy
RPK Structural Mechanics Consultants
18971 Villa Terr
Yorba Linda, CA 92886

Social Economic and Policy Panel

Martha Cox-Nitikman
Building and Owners and Managers
Association, Los Angeles
700 South Flower, Suite 2325
Los Angeles, CA 90017

Karl Deppe
27502 Fawnskin Dr.
Rancho Palos Verdes, CA 90275

Eugene Lecomte
Institute for Business and Home Safety
6 Sheffield Drive
Billerica, MA 01821

James Madison
Attorney at Law, Mediator and Arbitrator
750 Menlo Avenue, Suite 250
Menlo Park, CA 94025

Alan Merson
Morley Builders
2901 28th Street, Suite 100
Santa Monica, CA 90405

Joanne Nigg
University of Delaware
Disaster Research Center
Newark, DE 19716

William Petak
University of Southern California
Lewis Hall, Room 201
650 Childs Way
Los Angeles, CA 90089

Francine Rabinovitz
Hamilton, Rabinovitz and Alschuler
1990 South Bundy Drive, Suite 777
Los Angeles, CA 90025

Dennis Randall
SME Steel Contractors
5955 West Wells Park Road
West Jordan, UT 84088

David Ratterman
Stites and Harbison
400 West Market St., Suite 1800
Louisville, KY 40202-3352

L. Thomas Tobin, Panel Coordinator
134 California Ave.
Mill Valley, CA 94941

Stephen Toth
TIAA-CREF
730 Third Avenue
New York, NY 10017-3206

John H. Wiggins, POC
J.H. Wiggins Company
1650 South Pacific Coast Hwy, Suite 311
Redondo Beach, CA 90277

Performance of Steel Buildings in Past Earthquakes Subcontractors

David Bonowitz
887 Bush, No. 610
San Francisco, CA 94108

Peter Clark
SAC Steel Project Technical Office
1301 South 46th St.
Richmond, CA 94804

Michael Durkin
Michael Durkin & Associates
22955 Leanora Dr.
Woodland Hills, CA 91367

James Goltz
California Institute of Technology
Office of Earthquake Programs
Mail Code 252-21
Pasadena, CA 91125

Bruce Maison
7309 Lynn Ave
Elcerrito, CA 94530

Peter Maranian
Brandow & Johnston Associates
1660 West Third Street
Los Angeles, CA 90017

Terrence Paret
Wiss Janney Elstner Associates, Inc.
2200 Powell St. Suite 925
Emeryville, CA 94602

Maryann Phipps
Degenkolb Engineers
225 Bush Street, Suite 1000
San Francisco, CA 94104

Allan Porush
Dames & Moore
911 Wilshire Blvd., Suite 700
Los Angeles, CA 90017

Access Current Knowledge Subcontractors

David Bonowitz
887 Bush , No. 610
San Francisco, CA 94108

Stephen Liu
Colorado School of Mines
Mathematics and Computer Science Department
Golden, CO 80401

Materials and Fracture Subcontractors

Robert Dexter
University of Minnesota
122 Civil Engineering Building
500 Pillsbury Drive SE
Minneapolis, MN 55455-0116

Karl H. Frank
University of Texas at Austin
10100 Bornet Rd.
Ferguson Lab, P.R.C. #177
Austin, TX 78758

Welding and Inspection Subcontractors

Pingsha Dong / Tom Kilinski
Center for Welded Structures Research
Battelle Memorial Institute
501 King Avenue
Columbus, OH 43201-2693

Matthew Johnson
Edison Welding Institute
1250 Arthur E. Adams Drive
Columbus, OH 43221

Glenn M. Light / George Gruber
Southwest Research Institute
6220 Culebra Road, P. O. Drawer 28510
San Antonio, TX 78228-0510

William C. Mohr
Edison Welding Institute
1250 Arthur E. Adams Drive
Columbus, OH 43221

Connection Performance Subcontractors

Gregory Deierlein
Stanford University
Terman Engineering Center
Department of Civil and Enviromental Engr.
Stanford, CA 94305-4020

Charles W. Roeder
University of Washington
233-B More Hall FX-10
Seattle, WA 98195-2700

Sherif El-Tawil / Sashi Kunnath
University of Central Florida
Civil and Environmental Engr. Department
Orlando, FL. 32816-2450

Anthony Ingraffea
Cornell University
School of Civil Engineering
363 Hollister Hall
Ithaca, NY 14853

System Performance Subcontractors

Paul Somerville
Woodward-Clyde Federal Services
566 El Dorado St., Suite 100
Pasadena, CA 91101-2560

Farzad Naeim
John A. Martin & Associates
1212 S. Flower Ave.
Los Angeles, CA 90015

Andrei M. Reinhorn
State University of New York at Buffalo
Civil Engineering Department
231 Ketter Hall
Buffalo, NY 14260

C. Allin Cornell
Stanford University
Terman Engineering Center
Stanford, CA 94305-4020

Helmut Krawinkler
Dept. of Civil Engineering
Stanford University
Stanford, CA 94305

Gregory MacRae
University of Washington
Civil Engineering Department
Seattle, WA 98195-2700

Kazuhiko Kasai
Tokyo Institute of Technology
Structural Engineering Research Center
Nagatsuta, Midori-Ku
Yokohama 226-8503, JAPAN

Bruce F. Maison
7309 Lynn Avenue
El Cerrito, CA 94530

Performance Prediction and Evaluation Subcontractors

James Anderson
University of Southern California
Civil Engineering Department
Los Angeles, CA 90089-2531

Douglas A. Foutch
University of Illinois
MC-250, 205 N. Mathews Ave.
3129 Newmark Civil Engineering Lab
Urbana, IL 61801

Gary C. Hart
Department of Civil and Environmental Engineering
University of California
Los Angeles, CA 90095

Y.K. Wen
University of Illinois
3129 Newmark Civil Engineering Lab
205 N. Mathews Ave.
Urbana, IL 61801

Testing Subcontractors

Subhash Goel / Bozidar Stojadinovic
University of Michigan
Civil Engineering Department
Ann Arbor, MI 48109

Roberto Leon
Georgia Institute of Technology
School of Civil & Environmental Engr.
790 Atlantic Ave.
Atlanta, GA 30332-0355

Vitelmo V. Bertero / Andrew Whittaker
UC Berkeley
Pacific Earthquake Engr. Research Center
1301 S. 46th St.
Richmond, CA 94804

Thomas Murray
Virginia Tech, Dept. of Civil Engineering
200 Patton Hall
Blacksburg, VA 24061

James M. Ricles / Le-Wu Lu
Lehigh University
c/o ATLSS Center
117 ATLSS Drive, H Building
Bethlehem, PA 18015-4729

John M. Barsom
Barsom Consulting, Ltd.
1316 Murray Ave, Suite 300
Pittsburgh, PA 15217

Hassan Astaneh
University of California at Berkeley
Dept. of Civil and Environmental Engr.
781 Davis Hall
Berkeley, CA 94720

Michael Engelhardt
University of Texas at Austin
Ferguson Laboratory
10100 Burnet Road, Building 177
Austin, TX 78712-1076

Gary T. Fry
Texas A&M University
Department of Civil Engineering
Constructed Facilities Division, CE/TTI
Building, Room 710D
College Station, TX 77843-3136

Chia-Ming Uang
University of California at San Diego
Dept. of AMES, Division of Structural Engr.
409 University Center
La Jolla, California 92093-0085

Stephen Schneider
University of Ilinois at Urbana-Champaign
3106 Newmark Civil Engr. Lab, MC-250
205 N. Mathews Avenue
Urbana, IL 61801

Matthew Johnson
Edison Welding Institute
1250 Arthur E. Adams Drive
Columbus, OH 43221

James Anderson
University of Southern California
Civil Engineering Department
Los Angeles, CA 90089-2531

Bozidar Stojadinovic
Dept. of Civil & Environmental Engr.
University of California
Berkeley, CA 94720

Inspection Procedure Consultants

Thomas Albert
Digiray Corporation
2235 Omega Road, No. 3
San Ramon, CA 94583

Randal Fong
Automated Inspection Systems, Inc.
4861 Sunrise Drive, Suite 101
Martinez, CA 94553

Andre Lamarre
R.D Tech, Inc.
1200 St. Jean Baptiste, Suite 120
Quebec City, Quebec, Canada G2ZE 5E8

Glenn Light
Southwest Research Institute
6220 Culebra Road
San Antonio, TX 78228

Andrey Mishin
AS & E High Energy Systems
330 Keller Street, Building 101
Santa Clara, CA 95054

Robert Shaw
Steel Structures Technology Center, Inc.
42400 W. Nine Mile Road
Novi, MI 48375-4132

Carlos Ventura
Dept of Civil Engineering
University of British Columbia
2324 Main Hall
Vancouver, BC, Canada V6T 1Z4

Guideline Trial Applications Subcontractors

John Hopper
Skilling Ward Magnusson Barkshire, Inc.
1301 Fifth Avenue, Suite 320
Seattle WA 98101-2699

Lawrence Novak
Skidmore, Owings, and Merrill
224 S. Michigan Ave, Suite 1000
Chicago, IL 60604

Leonard Joseph
Thornton-Tomassetti Engineers
641 6th Avenue, 7th Floor
New York, NY 10011

Maryann Phipps
Degenkolb Engineers
225 Bush Street, Suite 1000
San Francisco, CA 94104

Economic and Social Impact Study Subcontractors

Ronald Eguchi
EQE Engineering and Design
300 Commerce Dr., Ste. 200
Irvine, CA 92602

Charles Kircher
Charles Kircher & Associates
1121 San Antonio Road, Suite D-202
Palo Alto, CA 94303

Martin Gordon / Peter Morris
Adamson Associates
170 Columbus Avenue
San Francisco, CA 94133

Lizandro Mercado
Brandow & Johnston Associates
1600 West 3rd St.
Los Angeles, CA 90017

Richard Henige
Lemessurier Consultants Inc.
675 Massachusetts Ave.
Cambridge, MA 02139-3309

Greg Schindler
KPFF Consulting Engineers
1201 3rd Ave.
Seattle, WA 98101-3000

Report Production and Administrative Services

A. Gerald Brady, Technical Editor
Patricia A. Mork, Administrative Asst.
Peter N. Mork, Computer Specialist
Bernadette A. Mosby, Operations Admin.
Michelle S. Schwartzbach, Pub. Specialist
Applied Technology Council
555 Twin Dolphin Drive, Suite 550
Redwood City, CA 94065

Carol Cameron, Publications Coordinator
Ericka Holmon, Admin. Assistant
California Universities for Research in Earthquake Engineering
1301 S. 46th Street
Richmond, CA 94804

*indicates industrial or organizational contact representative